On the State of Pentosan in Wood Pulps

By Kei MATSUZAKI, Akira HATANO, Tōru ABE and Hiroshi SOBUE

(Received October 9, 1953)

1. Introduction

Many discussions[1,2] have been made on the state of pentosan in wood pulps. However, as our previous report[3] showed, it is difficult to determine a small quantity of pentosan by the phloroglucin or bromate method. Accordingly, the conclusions reached do not seem to be correct. In this research, pentosan determinations by paper chromatography and by the colorimetric method with aniline were applied to the acid-hydrolyzed samples as well as to the alkali-extracted samples, and the state of pentosan in wood pulps was discussed.

2. Experimental Procedures and Results

(1) The Pentosan Contents of Acid-hydrolyzed Pulps.—Five g. each of sulfite rayon pulps from red pine (*Pinus densiflora* S. et Z.) and beech (*Fagus crenata* Blume) were hydrolyzed with 300 cc. of boiling 4N hydrochloric acid for 1, 3, 5 and 7 hours. Since recrystallization of split chains was observed during acid-hydrolysis,[4] the acid-hydrolyzed samples were treated with a boiling 1% sodium hydroxide solution for half an hour to eliminate[5] the recrystallized particles. The pentosan contents of the acid- and acid-alkali-treated samples were determined by paper chromatography.[6] The result is tabulated in Table I. The degrees of polymerization were determined from the viscosities of cupri-ethylene diamine solutions[7] of the samples.

TABLE I

THE PENTOSAN CONTENTS AND DEGREES OF POLYMERIZATION OF ACID-HYDROLYZED AND ACID-ALKALI TREATED PULPS

Time of Acid-Hydrolysis	Treatment	Red Pine			Beech		
		yield %	pentosan* %	D.P.**	yield %	pentosan* %	D.P.**
0	original	···	2.0	720	···	3.0	650
	alkali	88.2	1.25	710	92.6	2.0	620
1	acid	70.5	0.45	111	72.4	0.60	113
	acid-alkali	36.0	0.31	121	41.1	0.50	120
3	acid	47.9	0.30	102	49.2	0.30	102
	acid-alkali	23.9	0.22	87	25.0	0.20	98
5	acid	33.3	0.15	87	35.8	0.10	87
	acid-alkali	11.0	0.10	80	12.7	trace	92
7	acid	23.6	0.13	81			
	acid-alkali	7.1	0.05	80			

* % in the residue, determined by paper chromatography
** Cupri-ethylene diamine solution, $Km = 8.0 \times 10^{-4}$

(2) The Pentosan Contents of Cold Alkali-treated Pulps.—Two g. each of red pine and beech pulps were treated with 50 cc. of 4–17.5% sodium hydroxide solutions for half an hour at 20°C, stirring every five minutes. The samples, pressed on a glass filter to make them free from the residual alkaline solution as far as possible, were treated again with 50 cc. of a sodium hydroxide solution of the same concentration and processed as before, washed successively with water, and 1% acetic acid solution and water, and dried. In another series of experiments, the cold alkali-treated samples whose cellulose micelles are more or less disordered were treated with 200 cc. of 2.5N sulfuric acid at 95–100°C for an hour to remove pentosan thoroughly. The pentosan contents of the samples were determined by the colorimetric method[3] and partly by paper chromatography. The results are tabulated in Table II and Table III.

1) K. H. Meyer, "Hoch polymere Chemie" Vol. 2 (1940) p. 216; H. Maeda, *J. Text. Cell. ind. Japan*, **1**, 669 (1945); H. Sobue, K. Matsuzaki, A. Hatano and Y. Arisawa, ibid., **8**, 79 (1952).
2) A. Meller, *Paper Trade J.*, **124**, No. 9, 101 (1947).
3) T. Abe, K. Matsuzaki, A. Hatano and H. Sobue, This Bulletin, **26**, 255 (1953).
4) H. G. Ingersoll, *J. Applied Phys.*, **17**, 921 (1946); J. A. Howsmon, *Textile Research J.*, **19**, 152 (1949); O. A. Battista, *Ind. Eng. Chem.*, **42**, 502(1950); A. Meller, *J. Polymer Sci.*, **4**, 619(1949); P. H. Hermans and A. Weidinger, ibid., **4**, 317 (1949).
5) H. Maeda, *J. Text. Cell. Ind. Japan.*, **1**, 651 (1945).
6) H. Sobue and A. Hatano, *J. Chem. Soc. Japan, Ind. Chem. Sec.*, **54** 460(1951); **55**, 131(1952).
7) Tappi Standard T230 Sm-50.

TABLE II

THE PENTOSAN CONTENTS OF COLD ALKALI- AND ALKALI-ACID-TREATED RED PINE PULPS

NaOH, %	Treatment	Yield, %	Pentosan,* %
4	Alk.	97.1	0.93 (0.9)
	Alk.-acid	92.4	0.69
6	Alk.	93.7	0.69 (0.6)
	Alk.-acid	90.4	0.46
8	Alk.	88.9	0.53 (0.5)
	Alk.-acid	85.4	0.35
10	Alk.	85.6	0.42 (0.3)
	Alk.-acid	82.6	0.24
12	Alk.	88.9	0.32
	Alk.-acid	85.4	0.21
14	Alk.	89.0	0.39
	Alk.-acid	86.4	0.19
17.5	Alk.	91.2	0.38
	Alk.-acid	87.5	0.22

* By colorimetric method, except ( ) which was determined by paper chromatography

TABLE III

THE PENTOSAN CONTENTS OF COLD ALKALI- AND ALKALI-ACID-TREATED BEECH PULPS

NaOH, %	Treatment	Yield, %	Pentosan,* %
4	Alk.	95.7	0.73
	Alk.-acid	92.9	0.68
6	Alk.	94.2	0.65
	Alk.-acid	91.4	0.52
8	Alk.	89.8	0.53
	Alk.-acid	86.9	0.38
10	Alk.	88.3	0.48
	Alk.-acid	82.8	0.22

* By colorimetric method

3. Discussion

The foremost interest would be the problem of whether or not the pentosan penetrates into the crystalline region.

From Table I, it is seen that the pentosan contents of the acid-treated pulps and acid-alkali-treated pulps decrease with the time of hydrolysis. The relationship between the yield of residue and the quantity of pentosan removed is shown in Fig. 1. Both the acid- and acid-alkali-treated pulps show a similar tendency, and it is seen that the pentosan content depends mainly on the yields of the residues. If the alkali-treatment helps to remove[5] the particles produced by recrystallization of split molecules in the amorphous region containing most of the pentosan, it would be expected that almost all of the pentosan could be removed. This, however, is not the case as can be seen from Table I and Fig. 1. In Fig. 1, the pentosan contents of the acid-alkali-treated pulps are somewhat higher than those of the acid-treated pulps, when the comparison is made between the samples whose yields of the residues are the same.

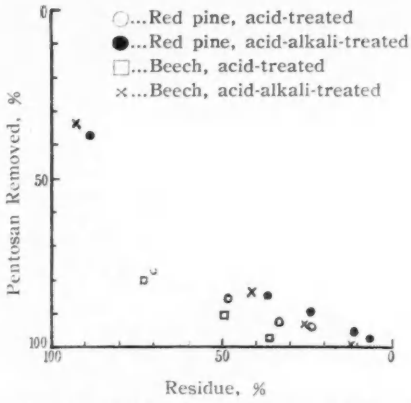

Fig. 1.—Relationship between residue and pentosan removed.

Pentosan removed is expressed as $(1-r)\times 100\%$, where r is the ratio of pentosan content in the treated pulp to that of the original pulps.

It has been asserted that the crystalline region of wood cellulose is 65% by X-ray method[3], and 60–70% by acid hydrolysis followed by dilute alkaline treatment.[5] In Fig. 1, even at 60–70% residue which is thought to consist almost entirely of the crystalline region, 0.5% of pentosan remains in the pulp.

The degrees of polymerization of the acid-alkali-treated pulps were expected to increase for the removal of the recrystallized particles (perhaps of very low D.P.). In Table I, the D.P.'s of the acid-alkali-treated pulps are not apparently different from those of the samples before alkaline treatment. This would be due to the degradation of the high molecular portion.

By using cold caustic solutions of concentrations over 10%, which are believed to be able to penetrate into the crystalline region of cellulose, the pentosan content was reduced to under 0.5%. The after-treatment by the acid of the residues thus treated gave a good effect for pentosan removal. Both pentosan and cellulose molecules in the crystalline region would have been disordered by the conc. alkalies to such an extent that they were readily attacked by the acid solution. Thus wood pulps containing 0.2% of pentosan

8) P. H. Hermans, "Physics and Chemistry of Cellulose Fibers", (1949), p. 517.

were obtained with 82–87% yield, although they are unsuitable for practical use.

These results suggest that the resistant pentosan chains share in building the crystalline region with cellulose chains, although larger portion of pentosan is found in the amorphous region. There remain as yet questions, whether or not the xylose units participate in mixed chain formation.

No great difference was observed between the behavior of pentosan in red pine and beech pulps.

It seems reasonable to deduce the following conclusion from the above discussion.

By intermicellar reactions such as hot alkaline treatment, the pentosan content in the purified pulp would not be reduced to under 0.5%, whereas by intramicellar reactions, such as cold alkaline refinement, the pentosan content could easily be reduced to under 0.5%. This will contribute to the purification processes of wood pulps, since the presence of pentosan is thought to be a cause of poorness in the reactivity of pulps to acetylation and xanthation.[9]

Summary

1. The pulps from the red pine and beech were hydrolyzed with boiling 4N hydrochloric acid solution for 1–7 hours and a part of the hydrolyzed pulps was treated with boiling 1% sodium hydroxide solution for half an hour to eliminate recrystallized particles. The pentosan content decreased as a function of the pulp yield. The degrees of polymerization of these samples were determined.

2. The pulps from the red pine and beech were treated with 4–17.5% sodium hydroxide solution for half an hour at 20° and this procedure was repeated. A part of the samples treated with the alkali was hydrolyzed with 2.5N sulfuric acid solution for one hour at 95–100°. The pentosan contents of these samples were determined.

3. The results show that it is difficult to reduce the pentosan content of wood pulp to under 0.5% by intermicellar reactions such as acid-hydrolysis or dilute hot alkaline refinement, whereas by intramicellar reactions such as cold concentrated alkaline refinement, it is easy to reduce the pentosan content to under 0.5%. The resistant pentosan seemed to be built in the crystalline region of wood cellulose.

4. It has no good effect for pentosan removal to eliminate the recrystallized particles produced by acid hydrolysis with dilute alkali, while acid treatment after cold alkaline refinement gave good result for pentosan removal.

The authors express thanks to Mr. M. Moriya and S. Fukuhara for their aid to the experiment. The expense of the work was defrayed from the Scientific Research Encouragement Grant of the Department of Education.

Department of Applied Chemistry,
Faculty of Engineering,
Tokyo University, Tokyo

9) W. Klauditz, *Holz Roh-u. Werkstoff*, **4**, 314(1941); G. Jayme, *Svensk Papperstidn.*, **50**, Häggland Issue 117(1947); R. E. Dörr, *Angew. Chem.*, **53**, 292(1940).

Molecular Structural Studies on Compounds Containing C—O Bond by Electron Diffraction. II. The Molecular Structure of Anhydrous Oxalic Acid[1]

By Shuzo SHIBATA and Masao KIMURA

(Received March 31, 1954)

Introduction

A number of studies[2] have been carried out on the structure of carboxyl group by use of x-ray diffraction, electron diffraction and molecular spectra. However systematic conclusion has not yet been reached for the structure of a carboxyl group. Hence it seems to be desirable to have more abundunt informations regarding the geometrical configuration of the group in order to discuss the character of carboxyl group by theoretical treatments. An oxalic acid molecule contains two carbonyl groups in a conjugated system O=C–C=O. Therefore the structural determination will decide the degree of conjugation between the two carbonyl groups across the central C–C bond.

In the present study we dealt with anhy-

1) Presented at the 5th annual meeting of the Chem. Soc. Japan held on April 4, 1952.

2) Cf. O. Thomas, *J. Chem. Phys.*, **18**, 761 (1950); M. Davies and O. Thomas, "Discussion of the Faraday Soc." 335 (1950).

drous oxalic acid in order to investigate the two subject problems mentioned above, i.e. 1) the stereochemistry of the carboxyl group, 2) the degree of conjugation between the two carbonyl groups. Hendricks,[3] Cox et al.,[4] Robertson,[5,6] Brill et al.[7] and Ahmed et al.[8] have already determined the molecular structures of anhydrous oxalic acid and its dihydrate by x-ray diffraction. Their studies were also undertaken mainly to make clear the two problems mentioned above although the results of their analyses appear to be inconsistent as will be described later. According to their results there exists an intermolecular hydrogen bond in the crystal of dihydrate and the distance O−H···O has a value of about 2.50Å, which is considerably short. This suggests that the structure of a free molecule might be different appreciably from the molecular structure in the crystalline state.

Therefore we attempted to determine the structure of a free anhydrous molecule by gas electron diffraction method and to obtain informations on the properties of carbon-carbon and carbon-oxygen bonds as well as on the effect of a hydrogen bond upon these distances.

Experimental Results

The sample used in the present investigation was anhydrous oxalic acid prepared from oxalic acid dihydrate by heating at temperatures above its melting point and was purified by sublimation. Anhydrous oxalic acid readily sublimes on heating at temperatures above 100°C. The sample was sublimed at about 120°C in a high temperature nozzle.

Excellent photographs were taken using an electron wavelength of about 0.06 Å and a camera length of about 11 cm. The characteristic features of the photographs are represented by the visual curve V in Fig. 2, where the dotted portion is drawn by use of the theoretical intensity curves to be mentioned later. That the feature of photograph bears a close resemblance to that of dimethylglyoxal is reasonable on account of the similarity of molecular structure between them. The maxima and minima were measured on the photographs within q=83. These observed values are listed in Table I.

TABLE I

OBSERVED AND CALCULATED q VALUES

Max.	Min.	$q_{obs.}$	model L $q_{calc.}$	model L $q_{calc.}/q_{obs.}$	model J $q_{calc.}$	model J $q_{calc.}/q_{obs.}$
	2	14.91				
2		18.07	18.6	1.016	18.5	1.013
	3	21.60				
3		23.87	24.2	1.014	24.2	1.014
	4	26.30	26.0	0.989	26.2	0.995
4		28.94	29.6	1.022	29.6	1.022
	5	32.16	32.4	1.008	32.1	0.998
5		35.56	36.2	1.017	36.1	1.015
	6	40.80	41.6	1.018	41.8	1.025
6		45.40	45.9	1.012	46.0	1.013
	7	48.87	49.4	1.011	49.2	1.006
7		52.43	53.1	1.013	53.0	1.011
	8	56.18	57.0	1.016	56.4	1.005
8		58.93	60.2	1.021	59.9	1.017
	9	62.90	64.0	1.017	63.5	1.009
9		67.25	68.5	1.020	67.9	1.010
	10	71.13	72.4	1.018	72.1	1.013
10		74.34	75.8	1.021	75.4	1.014
	11	77.78	79.6	1.023	79.3	1.021
11		81.12	83.2	1.024	83.0	1.022
average				1.015		1.012
average deviation				0.005		0.006

3) S. B. Hendricks, *Z. Krist.*, **91**, 48 (1953).
4) E. G. Cox, M. W. Dougill and G. A. Jeffrey, *J. Chem. Soc.*, **1952**, 4854.
5) J. M. Robertson and I. Woodward, *J. Chem. Soc.*, **1936**, 1817.
6) J. D. Dunitz and J. M. Robertson, *J. Chem. Soc.*, **1947**, 142.
7) R. Brill, C. Herman and C. L. Peters, *Ann. Physik*, **42**, 357 (1947).
8) F. R. Ahmed and D. W. J. Cruickshank, *Acta Cryst.*, **6**, 385 (1953).

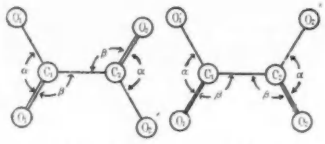

trans form *cis* form

Fig. 1.

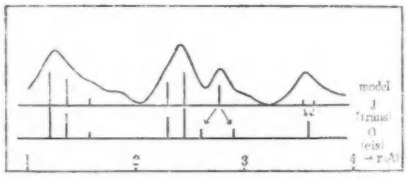

Fig. 2. The radial distribution curve for anhydrous oxalic acid.

The radial distribution curve was calculated by use of the formula

$$rD(r)=\sum_{q=1}^{q=\max.} I(q)\exp(-aq^2)\sin(\pi qr/10)$$

with $\exp(-aq^2_{\max.})=0.1$, and is shown in Fig. 2. The curve has maxima at 1.26, 2.40, 2.75 and 3.55 Å. Each peak may be regarded as made up of the contributions of several interatomic distances. The first peak may be interpreted as representing the bonded C_1-O_1 and C_1-O_1' distances, the second peak the non-bonded $C_1\cdots O_2'$, $C_1\cdots O_2$ and $O_1\cdots O_1'$, distances, and the third and the fourth peaks the non-bonded $O_1\cdots O_2'$, $O_1\cdots O_2$ and $O_1'\cdots O_2'$ (see Fig. 1). The last two peaks correspond to the long distances which are related to the rotational configuration about C—C axis. The existence of the third and fourth peaks shows that the four non-bonded O···O distances can be classified definitely into two groups. Accordingly the molecule seems to have, roughly speaking, either the *trans* form or the *cis* form. The sharp feature of the third peak seems to favor the trans form, because if the molecule takes the *cis* form, two equal distances $O_1'\cdots O_2$ and $O_1\cdots O_2'$ in the trans form will turn out to be two different distances $O_1\cdots O_2$ and $O_1'\cdots O_2'$. The possible O—O distances of trans (J) and cis (O) models are shown by bold lines in the radial distribution curve (Fig. 2).

The theoretical intensity curves were calculated with the following simplified equation,

$$I(q)=\sum_{i\neq j}\sum Z_iZ_j\sin(\pi qr_{ij}/10)/r_{ij}$$

Six parameters C=O, C—C, C—O, $\angle\alpha$, $\angle\beta$ and $\angle\gamma$ (a twisted angle) are required for settling molecular forms. The effect of hydrogen atoms is negligibly small on the theoretical intensity curves except the O—H distance which was assumed to be 0.96 Å. If the distance C=O is assumed to be equal to 1.20 Å and the molecule is planar, the parameters involved are as follows C—C/C=O, C—O/C=O, $\angle\alpha$ and $\angle\beta$. Fifty three theoretical intensity curves were calculated for the models with the values ranging from 1.44 to 1.60 Å for C—C, from 1.30 to 1.40 Å for C—O, from 116° to 131° for $\angle\alpha$ and from 112° to 134° for $\angle\beta$. Some of them are reproduced in Fig. 3. in order to illustrate the variation of the relative positions and intensities of maxima and minima with the change of the parameters.

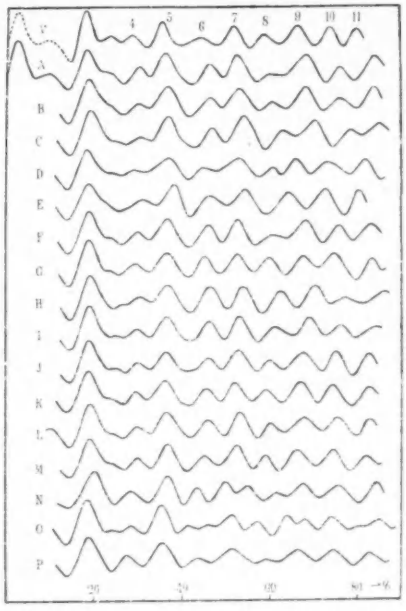

Fig. 3. The visual and theoretical intensity curves.

The models are listed in Table II. The curves A, B, D and E illustrate the effect of $\angle\beta$, the curves F and G that of C—O distance, the curves H, I and J that of C—C distance, and curves B, C, K and L that of $\angle\alpha$. Our analysis could be facilitated by the fact that the calculated intensity curves are not very sensitive to the parameter $\angle\beta$. The curve J in Fig. 3, which is one of the best models, is in good agreement with the observed scattering curve, except that the agreement is not perfect in regard to both the height of the third maximum and the depth of the fifth minimum, which appears stronger on photographs than would be suggested by the calculated intensity curves. This discrepancy may be considered to be due merely to a difficulty in the examination of photographs by visual method. It is found that the models with C—C distance smaller (or larger) than that of the best model can also give the theoretical intensity curves in agreement with the visual curve, if the value of $\angle\alpha$ is decreased (or increased) from that of the best model (e.g. curve L in Fig. 2). These circumstances are shown schematically in Fig. 4. Therefore it is impossible to determine the C—C distance very accurately. Further the theoretical intensity curves were calculated for the models with various twisted angles about C—C axis (Cf. Curves M and N in Fig. 2.). If a twisted angle from the

TABLE II

MODELS FOR ANHYDROUS OXALIC ACID

Model	C=O(Å)	C—O(Å)	C—C(Å)	∠α(degree)	∠β(degree)	∠γ and configuration
A	1.20	1.30	1.48	122	123	planar, *trans*
B	"	"	"	122	120	" "
C	"	"	"	125	"	" "
D	"	1.35	1.56	"	117.5	" "
E	"	"	"	"	112	" "
F	"	1.33	1.52	123.5	123	" "
G	"	1.37	"	"	"	" "
H	"	1.35	1.48	125	"	" "
I	"	"	1.52	"	"	" "
J	"	"	1.56	"	"	" "
K	"	"	1.52	122	"	" "
L	"	"	"	123.5	"	" "
M	"	"	1.56	125	"	twisted through 30° from the *trans* form.
N	"	"	"	"	"	twisted through 60° from the *trans* form.
O	"	"	"	"	"	planar, *cis*
P	"	"	"	"	"	free rotation

trans form is less than about thirty degrees, it is possible to obtain theoretical intensity curves in agreement with the visual curve, because the two distances which vary with internal rotation, O_1-O_2' and O_1-O_2 or $O_1'-O_2'$ change in opposite directions so that the effect of the changes is partly compensated each other. However the models with a twisted angle greater than about 30° are unacceptable because the third maximum disappears in the theoretical curves. Therefore electron diffraction data can give no conclusive value of the twisted angle about the C—C axis up to 30°. The free rotational and *cis* models are also discarded because of the disappearance of the third maximum and because of the changes of the 6th and 9th maxima into double maxima respectively. The effect of intramolecular vibrations was taken into account for the interatomic distances except for those related to the internal rotation. The mean amplitudes used in the calculation were estimated using the values for oxalyl chloride.[9] The results are practically the same as those obtained for the fixed models.

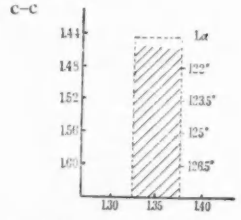

Fig. 4. Parameter chart for oxalic acid. The shaded part shows the region of parameters giving acceptable models when is assumed ∠β=123°.

The effect of the internal rotation can be found in the results obtained from the considerations of the theoretical intensity curves for the models with various twisted angles. But we could not obtain a definite conclusion for the rotational vibration because we must take into account at the same time both the twisted angle in equilibrium and the rotational vibration as well as internal vibrations.

Finally a quantitative comparison with the observed values was made for the maxima and the minima of the best theoretical intensity curves. The results are shown in Table I. For the 2nd and 3rd minima a comparison was not made on account of the inaccuracy of the observed values.

Thus the molecular structure of anhydrous oxalic acid was obtained as follows: C=O 1.22Å ±0.02 Å, C—O 1.37 Å±0.02 Å, C—C 1.54 Å±0.06 Å, ∠O=C—O 125°±3°, ∠O=C—C 122°±5°, and the *trans* form. But the deviation from the *trans* form is permissible within a twisted angle of about thirty degrees.

Although the existence of dimers as in formic acid[10] might be improbable in the gaseous state, the theoretical intensity curves were calculated for the model dimerized in the same type as β form of anhydrous oxalic acid.[2] When O···O distance is equal to about 2.70 Å, the dimerized model gives a theoretical intensity curve in fair agreement with the visual curve. Further investigation on this point, however, has not been carried out.

Discussion of Results

Our analysis gave the following results: First, the length of the central C—C bond is 1.54 Å, a value generally ascribed to a normal single bond, secondly the molecule is

9) Y. Morino, private communication.

10) I. L. Karle and L. O. Brockway, *J. Am. Chem. Soc.*, **66**, 574 (1944).

planar despite the single bond character of the C−C bond. We shall explain the above results and compare the molecular structure of oxalic acid in the gaseous state with that in the crystalline state which has hitherto been reported.

The value of 1.54 Å±0.06 Å was obtained for C−C bond length. This value is equal to C−C bond length in ethane and other saturated hydrocarbons. Therefore C−C bond in an oxalic acid molecule seems to have a small degree of double bond character. Though we cannot say definitely because of the probable errors, the double bond character seems to be less in an oxalic acid molecule than in glyoxal[14] (C−C=1.47 A± 0.02 Å) and in oxalyl chloride.[15] The molecules of these compounds contain carboxyl groups in a conjugated system similar to that of oxalic acid, i.e. O=C−C=O to which the resonating electronic structures such as $O^+-C=C-O^-$ contribute. This suggests that two carbonyl groups in the molecule are not conjugated very much with each other, presumably because the strongly electronegative hydroxyl oxygen atoms prevent an appreciable π electron conjugation across the C−C bond. Therefore the structure of the carboxyl group will be similar to that of a monobasic acid having only one carboxyl group. According to the recent data obtained by Schomaker and O'Gorman,[11] and Karle[13] shown in Table III, the structure of the carboxyl group in anhydrous oxalic acid is in good agreement with that in a formic acid monomer. The dimensions of the carboxyl group obtained have revealed a significant difference of about 0.15 Å, between the two carbon-oxygen bonds, although the difference between them is less than that expected between a pure single and a pure double bond. Accordingly it follows that the resonance form (B2) to be shown later does not contribute very much to the normal state of a carboxyl group in a gaseous oxalic acid molecule.

Table III

Structures of carboxyl group, especially oxalic acid

	C=O	C—O	C—C	material	method
Shibata and Kimura	1.22	1.37	1.54	anhydrus oxalic acid	electron diffraction
Hendricks[3]	1.22	1.29	1.57	„ (α form)	x-ray
Cox, Dougill and Jeffrey[4]	1.19	1.29	1.56	„ „	„
Hendricks[3]	1.20	1.30	1.59	„ (β form)	„
Robertson and Woodward[5]	1.24	1.30	1.43	oxalic acid dihydrate	x-ray
Brill, Herman and Peters[7]	1.21	1.28	1.55	„	„
Dunitz and Robertson[6]	1.24	1.25	1.46	„	„
Ahmed and Cruickshank[8]	1.19	1.29	1.53	„	„
Jeffrey and Parry[17]	1.23	1.25	1.56	ammonium oxalate monohydrate	„
Karle and Brockway[10]	1.24	1.42		formic acid monomer	electron diffraction
„ „	1.25	1.36		„ dimer	„
Schomaker and O'Gorman[11]	1.213	1.368		formic acid monomer	„
Karle[13]	1.23	1.36		„	„
Williams[12]	1.225	1.41		„	spectrum
Karle and Brockway[8]	1.24	1.43	1.54	acetic acid monomer	electron diffraction
„ „	1.25	1.36		acetic acid dimer	„
LuValle and Schomaker[14]	1.20		1.47	glyoxal	„
Schomaker[15]	1.20		1.50	oxalyl chloride	„

We have come to the conclusion that the molecule takes a planar configuration. To account for this fact some interpretation other than resonance interaction between carboxyl groups is necessary. According to the results obtained from Raman spectra and infrared absorption spectra, oxalyl chloride molecule in the liquid state takes a planar trans configuration rather than the *cis* configuration at room temperature and at higher

11) V. Schomaker and J. M. O'Gorman, *J. Am. Chem. Soc.*, **69**, 2638 (1947).
12) V. Z. Williams, *J. Chem. Phys.*, **15**, 232 (1947).
13) I. L. Karle and J. Karle, *J. Chem. Phys.*, **22**, 43 (1951).
14) J. E. LuValle and V. Schomaker, *J. Am. Chem. Soc.*, **61**, 3520 (1939).
15) The results by V. Schomaker cited in L. E. Sutton and P. W. Allen, *Acta Cryst.*, **3**, 46 (1950).

temperatures.[16] The molecular structure in the gaseous state was also confirmed to be the trans configuration by electron diffraction.[15] Moreover the molecular structure of glyoxal in the gaseous state was found to be the trans configuration, by electron diffraction experiment. The coplanarity of oxalyl chloride and glyoxal may be due to the stabilizing resonance energy associated with some double bond character of carbon-carbon bond. If molecule is planar, a consideration of electrostatic interaction and steric hindrance indicates that these molecules should take the trans rather than the *cis* configuration. On the other hand, since the double bond character which restricts rotation seems to be weak in oxalic acid, a consideration of electrostatic interaction and steric hindrance will indicate the possibility of a nonplanar form. Thus the fact that the molecule have the planar and trans configuration or the form similar to it seems to be due partly to the O—H···O intramolecular hydrogen bond similar to that in salicylic acid. This possibility may be supported by the fact that the distance 2.76 Å between the oxygen atoms (for the best model) is appropriate.

Recently Cox, Dougill and Jeffrey determined the molecular structure of anhydrous oxalic acid (α form)[1] in agreement with a work by Hendricks. Ahmed and Cruickshank carried out a refined analysis using the data obtained by Robertson and his coworkers and by Brill et al. They proposed a new molecular structure of oxalic acid dihydrate. According to these results, as shown in Table III, the C—C bond length is nearly equal to that a normal single bond, 1.54 Å, and two kinds of C—C bonds are equal to 1.29 Å and 1.19 Å respectively, and the molecule is planar.

In general the structure of oxalic acid dihydrate in the crystalline state may be represented by the following schematic formula,[1]

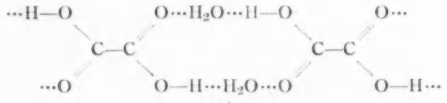

(A)

A carboxyl group may resonate between the two forms,

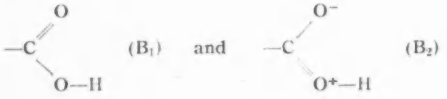

(B_1) and (B_2)

Accordingly the resonance form,

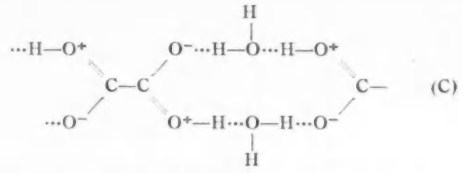

(C)

may contribute to the normal state of oxalic acid dihydrate. If very strong hydrogen bonds are present in a crystal, the contribution of such resonance from (C) will be appreciably large. As an extreme case, a resonance form

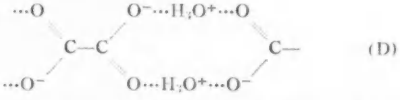

(D)

may be considered. If H_3O^+ is separated completely from other part of oxalic acid dihydrate, two C—C bonds in an oxalate ion should be equal to each other as shown by an x-ray analysis of the crystal structure of ammonium oxalate monohydrate.[17]

Taking into account the data of themselves and of Brill et al., Dunitz and Robertson proposed a remarkable feature of results for the structure of oxalic dihydrate, i.e. the C—C bond length 1.46 Å and two C—C bonds, differing in their lengths, 1.24 Å and 1.25 Å. These results are contradictory to that of Ahmed et al. in regard to the C—C double bond character and to the equality of C—C bond length, owing to the contribution of resonance form (D) to a molecule in the crystalline state. If such is actually the case in the crystalline state, the significant discrepancies between their results and ours suggest that the molecular structure is dependent on the molecular environment.

On the otherh and, Ahmed et al. and Cox et al. concluded that the appareciable difference in two C—C bond lengths suggests the absence of H_3O^+ ion in a dihydrate and that the similarity of the molecular structure of anhydrous oxalic acid to that of its dihydrate indicate the interatomic distances unaffected by the environment of the molecule. However more remarkable difference will be found between vapor and solid than between anhydrous oxalic acid (α-form) and dihydrate.

Upon comparison of their data obtained by x-ray with our data obtained by gas electron diffraction, the following facts are found to be noteworthy: the C—C bond has a normal single bond length and two C—O bond lenghts

16) J. S. Ziomek, A. G. Meister, F. F. Cleveland and C. E. Decker, *J. Chem. Phys.*, **21**, 90 (1953).
17) G. A. Jeffrey and G. S. Parry, *J. Chem. Soc.*, **1952**, 4864.

differ from each other. But the hydroxyl C—O bond is very short in crystals than in free molecules by an amount of about 0.07 Å.

The difference between the C—O and C=O bond is less in crystals than in gaseous state. If such is actually the case, this will be due to the difference between the crystalline state and the gaseous state, in other words to the difference in the environment around a molecule. Such changes of interatomic distances owing to intermolecular hydrogen bonds, have already been pointed out, for example, in the cases of acetamide[18] and hydroquinone[19] and also in the difference of the structures between the monomer and the dimer of formic acid. Therefore it seems to be probable that the structure of anhydrous oxalic acid is not exactly the same as that of its dihydrate, because the length of a hydrogen bond of 2.5 Å in a dihydrate crystal is considerably small. However the results of the molecular structure of oxalic acid dihydrate by x-ray method are not conclusive. The result obtained by Ahmed and Cruickshank seems to be more reliable than those by others, since they carried out a refined analysis using the data obtained by Robertson et al. and by Brill et al. But reinvestigation by x-ray diffraction seems to be desirable on the structure of oxalic acid dihydrate.

Summary

The molecular structure of anhydrous oxalic acid was studied by electron diffraction method. The interatomic distances and valency angles were found as follows: C=O 1.22 Å, C—O 1.37 Å, C—C 1.54 Å, ∠O=C—O 125°, and ∠O=C—C 122° with possible errors within 0.02 Å, 0.02 Å, 0.06 Å, 3° and 5° respectively. The molecule takes planar trans configuration. From these data the following conclusions were derived. The central C—C bond seems to have a small degree of double bond character with no appreciable conjugation between two carbonyl groups. The molecule takes the planar trans configuration in spite of the small degree of double bond character in the C—C bond. This fact in connection with the data of other compounds seems to suggest the possibility of the existence of intermolecular hydrogen bonds in a free oxalic acid molecule. Our data of oxalic acid in the gaseous state were compared with the data of oxalic acid in the crystalline state from x-ray diffraction. Significant differences was found between the results on molecular dimensions, especially in hydroxyl C—O bond lengths. From these fact it was inferred that the structure of a molecule (or a carboxyl group) is affected by the molecular environment such as hydrogen bond formation between molecules.

We wish to express our thanks to Prof. M. Kubo of Nagoya University for his helpful advice. Our thanks are also due to Dr. S. Seki and Dr. K. Osaki of Osaka University for their valuable suggestion regarding the x-ray diffraction data.

Department of Chemistry, Faculty of Science, Nagoya University, Nagoya

18) M. Kimura and M. Aoki, This Bulletin, **26**, 429 (1953).
19) M. Kimura and S. Shibata, Presented at the 4th annual meeting of the Chem. Soc. Japan held on April 7, 1951.

Zur Kenntnis über die Hochdrucksynthese von Acrylester. I. Erkenntnisse bei der Acrylestersynthese unter der Anwendung von Nickelhalogenid-Katalysator

Von Kazumi YAMAMOTO

(Eingegangen am 24. April 1954)

Einleitung

Bei der Acrylestersynthese nach dem Reppe-Verfahren er gibt sich zweierlei; das erste ist das stoichiometrische Verfahren (oder die Gewöhnliche-Druck-Synthese), in dem Metallcarbonyl als Kohlenoxydträger verwendet wird, und das andere das katalytische, (oder die Hochdrucksynthese), in dem Kohlenoxyd und Acetylen sich auf Alkohol unter katalytischer Wirkung von Salzen der carbonylbildungsfähigen Metalle, wie Nickel, unter erhöhtem Druck und bei erhöhter Temperatur einwirken lassen.

Die Abhandlungen, die fortlaufend veröffentlicht werden sollen, handeln über den Mecha-

nismus der Reaktion, insbesondere über den der Aktivierung des Kohlenoxyds bei dem letzteren.

Die Bildung von Acrylester wird im Sinne der folgenden Gleichung erläutert:

$$CH{\equiv}CH+CO+ROH \longrightarrow CH_2:CHCOOR$$

Reppe[1] hat geschickt die Bildung von Acryl-ester oder Säure aufgeklärt, durch die intermediäre Bildung eines hypothetischen Cyclopropenon-Rings aus Acetylen und Kohlenoxyd, der dann durch Verbindung mit beweglichem Wasserstoffatom, wie Wasser, Alkohol, usw. nach folgendem Schema aufgespalten wird:

$$CH{\equiv}CH+CO \longrightarrow \begin{matrix} CH:CH \\ \diagdown\ \diagup \\ C \\ \| \\ O \end{matrix}$$

$$\begin{matrix} CH:CH \\ \diagdown\ \diagup \\ C \\ \| \\ O \end{matrix} \begin{matrix} +ROH \longrightarrow CH_2:CHCOOR \\ +HOH \longrightarrow CH_2:CHCOOH \end{matrix}$$

Aber man kann den genügenden experimentellen Grund darüber nicht finden, in welcher Weise das Kohlenoxyd an dem Katalysator aktiviert wird, den Cyclopropenonring zu bilden. Darüber nimmt Reppe die Bildung von aktivem, nicht isolierbarem Zwischenprodukt wie $NiBr_2(CO)$, das von Kohlenoxyd und Nickelhalogenid unter der Reaktionsbedingung entsteht, unter Berücksichtigung der Arbeit von Hieber[2] über Kobaltcarbonyljodid $CoJ_2(CO)$ an.

Ausser dem oben erwähnten Metallhalogenid hat Reppe die Komplexverbindungen von demjenigen mit Triphenylphosphin als Katalysator bei der Acrylestersynthese vorgebracht. Was den Mechanismus, wodurch Kohlenoxyd aktiviert wird, anbelangt, ist die zuverlässige Theorie, worüber ich später schreiben werde, bisher nicht veröffentlicht.

Das Allgemeine

Wie vorher erwähnt, werden die Halogenide der carbonylbildenden Metalle als Katalysatoren bei der Hochdrucksynthese von Acrylester aus Acetylen, Kohlenoxyd und Alkohol verwendet. Als solche eignen sich in erster Linie Nickelhalogenide. Die im Experiment benützten Nickelhalogenide wurden nach folgenden Methoden hergestellt.

1. Nickelbromid und Jodid.—Sowohl wasserfreies Nickelbromid als auch Jodid wurde leicht dadurch in einer Form der Lösung erhalten, indem man Brom oder Jod auf Nickelcarbonyl oder auf reduziertes Nickel in Alkohol bei gewöhnlicher Temperatur einwirken lässt.[3,4] Nickelgehalt in der alkoholischen Lösung wurde entweder durch Verdampfung von Alkohol unter erniedrigtem Druck oder durch Titrieranalyse bestimmt. Zu der alkoholischen Lösung des Nickeljodids muss man kleine Mengen reduziertes Nickel beimengen, da es durch Luftsauerstoff unter Jodabspaltung oxydiert wird.[5]

2. Nickelchlorid.—Wasserfreies Nickelchlorid wurde zweckmässig aus Nickelhexaminchlorid hergestellt, das im Vakuum bei etwa 220° über die Stufe Diaminsalz zum Nickelchlorid abgebaut wird.

Acetylen, das von Calciumcarbid erzeugt wurde, wurde durch das übliche Mittel gereinigt, und die Reinheit war mehr als 99% und der Sauerstoffgehalt unter 0.2%.

Kohlenoxyd wurde aus Ameisensäure und Schwefelsäure entwickelt und der darin enthaltene Sauerstoff wurde durch Leitung auf das bei 300° bis 400° erhitzte, reduzierte Kupfer in Kohlensäure umgewandelt, die durch Alkalilauge beseitigt wurde.

Auf solche Weise erhaltenes Acetylen und Kohlenoxyd wurde im Gasometer in gleichem Verhältnis vermischt. Alkohol, wie Äthanol, bzw. Butanol, wird mit Calciumcarbid völlig getrocknet und so verwendet.

Die Aufarbeitung der Acrylestersynthse wurde entweder nach der diskontinuierlichen oder nach der halbkontinuierlichen Methode durchgeführt. Die einzelnen Bedingungen sind je nach den Umständen beschrieben und können folgendermassen zusammengefasst werden:

Diskontinuierliche Methode.—In den Schüttelautoklav, der elektrisch regulierend erhitzt wird, tut man Alkohol und Katalysator hinein und komprimiertes Acetylen-Kohlenoxyd-Gemisch bie zum bestimmten Druck nach dem Verblasen der Luft im Autoklav mit dem Gasgemisch. So beobachtet man hauptsächlich nur die Druckveränderung mit der steigenden Temperatur unter Schüttelung.

Halbkontinuierliche Methode.—Den Autoklav mit dem Verdichter durch biegsames Kapillarrohr verbindend, arbeitet man der Methode (1) gemäss auf. Wenn der Innendruck des Autoklavs bis zu einem Gebiet mit dem Reaktionsverlauf abfällt, so wird frisches Gas-gemisch jederzeit vom Verdichter eingepresst. Die bestimmte Gasmenge, die mittels des Gasometers gemessen wird, wird durch Wiederholung solcher Operation eingepresst. Im allgemeinen verläuft die Reaktion bei 180° unter Gesamtdruck von 30 bis 40 Atm. Die Ausbeute von Acrylester an Alkohol wurde davon ausgerechnet, soweit es nicht anders bestimmt wurde, dass man das ausgewaschene und mit Calciumchlorid getrocknete Öl, das vom Reaktionsprodukt mit Wasserdampf abdestilliert wurde, für Rohacrylester hält.

1) W. Reppe, „Neue Entwicklungen auf dem Gebiet der Chemie des Acetylens und Kohlenoxyds", Springer Verlag, (1949), S. 97.
2) W. Hieber, *Z. anorg. allg. Chem.*, **243**, 145 (1939).
3) K. Yamamoto und K. Sato, *J.P.*, 187, 504.
4) K. Yamamoto und K. Sato, M. Oku, *J.P.*, 195, 106.
5) K. Yamamoto und M. Oku, *J.P.*, 192, 733.

Erkenntnisse bei Äthylacrylat-Synthese

Es dürfte notwendig sein, etwas über die Erkenntnisse bei der Äthylacrylat-Synthese zu beschreiben, z. B. über den Unterschied der katalytischen Fähigkeiten der Nickelhalogenide,*) über die Reaktionsbedigungen, Nebenreaktionen usw.

a) Unterschied der katalytischen Fähigkeiten von Nickelhalogeniden.—Es wurde von Reppe veröffentlicht, dass als Katalysatoren Nickelhalogenide in erster Linie geeignet sind, und dass die wirksamkeit der Halogenide (Nickelfluorid ist unbrauchbar) vom Chlorid zum Jodid stark zunimmt. Bei meiner Nachprobe wurde dies festgestellt, d.h., der Unterschied der katalytischen Fähigkeiten von Nickelhalogeniden ist eindeutig, wie in der Tabelle I gezeigt ist. Das Experiment wurde nach dem halbkontinuierlichen Veafahren durchgeführt.

TABELLE I

Äthanol (g)	NiX_2 (g)		Einleitgsatz. von Gasgem.(%)	Reaktionstemp. (°C)	Laufzeit (Std)	Äthylacrylat (g)	(%)
50	$NiCl_2$	1.5	40	170	20	—	—
50	$NiBr_2$	2.5	100	180	18	45.5	42
50	NiJ_2	3.6	100	165	5	62.5	58

Anmerkung: Autoklavinhalt 600 cm³, Operierender Druck 40 Atm.
Die Kontaktmenge wurde so bestimmt, dass das dem Bromid (5% an Alkohol) entsprechende Nickel erhalten wird, da es mir scheint, dass das katalytische Zentrum das Nickelatom ist. Theoretische Gasgemischmenge ist 48.7 *l.* für 50 g. Alkohol unter normalem Zustand.

b) Reaktionsbedingungen durch Nickeljodidkatalysator.—Wenn man nach dem diskontinuierlichen Verfahren den Reaktionsverlauf beobachtet, so kann man finden, dass die Reaktion in kurzer Zeit über die Latenzperiode (L.P.) hinaus mit dem die Wärmeerzeugung begleitenden Druckabfall verläuft. Die experimentellen Resultate sind unten zusammengefasst. Das Experiment wurde im Autoklav vom 600 cm³ Inhalt, in dem 46 g Äthanol und die bestimmte Menge Nickeljodid (in irgendeinem Falle mit reduziertem Nickel) enthalten sind, dadurch ausgeführt, dass das Gasgemisch (C_2H_2 : CO ist 1 : 1) bis 30 at. eingepresst und unter Schütteln erhitzt wird.

1. Nickeljodidmenge.—In der Tabelle II drückt Atm/Min den verhältnismässig schnellen Druckabfall aus und L.P. die Latenzperiode.

TABELLE II

Nr.	NiJ_2 (g)	Reaktionstemp. (°C)	L. P. (Std)	(Min)	Laufzeit (Std)	(Min)	Atm/Min
625	2.3	140	6	45	8	—	15/15
627	3.2	140	2	—	2	50	18/6
628	4.6	140	1	15	2	30	31/14

Man kann aus obiger Tabelle ersehen, dass man zur Gewinnung von genügender Reaktionsgeschwindigkeit nur mit Nickeljodid eine ziemlich hohe Konzentration dessen bedarf, und dass die Latenzperiode desto kürzer wird, je höher die Konzentration ist.

2. Reaktionstemperatur. — Unter den gleichen Bedingungen wurde der Einfluss der Temperatur unter Anwendung von Nickeljodid (5% an Äthanol) untersucht.

TABELLE III
EINFLUSS VON TEMPERATUR

Nr.	L. P. (Std)	(Min)	Reaktions-temp. (°C)	Atm/Min
620	—		120	—
625	6	45	140	15/15
633	2	—	150	20/15
626	1	—	160	30/30

3. Rolle des reduzierten Nickels als Hilfskatalysator.—Es ist bekannt, dass die Hinzufügung von reduziertem Nickel als Hilfskatalysator die Wirkung von Nickeljodid verstärkt. Darauf erforschte ich dessen Effekt unter den bestimmten Bedingungen (Äthanol 46 g. NiJ_2 2.3 g. bei 140°), um den Umfang zu erkennen.

TABELLE IV
NICKEL ALS HILFSKATALYSATOR

Nr.	Nickel (g)	L. P. (Std)	(Min)	Laufzeit (Std)	(Min)	Atm/Min
625	0	6	45	8	—	15/15
635	0.23	3	—	3	30	28/30
636	0.50	1	15	2	30	20/15

*) Jüngst hat Reppe etwas eingehend darüber veröffentlicht: *Ann.*, **582**, 26 (1953).

Es ist hieraus selbstverständlich, dass die Anwesenheit des Nickels im Vergleich mit seiner Abwesenheit entweder die Reaktionstemperatur um ca. 20° erniedrigt oder die Nickeljodidmenge 30 bis 50 % ersparen lässt.

In der Tabelle V wurde der Effekt von dem in verschiedenem Verhältnis beigefügten Nickel dargestellt. In solcher Weise ist der Effekt der Beifügung von Nickel als Hilfskatalysator sehr bemerkenswert.

TABELLE V
EFFEKT DER NICKELMENGE

Nr.	NiJ_2 (g)	Nickel (g)	L. P. (Std)	L. P. (Min)	Laufzeit (Std)	Laufzeit (Min)	Reaktionstemp. (°C)	Atm/Min
635	2.3	0.2	3	—	3	30	140	20/30
636	2.3	0.5	1	15	2	—	140	15/20
640	0.93	1.0	3	10	2	30	140	17/15
641	0.69	1.2	2	—	3	—	140	35/25
642	0.69	1.2	4	—	5	—	130	25/25
643	0.94	1.0	4	30	5	30	120	25/25

Die Lage der Latenzperioden und Laufzeiten bei den oben beschriebenen Experimenten sind, z.B. in Bezug auf Nr. 627, 628 und 640 aus den Figuren 1, 2 und 3 zu ersehen.

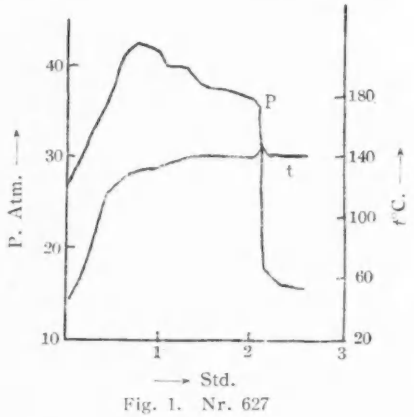

Fig. 1. Nr. 627

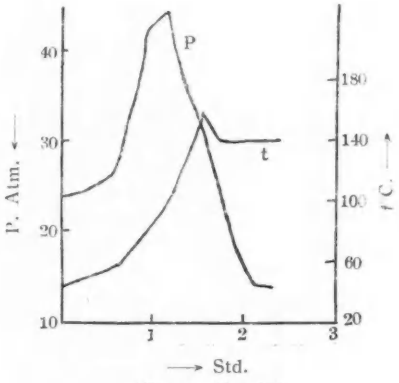

Fig. 2. Nr. 628

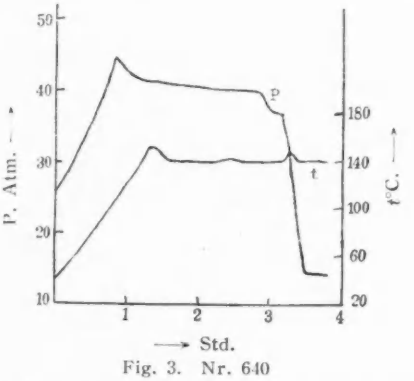

Fig. 3. Nr. 640

c) Über die Nebenreaktionen. — Wenn die eingeleitete Menge von Gasgemisch klein ist, finden die Nebenreaktionen auch in geringem Umfang statt. Mit steigender Gasmenge jedoch werden sie verschieden beobachtet. Abgesehen von der Polymerisation des gebildeten Acrylesters werde ich hier über diese berichten, welche zu dem Reaktionsmechanismus in Beziehung stehen.

1. Nebenprodukte mit niedrigem Siedepunkt. — Man liess das vom Reaktionsprodukt mit Wasserdampf abdestillierte Rohacrylester nach Waschen und Trocknen mit Calciumchlorid abtropfen. 383 g Vorlauf (bis 70°) fraktionierte man als Probe mit Widmer's Kolonne 2 m lang und erhielt die folgenden Resultate.

Die Fraktion 1 enthält eindeutig etwas Acetaldehyd und Äthyläther, welche beide sich von Äthanol herausbildeten. Die Fraktionen 2 und 3, die schwerer als Wasser sind, enthalten noch eine ziemliche Menge Äthyl-

TABELLE VI

FRAKTIONIERUNG VON VORLAUF

Fraktion	Kp. (°C)	Gewicht (g.)	n_D^{20}	Note
1	20— 50	13.3	1.3575	Starker Geruch von CH_3CHO u. $(C_2H_5)_2O$
2	70— 80	29.8	1.4000	Schwerer als Wasser
3	80— 98	103.8	1.3796	Äthylacrylatreich
4	98—100	176.0	1.3990	Reines Äthylacrylat
5	Rest	10.0		

acrylat, das durch Verseifung unter Schütteln mit 2N-Natronlauge bei gewöhnlicher Temperatur grösstenteils beseitigt wird. Von diesen Fraktionen wurde eine Probe als Hauptteil bei der Wiederfraktionierung erhalten, die die physikalischen Eigenschaften, Kp. 73°, n_D^{20}, 1.4980 d_{15}^{20} 1.8158 besass, und deren Jodgehalt 73% analytisch bestimmt wurde. Folglich kann man vermuten, dass der Hauptbestandteil von diesen Fraktionen Äthyliodid (Kp. 72.5°, n_D^{25} 1.5125, d_{15}^{20} 1.9330, Jodgehalt 81.8%) sein dürfte, und dass es sich bei der Acrylesterbildung nebenbei bildet.

Wie es später noch näher beschrieben ist, nimmt die folgende Reaktion eng an dem Mechanismus teil, wodurch das Kohlenoxyd aktiviert wird.

$$NiX_2 + 4CO \longrightarrow Ni(CO)_4 + 2X$$

Die Bildungen solcher Nebenprodukte werden demnach unter Annahme der Wirkungen des Jods in naszierendem Zustand völlig aufgeklärt, d.h., wie folgt;

$$\left.\begin{matrix} CH_3CH_2OH \\ CH_3CH_2OH \end{matrix}\right\} + 2J \longrightarrow \left.\begin{matrix} CH_3CH_2OJ \\ CH_3CH_2J \end{matrix}\right\} \longrightarrow \begin{matrix} CH_3CH_2 \\ CH_3CH_2 \end{matrix}\!\!>\!O + J_2 + H_2O$$

$$J_2 + H_2O \longrightarrow HJ + HJO; \quad C_2H_5OH + HJ \longrightarrow C_2H_5J + H_2O$$

$$C_2H_5OH + HJO \longrightarrow CH_3CHO + H_2O + HJ$$

Die Annahme kann ferner dadurch unterstützt werden, dass die Anwesenheit von Jodwasserstoffsäure im Abgase bei der Acrylester-Synthese durch die Behandlung mit Silbernitratlösung bestätigt wird.

2. Hochsiedende Nebenprodukte. — Am Ende der Wasserdampfdestillation vom Reaktionsprodukt wird das als Wasser schwerere Öl produkt erhalten. Dies siedet bei 78° bis 81° unter vermindertem Druck von 4 mm. Hg. und wird mit der empirischen Formel $C_2H_{3-4}O$ repräsentiert. Behandelt man dies mit konzentriertem wässrigem Ammoniak, so kann man zweierlei kristallinische Substanzen erhalten. Die eine schmilzt bei 242 bis 243° und wird mit der empirischen Formel C_2H_4ON repräsentiert, dementgegen schmilzt die andere bei 262° unter Zersetzung und wird mit der Formel C_2H_3ON benannt. Da die erstere dem Bernsteinsäurediamid ($(CH_2CONH_2)_2$ Smp. 243°) und die letztere dem Fumarsäurediamid ($(CHCONH_2)_2$ Zers. 267°) entspricht, so wird die Anwesenheit von Bernsteinsäure- und Fumarsäurediäthylester in dem ursprünglichen Produkt bestätigt. Ich[6] teilte früher mit meinem Mitarbeiter darüber mit, dass die Bildung von Fumarsäureester ihren Ursprung in der Dehydrierung von Bernsteinsäureester, das sich durch die Anlagerung von Alkohol und Kohlenoxyd an der Doppelbindung von Acrylester bildet, hat. Auch Pino[7] hat jüngst eine derartige Meinung veröffentlicht.

6) K. Yamamoto und K. Sato; Vortrag im Kongress der japanischen chemischen Gesellschaft-Kyuschu-Zweigabteilung am 24. 11. 1950.

Schlusswort

In vorliegender Abhandlung habe ich vorbereitend die Arbeitsmethode und einiges über die Erkenntnis bei der Acrylestersynthese unter der Anwendung vom Nickelhalogenid-Katalysator mitgeteilt, welche alle bei den folgenden Erörterungen über den Mechanismus der Aktivierung des Kohlenoxyds nötig sein dürften.

Herr Dr. K. Yoshikawa hat mich stets bei meinen Arbeiten leitend unterstützt und ermutigt. Herr K. Sato hat mit mir eifrig mitgearbeitet. Und ich spreche diesen Herren und der Mitsui Chemical Industry Co., die mir diese Veröffentlichung meiner Arbeiten erlaubte, hierdurch meinen herzlichen Dank aus.

Mitsui Chemical Industry Co. Ltd.
Miike Dyestuff and Chemical Works.
Omuta, Fukuoka

7) P. Pino, *J. Am. Chem. Soc.*, **74**, 5551 (1952).

Zur Kenntnis über die Hochdrucksynthese von Acrylester. II. Über das Verhalten des unter Druck Stehenden Kohlenoxyds auf das Nickelhalogenid

Von Kazumi YAMAMOTO und Kazutoshi SATO

(Eingegangen am 24. April 1954)

Einleitung

Yamamoto[1] hat in Bezug auf die Acrylestersynthese aus Acetylen, Kohlenoxyd und Alkohol unter der katalytischen Wirkung von Nickelhalogenid mitgeteilt, dass die Reaktion über eine Latenzperiode schnell verläuft, und dass die Aktivität von Nickelhalogenide in einer Reihe Jodid, Bromid, Chlorid stark abfällt, und dass sowohl das Alkylhalogenid als auch der Halogenwasserstoff für Nebenprodukte nachgewiesen werden, usw.

Wir möchten hier über die Beziehung zwischen diesen Erscheinungen und dem Reaktionsmechanismus, insbesondere über das Verhalten des Kohlenoxyds, erwähnen. Wie in Mitteilung I erwähnt, wird die Bildung von Acrylester nach der Cyclopropenon-Hypothese von Reppe künstlich aufgeklärt. Auch die von Bernsteinsäureester kann ebenso dieser Hypothese gemäss einbegriffen werden;

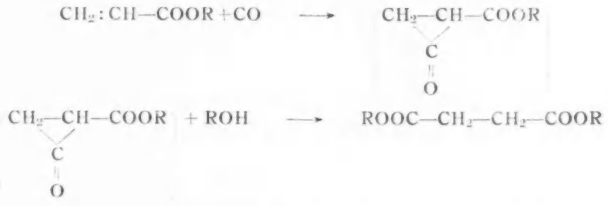

Folglich kommt es darauf an, auf welche Weise das Kohlenoxyd aktiviert wird. Reppe hat, wie schon erwähnt, diesen Mechanismus dadurch erklärt, dass mit Kohlenoxyd zunächst das unbekannte, sehr instabile und deshalb sehr reaktionsfähige $NiCOX_2$ entsteht, das unter Abgabe von aktiviertem Kohlenoxyd wieder als rückgebildetes $NiBr_2$ von neuem mit Kohlenoxyd reagiert.

$$NiX_2 + CO \rightleftarrows CO\text{-}NiX_2$$

Aber der experimentelle Beweis darüber wird nicht gezeigt.

Unsere Arbeiten hatten ihren Ursprung an dem grossen Interesse der "Latenzperiode", die in voriger Mitteilung beschrieben wurde. Als wir während der Latenzperiode den Autoklav schnell abkühlten und dessen Inhalt untersuchten, wiesen wir zufällig eine erhebliche Menge Nickelcarbonyl nach. Demnach führte uns das zu einem Zweifel, dass der wirkliche Katalysator nicht das Nickelhalogenid sein könnte, ja vielmehr Nickelcarbonyl ist. Aus diesem Grunde fassten wir damals die erhebliche Wirkung des Nickelhilfskatalysators oder die Erscheinung der Latenzperiode so auf, dass jene als Akzeptor des von Nickelhalogenid freigemachten Halogens wirken, und die Bildung von echtem Katalysator Nickelcarbonyl erleichtern könnte;

$$NiX_2 + 4CO \longrightarrow Ni(CO)_4 + 2X$$
$$2X + Ni \longrightarrow NiX_2 \qquad Ni(CO)_4 \longrightarrow Ni + 4CO$$

und dass die Latenzperiode die Periode zur Erreicherung einer Konzentration von Nickelcarbonyl sein könnte. Dann haben wir es experimentell feststellen wollen. Diese Arbeiten werden hauptsächlich in vier Klassen eingeteillt, d.h.:

1) Die Bildung von Nickelcarbonyl aus den verschiedenen Nickelverbindungen.
2) Die Bildung von Nickelcarbonyl aus den Nickelhalogeniden in Anwesenheit von dem Zusatzmetell.
3) Der Zusammenhang zwischen der Acrylestersynthese und den oben erwähnten Faktoren.
4) Die Ätzung von dem Reaktionsgefäss.

Reaktion verschiedener Nickelverbindungen mit Kohlenoxyd in Anwessenheit von Alkohol

Nimmt man an, dass Nickelcarbonyl, das mit Acetylen und Alkohol reagiert, durch die Einwirkung von Kohlenoxyd auf das Nickelhalogenid in Alkohol gebildet wird, so

1) K. Yamamoto, Dieses Bulletin, **27**, 491 (1954).

müsste es ein wichtiger Leitfaden zur Lösung vom Mechanismus sein, die Neigung des Nickelcarbonylbildungsbestrebens der Nickelverbindungen zu erkennen.

Das Experiment wurde wie folgt durchgeführt. Man zog 30 cm^3 Äthanol und einige Gramm Nickelverbindung in das Druckgefäss von 130 cm^3 Inhalt (18:8-Stahl) hinzu und erwärmte es nach der Einpressung von Kohlenoxyd (Anfangsdruck 70 Atm). Dieser Kohlenoxyddruck war zwar höher im Vergleich mit dessen Teildruck bei der Acrylestersynthese, aber es dürfte unter Berücksichtigung folgender Sachen zweckmässiger sein:

1) Unterdrückung vom Zerlegen des gebildeten Nickelcarbonyls der erhöhten Temperatur wegen.
2) Vergrösserung vom Reaktionsverlauf.
3) Im Falle der Acrylestersynthese gibt es den Akzeptor von Nickelcarbonyl.

Im Experiment wurde die qualitative Beobachtung gemacht, und die Ausbeute von Nickelcarbonyl vom Unterschied zwischen dem Anfangs-und Enddruck vom Kohlenoxyd berechnet. Man liess den Autoklav langsam erwärmen und hielt die Temperatur, wobei der Druckabfall stattzufinden begann. Als der Druckabfall sehr langsam wurde, steigerte die Temperatur sich wieder. Auf solche Weise beobachtete man den Verlauf der Hauptreaktionstemperatur, der als Kennzeichnung der Reaktionsfähigkeit der Nickelverbindung von Bedeutung wäre. Die Resultate sind in der Tabelle I gezeigt.

TABELLE I

NICKELCARBONYL AUS NICKELVERBINDUNGEN

Nr.	Ni-Verbg. (g)	Reaktionstemp. in°		Laufzeit		$Ni(CO)_4$ (%)	Aufgelös. Fe
		Haupt.	Max.	(Std)	(Min)		
C-12	Ni 6 auf Kiesg.	Raumtemp.	155	4	10	78	+
C-13	Ni 4 auf Kiesg. $(NH_4)_2S$ aq. 0.5	,,	110	1	45	83	+
C-14	NiS 6 $(NH_4)_2S$ aq. 0.5	90–110	170	4	45	24	
C-30	$NiCl_2$6 $(NH_4)_2S$ aq. 0.5	120–150	160	6	—	10	++
C-17	$NiJ_2$10	120–150	180	3	30	100	+++
C-29	Ni-Acetat 8	—	190	2	30	—	
C-31	$NiCl_2$ 5.7	120–150	210	2	30	78	+++

Note: Die letzte Spalte stellt die aufgelöste Eisenmenge qualitativ dar.

Das in den Experimenten Nr. C-12 und C-13 benutzte Nickel ist eben ein und dasselbe, welches als Hilfskatalysator bei der Acrylestersynthese angewandt wurde. Folglich würde vermutlich bei der Acrylestersynthese trotz des niedrigen Teildrucks von Kohlenoxyd eine ziemliche Menge Nickelcarbonyl daraus gebildet werden. Als Eigentümlichkeit der Nickelhalogeniden wie C-17 und C-31 kann man folgendes erörtern:

1) Erhebliche Menge Eisenion ist nachweisbar.
2) Ausser dem Nickelcarbonyl bildet sich die flüchtige Substanz Eisenpentacarbonyl, dessen Nachweis mit der wässrigen Lösung von Sublimat[2] durchgeführt wird.

Da die Quelle von diesem Eisen nichts anderes als die Gefässwand ist, könnte dies als Resultat der folgenden Reaktion aufgeklärt werden;

$$NiX_2 + 4CO + Fe \longrightarrow Ni(CO)_4 + FeX_2$$
(Gefässwand)

Eisenhalogenid löst sich in Alkohol und dadurch wird die folgende Ätzung der Gefässwand erleichtert. Die Bildung von Eisenpentacarbonyl dürfte gleich mit der des Nickelcarbonyls sein;

$$FeX_2 + 5CO \longrightarrow Fe(CO)_5 + 2X$$

Dies ergibt die Auflösung von 0.05 bis 0.2% Eisen bei der Acrylestersynthese.

Bildung von Nickelcarbonyl in Anwesenheit von verschiedenen Beimetallen oder verschiedener Verbindung

Von den Resultaten voriger Paragraphen wird vermutet, dass die Bildung von Nickelcarbonyl weitaus leichter wird, wenn das mit dem von Nickelhalogenid freigemachten Halogenatomen leicht zu verbindende Metallpulver hinzugefügt wird. Die unter dieser Annahme durchgeführten Resultate sind in der Tabelle II zusammengefasst.

2) H. Hock u.a., *Ber.*, **61**, 2037 (1928).

TABELLE II

NICKELCARBONYL AUS HALOGENIDEN

Nr.	NiX_2 (g)	Anlage (g)	Reaktionstemp. Haupt.	Reaktionstemp. Max.	Laufzeit (Std)	Laufzeit (Min)	$Ni(CO)_4$ (%)	Gelös. Fe	Note
C-17	NiJ2 10	—	120–150	180	3	30	100	+++	
C-20	,,	Cu 4	Raumtemp.	150	2	30	77		CuJ-Bild.
C-22	,,	Hg_2O 5	,,	180	2	00	39		HgJ_2– ,,
C-31	$NiCl_2$ 5.7	—	120–150	180	2	30	78	+++	
C-23	,,	Cu 4	60–130	142	2	10	43	+	
C-25	,,	Al 2	60–160	178	2	10	34	++	

Note: Jede Anlage kam im Überschuss zur Verwendung. Die Ausbeute von Nickelcarbonyl wurde von dem Druckabfall berechnet.

Wie vermutet erschienen die Effekte der Anlage im Fall des Nickeljodids eindeutig als Erniedrigung der Reaktionstemperatur und Verminderung der Ätzung von der Gefässwand. Bei dem Chlorid war die Lage analog, wenn der auch Grad niedrig gewesen ist. Dies zeigt, dass der Unterschied zwischen dem Jodid und Chlorid in der Bindung Nickel-Halogen sehr wesentlich ist, d.h., bei dem Jodid ist die Bindung mehr nichtionisch als bei dem Chlorid. Der Unterschied ist mit dem der katalytischen Wirkung in der Ordnung analog. Folglich deutet dies auf eine Richtung zur Forschung von neuem Katalysator. Die anfängliche Erwartung war, dass der wesentliche Katalysator bei der Acrylestersynthese nicht das Nickelhalogenid sein könnte, sondern Nickelcarbonyl. Den Fall gesetzt, dass man Nickeljodid mit dem Beimetall wie Cu, Hg, Ag oder Zn verwendet, so könnte unter der Bildung von Nickelcarbonyl die Acrylestersynthese erleichtert werden. Dieses trat nicht ein sondern darüber hinaus wurde die Bildung von Acrylester bei der Verwendung von Nickelcarbonyl vielmehr erschwert. Es bedeutet dies, welche wichtige Rolle die Halogenatome spielen, denn das Beimetall wie Cu nimmt unter der starken Verbindung mit dem Halogenatom dessen Funktion fort.

Beziehung zwischen dem Beimetall und der Ätzung von Gefässwand

Wie schon nach Hieber[3] in Bezug auf die Kobaltverbindung beschrieben, wird die Reaktion von Nickelhalogenid mit Kohlenoxyd in Anwesenheit vom Beimetall im Sinne der Gleichungen dargestellt:

$$NiX_2+4CO \longrightarrow Ni(CO)_4+X_2+Q_1 \quad (1)$$

$$M+X_2 \longrightarrow MX_2+Q_2 \quad (2)$$

wobei das Beimetall M mit der grösseren Wärmetönung Q_2 fester mit den Halogenatomen verbindet, sodass es die Reaktion (1) leicht nach rechts dringen lässt.

Die betreffenden Werte sind hinsichtlich der Jodide und Chloride in den Literaturen wie folgt veröffentlicht:

Jodid	Mg	Zn	Hg	Al	Cu	Fe	Ni
Q_2 in kcal./mol.	84.8	49.8	47.8	44.0	32.2	30.1	23.0
Chlorid	Mg	Al	Zn	Fe	Ni	Cu	Hg
Q_2 in kcal./mol.	151.0	111.3	98.4	82.1	74.5	65.2	61.8

In der obigen Tabelle wechselt die Zusammensetzung der Metalle bei Jodide mit denen von Chloride. Demnach sollten die Zustände der Ätzung von der Gefässwand zwischen der Reaktion von Nickeljodid mit Kohlenoxyd in Anwesenheit von solchen Beimetallen wie Cu oder Hg, entgegengesetzt von denen wie Nickelchlorid unter den gleichen Bedingungen, gehen. Die Folgenden experimentellen Resultate stellen dies dar. In den Tabellen III und IV sind die Bedingungen zur Bildung von Nickelcarbonyl aus Nickelchlorid und Jodid in Anwesenheit von Beimetall gezeigt.

Diese Experimente wurden mehr quantitativ durchgeführt als die in der Tabelle II gezeigten. Die Ausbeuten wurden auf Grund von dem verbrauchten Nickelhalogenid berechnet. Auf solche Weise wurde der Wert von Nr. C-25 in der Tabelle II durch den von C-36 in der Tabelle III korrigiert. Wie aus dem Vergleich der Werte in C-41 und 42 ersehen, ist die Korngrösse von dem Beimetall bemerkenswert. Wenn man das feine Magnesiumpulver wie Korngrösse (c) unter der Berücksichtigung dieser Umstände benutzt, so würde man den grössten Erfolg haben. Dies zeigt, dass sowohl die Ätzung der Gefässwand als auch das Gebiet der Hauptreaktionstemperatur von der Bildungswärme Q_2 beherrscht wird. Ferner ist von dem Resultat in C-49, unter Verwendung

3) W. Hieber, *Z. anorg. allg. Chem.*, **243**, 145 (1939).

TABELLE III

NICKELCARBONYL AUS CHLORID

Nr.	Beimetall (Korngrösse)	Reaktionstemp. (°C)	Laufzeit (Std)	Laufzeit (Min)	Gelöst. Fe (g)	Unreag. $NiCl_2$ als Ni (g)	$Ni(CO)_4$ (%)
C-35	Hg	130–140	2	30	0.35	0.20	87
C-36	Al (c)	16– 70	1	30	0.04	0.00	100*
C-37	Cu (c)	80–120	5	20	0.39	0.47	70
C-41	Mg (a)	70–130	3	20	0.00	0.24	85*
C-38	Zn (c)	65– 80	2	10	0.03	0.33	79
C-42	Zn (b)	75– 85	3	50	0.04	0.26	83

Note: $NiCl_2$ 5.7 g Äthanol 30 cm³ CO-Anfangsdruck 70 Atm. Beimetallmenge etwas Überschuss. Korngrösse (a) ca. 20 Mesch, (b) ca. 50 Mesch und (c) ca. 100—200 Mesch. * Alkoholatbildung.

TABELLE IV

NICKELCARBONYL AUS JODID

Nr.	Beimetall (Korngrösse)	Reaktionstemp. (°C)	Laufzeit (Std)	Laufzeit (Min)	Gelöst. Fe (g)	Unreag. NiJ_2 als Ni (g)	$Ni(CO)_4$ (%)
C-43	Hg	90–100	2	00	0.03	0.51	73
C-46	Zn (c)	20– 50	3	00	Spur	0.06	96
C-20	Cu (c)	20–100	2	30	Spur	—	90
C-48	Ni (c)	20–100	6	00	0.37	0.11	95
C-49	Ni (b)	90–100	5	30	0.36	0.05	98

Note: NiJ_2 6.9 g Äthanol 30 cm³.

eines üblichen Nickelpulvers denkbar, dass die Hilfskatalysatorwirkung von Nickel wie anderer Beimetalle, bei der Acrylestersyntese, durch die Wirkung als Akzeptor für freigemachte Halogenatome sein kann.

$$NiJ_2 + 4CO + Ni^* \longrightarrow Ni(CO)_4 + Ni^*J_2$$

Wir sind demnach zum Schluss gelangt, dass das als Hilfskatalysator benutzte Nickel besonders in dem reduzierten, aktiven Zustand nicht zu sein braucht, sondern in der körnigen oder geschnittenen Form auch verwendbar ist.

Lebensdauer von Katalysator und Ätzung von Gefässwand

Wir dachten zuerst die Ätzung der Gefässwand hätte ihren Ursprung in der Bildung von Eisenpentacarbonyl, das sich durch die Einwirkung von Kohlenoxyd unter Druck auf die Gefässwand bildet. Daraufhin wurde Äthanol mit Kohlenoxyd unter 100 Atm Druck bei 150° zwei Stunden lang erhitzt, aber die Bildung von Eisencarbonyl konnte nicht beobachtet werden. Unter Berücksichtigung der Einwirkung von Jod im Molekularzustand wurde die alkoholische Lösung von Jod unter der gleichen Bedingung behandelt, jedoch die Auflösung von Eisen wurde gleichfalls nicht beobachtet, sondern nur die Bildung von Äther. Wir können also nicht umhin anzunehmen, dass die Ätzung ihren Ursprung hauptsächlich in der Einwirkung von Jod in dem naszierenden Zustand hat.

Eisenpentacarbonyl, dessen Anwesenheit durch die Reaktion mit der wässrigen Lösung von Sublimat[2] festgestellt ist, wird sich durch die Reaktion zwischen dem Eisenjodid und dem unter Hochdruck stehenden Kohlenoxyd bilden. Die Auflösung von Eisen bringt nicht nur die Ätzung von Autoklav bei der Acrylestersynthese, sondern gibt auch den Anlass von dem Verlust des Katalysators.

Auch der Zusatz von Nickelpulver kann die Auflösung von Eisen nicht hemmen, wird leicht davon verstanden werden, und wie aus der Tabelle III hervorgeht, ist die Bildungswärme von FeX_2 grösser als die von NiX_2. Wenn man auf Grund der in vorigem Paragraphen beschriebenen Schlussfolgerung, das Reaktionsgefäss mit Nickel bekleidet oder plattiert, so kann man das Hindernis der Ätzung und die Vergrösserung der Reaktionsgeschwindigkeit darauf erwarten. Das Experiment hatte dieses Ergebnis.

In 100 cm³ Inhalt Autoklav, der dicht vernickelt wurde, setzten wir 24 g Äthanol und 0.12 g Nickeljodid ein und erhitzten dieses Gemisch auf 150 bis 160° unter 30 Atm Druck vom Acetylen-Kohlenoxyd-Gasgemisch. Wir beobachteten dabei den sehr glatten Reaktionsverlauf.

Die starke kondensierende Wirkung des

gebildeten FeJ_2 oder FeJ_3 gibt einen Anlass für die nicht wünschenswerte Polymerisation oder Kondensation von Acetylen oder Acrylester.

Zum Beispiel, wenn die Reaktion in Anwesenheit von Nickelchlorid und Aluminium durchgeführt wird, ist die Bildung von dem harzartigen Produkt wunderbar. Somit wird aufgeklärt, dass die Auskleidung von Autoklav mit Nickel zur Verbesserung der Ausbeute von Acrylester beiträgt[4].

Betrachtungen über die Rolle der Halogenatome in NiX_2

Es wurde bisher beschrieben, dass das Nickelcarbonyl selbst als Katalysator für die Acrylestersynthese nicht genügend ist und dass die Halogenatome dabei eine wichtige Rolle spielen. Dies wurde auch durch das folgende Experiment gezeigt, welches diskontinuierlich im 270 cm^3 Inhalt Autoklav in Anwesenheit von Nickeljodid und Kupfer durchgeführt wurde. Die Resultate sind in der Tabelle V zusammengefasst.

TABELLE V

ACRYLAT-SYNTHESE MIT NiJ_2 UND Cu

Äthanol (g)	NiJ_2 (g)	Cu* (g)	Druck von Gasgemisch	Reaktionstemp. (°C)	Laufzeit (Std)	Laufzeit (Min)	Restdruck Atm
40	2	0	35 at.	160	2	30	0
40	2	1.0	35	150–180	6	40	26.5
40	2	1.0	35	150–180	14	00	25
40	2	0.3	35	160–200	7	00	21

* Die dem Jod in 2 g. NiJ_2 entsprechende Kupfermenge ist 0.4 g.

Mit Anwesenheit von Kupfer wurde die Bildung von Acrylat trotz der Bildung von Nickelcarbonyl beinahe nicht beobachtet.

Die Hinzufügung aber des metalischen Nickels erleichtert die Bildung von Acrylester. Von diesen Tatsachen könnte man erwarten, dass die Erniedrigung der zur Bildung des Cyclopropenons erforderlichen Aktivierungsenergie durch die Bildung irgendeines intermediären Zwischenproduktes erreicht wird, welches sich durch die Umsetzung von Kohlenoxyd und Nickelhalogenid, bevor das Nickelcarbonyl zusammengesetzt wird, bildet und dass das Halogenatom des Nickelhalogenids die wichtige Rolle spielen sollte, mit anderen Worten, dass das Halogenatom vom Nickelhalogenid nicht weggenommen werden müsste. Hierauf möchten wir etwas über die Latenzperiode ausführen. Während der Latenzperiode bei der Acrylestersynthese wurde das Nickelcarbonyl zufällig im Reaktionsgefäss gefunden, und wie schon gezeigt, liess uns diese Beobachtung eine Reihe der Arbeiten ausführen. Jedoch wurde es klar in den Arbeitungsvorgängen, dass die Latenzperiode nicht gerade mit der Bildung des Nickelcarbonyls zusammenhängt, sondern sie hauptsächlich von dem Sauerstoffgehalt im Gasgemisch abhängig ist, d.h., während sie in Abwesenheit von Sauerstoff kaum auftritt, beträgt sie 1 Stunde in Anwesenheit von 0.2% und 1.5 Stunden bei 0.3% bzw. unter den gleichen Bedingungen. Da Nickeljodid durch Sauerstoff unter der Abscheidung von Jod leicht oxydiert wird, so wird die Latenzperiode dargestellt als die beanspruchte Zeit bis zum Verschwinden des abgeschiedenen Jods unter der Umsetzung mit dem Alkohol oder mit der Gefässwand. Auch die Verkürzung der Latenzperiode durch die Hinzufügung von Nickel oder die Steigerung von der Temperatur wird dadurch erläutert. Zur Illustration des Schlusses kann man die folgende Beobachtung anführen. Fügt man absichtlich freies Jod und Eisenpulver ins Reaktionensystem hinzu, so kann man beobachten, dass die Reaktion erst nach der langen Latenzperiode stattfindet.

Selbst eine Nickelverbindung wie Borat, Formiat, Phosphat, Dimethylglyoxymnickel oder Acetoessigsäureester-Nickel als Katalysator für die Acrylestersynthese ist nicht erwünscht. Von den bisher erwähnten Tatsachen zieht man den Schluss, dass die aus Nickel und solchen negativen Atomen oder Atomgruppen zusammengesetzten Verbindungen als Hauptkatalysator gelten, wie sie sich mit dem Nickel nichtionisch verbinden und das Metall leicht angreifen können. Als solche Atome order Atomgruppen kann eine Reihe sogenannter Pseudohalogene von Birkenbach[5] angegeben werden. Deren elektrische Negativität nach folgender Reihe angeordnet sind:

F, CNO, Cl, N_3, Br, CN, SCN, J, SeCN.

Aus dem Resultat der Acrylestersynthese, welches in Anwesenheit von dem nach Grossmans Verfahren[6] hergestellten Nickelthio-

4) K. Yamamoto und K. Sato, *J.P.*, 197, 084.

5) L. Birkenbach, *Ber.*, **58**, 2377 (1925).

6) H. Grossman, *Ber.*, **37**, 565 (1904).

cyanat erfolgte, wurde wie in obiger Reihe vermutet, festgestellt, dass dessen katalytische Fähigkeit, abgesehen von der polymerisierenden Einwirkung, zwischen Nickelbromid und Jodid gestellt wird.[7]

Yatsimirskii[8] hat den Beteiligungsgrad von dem ionischen Charakter in der Bindung zwischen Nickel und Halogenatom wie folgt berechnet:

$NiCl_2$ 53%, $NiBr_2$ 48%, $Ni(SCN)_2$ 45%, NiJ_2 39%

Dies unterstützte auch unsere Meinung.

Zusammenfassung

In der vorliegenden Mitteilung wurde das Verhalten des unter Druck stehenden Kohlenoxyds gegen das Nickelhalogenid in Alkohol in Anwesenheit von den verschiedenen Beimetallen oder anderen Anlagen beschrieben. Zugleich wurde die Rolle des Halogenatoms von Nickel halogenid bei der Acrylestersynthese erörtert, von dem Gesichtspunkt der Ätzung der Gefässwand sowohl, als auch der Lebensdauer des Katalysators aus gesehen.

Darüber hinaus haben wir von diesen experimentellen Resultaten geschlossen, dass die katalytische Fähigkeit der Nickelhalogenide von dem Beteiligungsgrad des ionischen Charakters der Bindung zwischen dem Nickel- und Halogenatom abhängig ist.

Herr Dr. K. Yoshikawa hat uns stets bei unseren Arbeiten leitend unterstützt und ermutigt. Wir sprechen ihm und der Mitsui Chemical Industry Co. Ltd., die uns die Veröffentlichung dieser Arbeiten erlaubte, unseren herzlichen Dank aus.

Diese Arbeiten wurden am 24. 11. 1950 in Kumamoto im Rahmen des Kongresses der japanischen chemischen Gesellschaft — Kyushu — Zweigabteilung mündlich veröffentlicht.

Mitsui Chemical Industry Co. Ltd.
Miike Dyestuff and Chemical Works,
Omuta, Fukuoka

7) K. Yamamoto und K. Sato, *J.P.*, 197, 083.
8) K. B. Yatsimirskii, *Izvest. Akad. Nauk USSR.*, 590 (1948), *C.A.*, **43**, 2329 (1949).

Zur Kenntnis über die Hochdrucksynthese von Acrylester III. Zur Kenntnis über die Herstellung von Triphenylphosphin-Nickelkomplex Verbindungen

Von Kazumi YAMAMOTO

(Eingegangen am 24. April 1954)

Einleitung

In den bisherigen Mitteilungen[1] wurde das Verhalten des unter Druck stehenden Kohlenoxyds an Nickelhalogenid Katalysator erörtert. In der vorliegenden Mitteilung sind die Herstellungsverfahren der Triphenylphosphin-Nickelhalogenid-Komplexverbindungen beschrieben, die von Reppe[2] als Katalysator bei der Acrylatsynthese gefunden wurden. Diese Verbindungen, die in der ausgezeichneten Weise allen Anforderungen, z. B. kleine Nebenreaktion, lange Lebensdauer, leichte Zurückgewinnbarkeit wegen deren guter Kristallisierbarkeit, entsprachen, werden im allgemeinen in folgende vier Klassen eingeteilt:

1. $(Ph_3P)_xNi(CO)_{4-x}$
2. $(Ph_3P)_2NiX_2$
3. $(Ph_3P)_2NiX_2RX'$
4. $(Ph_3P)_2NiX_22RX'$

wobei Ph den Phenylrest (C_6H_5)- ausdrückt und x im allgemeinen 1 oder 2, R die Alkyl- oder Arylgruppe, und X und X' dasselbe oder verschiedene Halogenatom ausdrücken.

Über die Aufklärung des Mechanismus der Aktivierung des Kohlenoxyds könnte ich nur die in Copenhaverschem Buch[3] angeführte Annahme von Schweckendiek, der der Mitarbeiter von Reppe ist, und die von McKinley[4] angeben. Wie später ausführlich behandelt, dürfte die erstere einen Widerspruch enthalten und die letztere ginge nur von dem Rahmen des Gedankens nicht aus.

Ich habe darüber einen Erfolg aufgrund der zusammenfassenden Resultate betreffs der Verfahren zur Herstellung, und der chemischen, physikalischen Eigenschaften von Kom-

1) K. Yamamoto, Dieses Bulletin, **27**, 491, 496 (1954).
2) W. Reppe, "Neue Entwicklungen auf dem Gebiet der Chemie des Acetylens und Kohlenoxyds", Springer Verlag (1949) S. 103.
3) Copenhaver und M. Bigelow, "Acetylene and Carbonmonoxide Chemistry", Rheinhold Publ. Co. (1949) S. 259.
4) C. McKinley, *Ind. Eng. Chem.*, **44**, 995 (1952).

plexverbindungen und betreffs deren Verhalten bei der Acrylestersynthese zu verzeichnen.

Herstellung von Triphenylphosphin.—Triphenylphosphin, das der Grundstoff ist, wurde durch das Verfahren von Michaelis[5] aus Natrium, Chlorbenzol und Phosphortrichlorid hergestellt.

$$3C_6H_5Cl+6Na+PCl_3 \rightarrow 6NaCl+(C_6H_5)_3P$$

Nach Michaelis wird es unter Anwendung von Äther als Lösungsmittel durch Erhitzen bei dessen Kochpunkt 48 Stunden lang mit der Ausbeute von 30% der Theorie auf Grund von Chlorbenzol erhalten. Auch wurde mitgeteilt, dass die Bildung vom harzartigen Produkt erheblich war, wenn Benzol an statt Äthers verwendet wurde. Ich habe es aber dadurch in Benzol mit der Ausbeute von 50 bis 60% erhalten können[6], weil ich die Reaktion bei 60°, 6 Stunden lang in Anwesenheit vom Katalysator wie Äthylacetat, -Malonat, -Acetacetat durchführte.

Herstellung von $(Ph_3P)_xNi(CO)_{4-x}$.—Die Komplexverbindungen dieses Typus sind unmittelbar nicht wichtig für Katalysator bei der Acrylestersynthese und sie nützen zur cyclisierenden Polymerisation des Acetylens[7], aber ich möchte deren Herstellungsveafahren kurz darstellen, da es mit der Herstellung der Komplexverbindungen von $(Ph_3P)_2NiX_2$ und mit dem Mechanismus in Beziehung steht.

Wenn man Triphenylphosphin in Methanol auf Nickelcarbonyl einwirken lässt, so kann man Triphenylphosphin-Nickeltricarbonyl oder Bistriphenylphosphin-Nickeldicarbonyl bei 20° bzw. 50° erhalten:

$$Ph_3P+Ni(CO)_4 \xrightarrow[\text{Zp. } 123^\circ]{20^\circ} Ph_3PNi(CO)_3+CO$$

$$2Ph_3P+Ni(CO)_4 \xrightarrow[\text{Smp. } 206\text{–}9^\circ]{50^\circ} (Ph_3P)_2Ni(CO)_2+2CO$$

Anstatt des Triphenylphosphins kann man die Komplexverbindung von Triphenylphosphin mit Schwermetallhalogenid verwenden, z. B.;

$$(Ph_3P)_2ZnCl_2+2Ni(CO)_4 \rightarrow 2Ph_3PNi(CO)_3+2CO+ZnCl_2$$

$$(Ph_3P)_2ZnCl_2+Ni(CO)_4 \rightarrow (Ph_3P)_2Ni(CO)_2+2CO+ZnCl_2$$

In diesen Verfahren muss man sehr giftiges Nickelcarbonyl verwenden. Ich habe diese Verbindung dadurch quantitativ herstellen können[8], weil ich Triphenylphosphin und reduziertes Nickelpulver in Methanol bei 150° mit Kohlenoxyd unter Druck von 50 Atm unmittelbar behandelte:

$$2Ph_3P+Ni+2CO \rightarrow (Ph_3P)_2Ni(CO)_2$$

Herstellung von $(Ph_3P)_2NiX_2$.—Reppe hat die folgenden drei Verfahren zur Herstellung der Komplexverbindung von Typus $(Ph_3P)_2NiX_2$ veröffentlicht. Zwei derselben[7] bringen das oben beschriebene Bistriphenylphosphin-Nickeldicarbonyl als Ausgangsstoff zur Verwendung und das andere ist das Verfahren, wodurch die Komplexverbindung aus dessen Bestandteile aufgebaut wird[9].

1. $(Ph_3P)_2Ni(CO)_2+2C_4H_9X+2C_4H_9OH \rightarrow (Ph_3P)_2NiX_2+2C_4H_9COOC_4H_9+H_2$
2. $(Ph_3P)_2Ni(CO)_2+X_2 \rightarrow (Ph_3P)_2NiX_2+2CO$
3. $2Ph_3P+NiX_2 \rightarrow (Ph_3P)_2NiX_2$

Das Verfahren (1) muss im Druckgefäss bei 180° durchgeführt werden, darüber kann die Beimengung von der Komplexverbindung $(Ph_3P)_2NiX_2RX$ nicht vermieden werden. Das Verfahren (2) kann in Benzol bei der gewöhnlichen Temperatur durchgeführt werden. Aber es ist wegen der Bildung von dem harzartigen Nebenprodukt schwierig, den reinen Kristall zu erhalten. Beim Verfahren (3) wird die Komplexverbindung dadurch hergestellt, dass man Nickelhalogenid in das bei 280° geschmolzene Triphenylphosphin unter der Rührung hinzufügt und dann das Reaktionsgemisch schnell abkühlt. Dieses Verfahren ist infolge der thermischen Zersetzung desselben kein gutes, wie in der folgenden Mitteilung erwähnt wird.

Jensen[10] hat darüber mitgeteilt, dass Bistriäthylphosphin-Nickelchlorid aus Triäthylphosphin und Nickelchlorid in Äthanol bei der gewöhnlichen Temperatur hergestellt wurde aber keinen Triphenylphosphinabkömmling ergab. Dementgegen habe ich gefunden, dass diese Komplexverbindung aus dessen Bestandteil durch Erhitzung in Äthanol oder Butanol unter dem Rückfluss beinahe quantitativ erhalten werden kann. Ich habe die bisher nicht veröffentlichte Verbindung nach dieser Methode dargestellt (Tabelle I).

5) A. Michaelis, *Ann.*, **229**, 295 (1885).
6) K. Yamamoto und S. Kunisaki, *J.P.*, 200, 535.
7) W. Reppe und W. J. Schweckeudiek, *Ann.*, **560**, 104 (1948).
8) K. Yamamoto und M. Oku, Dieses Bulletin **27**, 383 (1954).
9) W. Reppe, *F.P.* 961.010, *C.A.*, **46**, 5617 (1952).
10) K. Jensen, *Z. anorg. allg. Chem.*, **229**, 273 (1936).

Tabelle I

Komplexverbindungen $(Ph_3P)_2NiX_2$

Verbindung	Farbe	Smp. in (°C)	P—Gehalt in % Gef.	Ber.
$(Ph_3P)_2NiBr_2$	Intensivgrün	221–22*	8.40	8.36
$(Ph_3P)_2NiCl_2$	Dunkelblau	205–6 **	9.51	9.48
$(Ph_3P)_2NiJ_2$	Violettbraun	225	7.38	7.42

* Nach Reppe[7] 223°. ** Nach Reppe[11] zähe Flüssigkeit.

Diese Verbindungen sind löslich in Aceton, Alkohol und Benzol und nicht in Äther. In der Lösung gibt es Dissoziationsgleichgewicht;

$$(Ph_3P)_2NiX_2 \rightleftarrows 2Ph_3P+NiX_2$$

insbesondere in Methanol ist das Gleichgewicht von links nach rechts bemerkenswert abweichend. Darüber will ich später noch näher beschreiben.

Herstellung von $(Ph_3P)_2NiX_2RX'$.—Reppe[7] hat drei Verfahren zur Herstellung von den Komplexverbindungen dieses Typus, die als Katalysator bei der Acrylestersynthese am wichtigsten sind, veröffentlicht:

1) $(Ph_3P)_2NiX_2+RX' \rightarrow (Ph_3P)_2NiX_2RX'$
2) $(Ph_3P)_2Ni(CO)_2+3RX+2ROH \rightarrow (Ph_3P)_2NiX_2RX+2RCOOR+H_2$
3) $(Ph_3RP)X'+NiX_2+Ph_3P \rightarrow (Ph_3P)_2NiX_2RX'$

In welchem Verfahren es auch sei, verläuft die Umsetzung in Anwesenheit von Alkohol wie Butanol bei 120 bis 200°. Beim Verfahren (1) kann man anstatt des $(Ph_3P)_2NiX_2$ dessen Bestandteile, d.h., Triphenylphosphin und Nickelhalogenid, verwenden[12].

Ich habe ein anderes Verfahren gefunden,[13] in dem das Halogen zusammen mit dem aus Alkylreste bestehenden Alkohol, der dem betreffenden Alkylhalogenid entsprechend ist, anstatt des Alkylhalogenids, verwendet wird. Die Umsetzung verläuft auch in diesem Falle im eingeschlossenen Rohre bei 150 bis 180° und im Endeffekt im Sinne der Gleichung quantitativ.

$$4(Ph_3P)_2NiX_2+6C_nH_{2n+1}OH+2X'_2 \rightarrow 4(Ph_3P)_2NiX_2C_nH_{2+1}X' + C_nH_{2n-1}COOC_nH_{2n+1}+4H_2O$$

Ich soll hier beschreiben, wie diese Umsetzung, die später erwähnt wird, im Zusammenhang mit der katalytischen Wirkung von der Komplexverbindung Typus $(Ph_3P)_2NiX_2$ eine Bedeutung hat.

Ich habe die bisher unveröffentlichten Komplexverbindungen dieses Typus dargestellt und in der Tabelle II zusammengefasst.

Tabelle II

Komplexverbindungen $(Ph_3P)_2NiX_2RX'$

Verbindung	Farbe	Smp. in (°C)	P-Gehalt in % Gef.	Ber.	Bemerk.
$(Ph_3P)_2NiBr_2C_2H_5Br$	Grün	162	7.15	7.28	
$(Ph_3P)_2NiBr_2C_2H_5J$	Violettbraun	160	6.98	6.90	
$(Ph_3P)_2NiBr_2C_4H_9Br$	Blaugrün	178*	6.98	7.04	*Reppe[7] 178°
$(Ph_3P)_2NiBr_2isoC_4H_9Br$	Blaugrün	167	6.90	7.04	
$(Ph_3P)_2NiBr_2C_4H_9Cl$	Hellblau	167–8	7.42	7.45	
$(Ph_3P)_2NiCl_2C_4H_9Br$	Hellblaugrün	167*	7.81	7.84	*Reppe[7] 148–50°
$(Ph_3P)_2NiCl_2C_4H_9Cl$	Blau	176	8.25	8.30	
$(Ph_3P)_2NiBr_2C_4H_9J$	Violettbraun	125	6.71	6.70	
$(Ph_3P)_2NiJ_2C_4H_9J$	Violettbraun	167–8	6.12	6.07	
$(Ph_3P)_2NiBr_2C_5H_5Cl$	Grün	203–5	7.09	7.26	
$(Ph_3P)_2NiBr_2C_5H_5Br$	Aschgrün	210	6.90	6.89	
$(Ph_3P)_2NiBr_2C_7H_7Br$	Gelbgrün	186	6.90	6.97	

Diese Komplexverbindungen sind in Aceton, und Alkohol löslich, dagegen schwer in Benzol und garnicht in Äther. Ich habe die folgende Regelmässigkeit von dem Verhalten dieser Verbindungen gegen Alkohol gefunden, in dem Falle, wenn R Alkyl ist:

1) Gegen gleichen Alkohol ist die Verbindung desto beständiger, je niedriger der Alkylrest in ihr ist.
2) Die eine Verbindung ist desto beständiger gegen Alkohol je höher er ist.

Über das Verhalten gegen Methanol und über die Bedeutung der Beständigkeit soll ich anderweitig noch eingehender sprechen. Darüber bietet die alkoholische Lösung der

11) s. 3) S. 298.
12) K. Yamamoto, H. Izawa und M. Oku, *J.P.* ausgelegt 1952-5625.
13) K. Yamamoto, M. Oku und M. Tanaka, *J.P.* ausgelegt 1952-5173.

Komplexverbindung das sehr charakteristische Verhalten, dass sie bei der Heizung die intensiv eigentümliche Farbe behält, aber beim Erkalten verliert.

Herstellung von $(Ph_3P)_2NiX_2 2RX'$.—Betreffs des Verfahrens zur Herstellung dieser Verbindungen gibt es keine Beschreibung. Wenn man jedoch darauf das Verfahren, nach der in vorigem Paragraph beschriebenen Methode (1) gemäss unter der Anwendung von überschüssigem Alkylhalogenid durchführt, kann man nichts weiter erhalten, als die Komplexverbindung mit einem Molekül von Alkylhalogenid. Wenn man Bistriphenylphosphin-Nickelhalogenid mit der überschüssigen Menge Alkylhalogenid im eingeschlossenen Rohre bei 150 bis 180° erhitzt, so kann man eine Verbindung, die in Alkylhalogenid unlöslich ist, erhalten. Jedoch bei der Umkristallisation mit Lösungsmittel wie Butanol wandert diejenige zum Monoalkylhalogenidkomplex um. Im Falle, dass R Phenyl ist, kann man die Komplexverbindung dieses Typus als definierter Kristall von dem nach oben beschriebener Methode erhaltenen Reaktionsprodukt durch die Entfernung von überschüssigem Phenylhalogenid unter erniedrigtem Druck gewinnen. Im Falle des Alkylhalogenids ist das Reaktionsprodukt zu zähflüssig, als dass man die Komplexverbindung als Kristall erhalten könnte, selbst durch eine derartige Aufarbeitung.

Falls X' das Halogen mit dem schwereren Atomgewicht als X ist, so darf nicht erlaubt werden, die überschüssige Menge RX' zu verwenden, da man, wegen der Austauschung von Halogen, die erforderliche Komplexverbindung $(Ph_3P)_2NiX_2 2RX'$ nicht erhalten kann, sondern nur $(Ph_3P)_2NiX'_2 2RX'$.

In Tabelle III sind diese Komplexverbindungen gezeigt, die von mir hergestellt wurden.

TABELLE III

KOMPLEXVERBINDUNGEN $(Ph_3P)_2NiX_2 2RX'$

Verbindung	Farbe	Smp. in (°C)	P-Gehalt % Gef.	P-Gehalt % Ber.	Ni-Gehalt % Gef.	Ni-Gehalt % Ber.
$(Ph_3P)_2NiBr_2 2PhBr$	Hellblaugrün	270	5.64	5.86	5.53	5.56
$(Ph_3P)_2NiCl_2 2PhCl$	Blau	260	7.65	7.68	6.31	6.68
$(Ph_3P)_2NiJ_2 2PhJ$	Braun	Unisolierbar				
$(Ph_3P)_2NiBr_2 2PhCl$	Hellblau	253–5	6.34	6.41	5.92	6.00
$(Ph_3P)_2NiCl_2 2PhBr$	Hellblau	253–5	6.37	6.41	6.26	6.00

Bemerkenswert ist das, dess die letzten zwei Verbindungeh als gleich angesehen werden könnten. Wie es anderweit beschrieben wird, wurde durch die Erforschung von dem Abbauprodukt bei Methanolyse festgestellt, dass diese Verbindungen mit zwei Arten Halogenatomen nicht nur das Gemisch von je gleicher Menge der einzelnen Homohalogenkomplexverbindungen sind.

Die Komplexverbindung dieses Typus liefert in Alkohol nicht bloss ein Molekül RX leicht, sondern zersetzt sich auch, je nach den Bedingungen, zu Phosphonium- und Nickelhalogenid.

Schwer löslich ist solche in Benzol und Aceton, aber leicht in Nitrobenzol.

Experimentelle Beispiele

1. Triphenylphosphin.—Man tut das Gemisch von 250 g Benzol, 5.7 g Diäthylmalonat und 51.6 g Natriumschnitzen in den Rundkolben vom 1000 cm³ Inhalt, der mit dem Rückflusskühler, Rührer und Tropfentrichter versehen ist, hinein.

Zu diesem Gemisch fügt man die aus 68 g Chlorbenzol und 32.3 g Phosphortrichlorid bestehende Mischung vom Trichter tropfenweise hinzu, wobei man die Reaktionstemperatur bei 60°C halten muss. Nach 6 Stunden endet die Umsetzung. Wenn man das Reaktionsgemisch nach dem Filtrieren konzentriert, so kann man den Rohkristall des Triphenylphosphins erhalten. Nach der Umkristallisierung aus Methanol erhält man 26.4 g reines Triphenylphosphin (Smp. 79°C).

2. $[(C_6H_5)_3P]_2Ni(CO)_2$.—Man erhitzt das Gemisch von 50 g Triphenylphosphin, 200 g Methanol und 5 g. reduzierten Nickelpulvern in 500 cm³ Autoklav bei 150°C drei Stunden lang unter 50 Atm Druck von Kohlenoxyd. Da das Reaktionsprodukt in Methanol unlöslich ist, dekantiert man es und zieht mit Benzol aus. Fügt man Methanol zur Benzollösung hinzu, so kann man 43 g $[(C_6H_5)_3P]_2Ni(CO)_2$ erhalten.

3. $[(C_6H_5)_3P]_2NiBr_2$.—Wenn man das Gemisch, bestanden aus 200 g Butanol 24 g Triphenylphosphin und 20 g wasserfreiem Nickelbromid, unter Rückfluss zwei Stunden lang erhitzt, so kann man den feinen, kristallinischen Niederschlag von $[(C_6H_5)_3P]_2NiBr_2$ erhalten.

Die Ausbeute beträgt 35 g nach der Umkristallisierung (aus Butanol).

4. $[(C_6H_5)_3P]_2NiBr_2C_2H_5J$.—Man erhitzt das Gemisch, bestehend aus 10.5 g Triphenylphosphin, 4.4 g wasserfreiem Nickelbromid, 3.1 g Äthyljodid und 15 g Äthanol, im eingeschlossenem Rohr bei 150°C, zewi Stunden lang und kann 15 g $[(C_6H_5)_3P]_2NiBr_2C_2H_5J$ (gef. C 50.3, P 6.98. Ni 6.55%, ber. C 50.8, P 6.90, Ni 6.57%) nach der Umkristallisierung erhalten.

5. $[(C_6H_5)_3P]_2NiBr_2 \cdot 2C_6H_5Br$.—Man erhitzt

das Gemisch, bestehend aus 10 g Triphenylphosphin, 4 g wasserfreim Nickelbromid und 15 g Brombenzol, in eingeschlossenem Rohr bei 250°C, zwei Stunden lang. Beim Erkalten scheidet sich das Reaktionsprodukt als feiner Kristal aus. Wenn man überschüssiges Brombenzol auf dem Wasserbad unter erniedrigtem Druck verdünstet, so kann man ca. 5 g $[(C_6H_5)_3P]_2NiBr_2 \cdot 2C_6H_5Br$ aus den reinen Teilen des Bodenkörpers erhalten.

Falls man den Komplex $[(C_6H_5)_3P]_2NiCl_2 \cdot 2C_6H_5Br$ herstellen will, muss man die stoichiometrischen Mengen Triphenylphosphin, wasserfreies Nickelchlorid und Brombenzol verwenden, dann muss man die betreffenden Kristalle vorsichtig aus den reinen Teilen des Bodenkörpers herausgreifen.

Schlusswort

Die Herstellungsverfahren und einige Eigenschaften von Triphenylphosphin-Nickelkomplexverbindungen, die als Katalysator für die Acrylestersynthese verwendet werden, sind beschrieben worden.

Die Eigenschaften und Struktur betreffender Verbindungen sollen später noch näher gesprochen werden.

Herr Dr. K. Yoshikawa hat mich stets bei meinen Arbeiten leitend unterstützt und ermutigt. Die Herren K. Sato und M. Oku haben mit mir eifrig mitgearbeitet. Ich spreche diesen Herren und der Mitsui Chemical Industry Co., die mir diese Veröffentlichung meiner Arbeiten erlaubte, hierdurch meinen herzlichen Dank aus.

Mitsui Chemical Industry Co. Ltd., Miike Dyestuff and Chemical Works, Omuta, Fukuoka

Zur Kenntnis über die Hochdrucksynthese von Acrylester. IV. Über die Acrylestersynthese unter Anwendung von Triphenylphosphin-Nickelkomplexkatalysator

Von Kazumi YAMAMOTO und Mitsuo OKU

(Eingegangen am 24. April 1954)

Einleitung

In der vorigen Mitteilung[1] wurden die Verfahren zur Herstellung von Triphenylphosphin-Nickelkomplexverbindungen beschrieben.

Es geht über den Rahmen der vorliegenden Abhandlung, die eingehenden Bedingungen über die Acrylestersynthese zu erwähnen. Deshalb sollen nur die Kenntnisse, die die wichtigen Tatsachen über die Forschung vom Mechanismus der Aktivierung des Kohlenoxyds am Komplexkatalysator sind, hier gegeben werden. In der Abhandlung bedeutet Ph den Phenylrest, R den Alkyl- oder Arylrest und X und X′ bedeuten das Halogenatom selber oder sich darauf beziehende Arten. Alle Experimente wurden durch das halbkontinuierliche Verfahren[2] durchgeführt.

Wie schon erwähnt, wurde es nach Reppe betont, dass die Triphenylphosphin-Nickelkomplexverbindung als Katalysator für die Acrylestersynthese eine ausgezeichnete Fähigkeit besitzt. Bei unserer Nacharbeitung ist dieses festgestellt worden.

1) K. Yamamoto, Dieses Bulletin, **27**. 501 (1954).
2) K. Yamamoto, Dieses Bulletin, **27**. 491 (1954).

Einfluss, welcher das verschiedene Halogen auf die katalytische Fähigkeit von $(Ph_3P)_2NiX_2$ oder $(Ph_3P)_2NiX_2RX$ ausübt

Es ist schon beschrieben worden, dass die katalytische Fähigkeit von Nickelhalogenid bei der Acrylestersynthese in einer Reihe Cl→Br→J stark zunimmt. Diese Reihe ist ja im Falle des Komplexkatalysators auffallend. Das Experiment wurde nach dem halbkontinuierlichen Verfahren unter der Anwendung vom 600 cm^3 Inhalt Druckgefäss hinsichtlich der Synthese von Butylacrylat, durchgeführt. Die verwendete Menge von Komplexverbindung wurde so bestimmt, dass dejenige menge als Nickelbromid 5% an Butanol erhalten wird, da das Zentrum der katalytischen Wirkung derjenigen katalysatoren das Nickelatom ist.

Unter der Berücksichtigung der Beständigkeit derjenigen katalysatoren für Butanol wurde Butylhalogenid als RX vom $(Ph_3P)_2NiX_2RX$ verwendet. Die Resultate sind aus den Tabellen I, II und beziehungsweise aus der Figur 1 zu ersehen.

TABELLE I

KATALYTISCHE FÄHIGKEIT VON $(Ph_3P)_2NiX_2$

Nr.	BuOH (g)	Katalysator (g)	Einführsatz. von Gasgem. (% d. Th.)	Reakttemp. (°C)	Laufzeit (Std)	(Min)
13	50	$NiBr_2$ 2.5	100	180–190	9	00
14	50	$(Ph_3P)_2NiCl_2$ 7.5	30	180	3	30
15	50	$(Ph_3P)_2NiBr_2$ 8.5	100	180	5	00
16	50	$(Ph_3P)_2NiJ_2$ 9.5	100	180	1	10

* Die theoretische Menge vom Gasgemisch für 50 g. Butanol ist 30.0 *l.* unter dem normalen Zustand.

TABELLE II

KATALYTISCHE FÄHIGKEIT VON $(Ph_3P)_2NiX_2RX$

Nr.	BuOH (g)	Katalysator (g)	Reakttemp. (°C)	Laufzeit (Std)	(Min)	Bu-Acrylat (% an BuOH)
35	50	$(Ph_3P)_2NiCl_2BuCl$ 8.5	165	8	00	60
36	50	$(Ph_3P)_2NiBr_2BuBr$ 10.1	165	3	00	76
37	50	$(Ph_3P)_2NiJ_2BuJ$ 11.7	140–50	0	50	50

Note: In allen Fällen war Einführungssatz von Gasgemisch 100% d. Th.

TABELLE III

KATALYTISCHE FÄHIGKEIT VON $(Ph_3P)_2NiX_2BuX'$

Nr.	BuOH (g)	$(Ph_3P)_2NiX_2BuX'$ (g)	Reakttemp (°C)	Laufzeit (Std)	(Min)	Bu-Acrylat (g)	(%)
35	50	„ $NiCl_2BuCl$ 8.5	165	8	00	51.5	60
36	50	„ $NiBr_2BuBr$ 10.1	165	3	00	65.5	76
51	50	„ $NiCl_2BuBr$ 9.1	165	3	40	56.0	65
52	50	„ $NiBr_2BuCl$ 9.5	165	4	00	57.0	66
53	50	„ $NiCl_2BuJ$ 9.7	140–50	0	55	46.5	54
37	50	„ NiJ_2BuJ 11.7	140–50	0	50	43.0	50

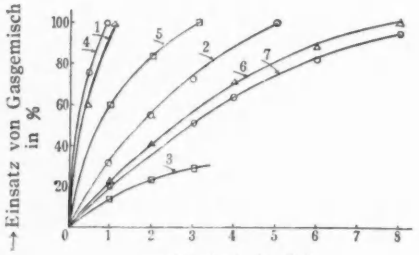

→ Laufzeit in Std.

1 $[(C_6H_5)_3P]_2NiJ_2$
2 $[(C_6H_5)_3P]_2NiBr_2$
3 $[(C_6H_5)_3P]_2NiCl_2$
4 $[(C_6H_5)_3P]_2NiJ_2C_4H_9J$
5 $[(C_6H_5)_3P]_2NiBr_2C_4H_9Br$
6 $[(C_6H_5)_3P]_2NiCl_2C_4H_9Cl$
7 $NiBr_2$

Fig. 1. Katalytische Wirkungen von $[(C_6H_5)_3P]_2NiX_2$ und $[(C_6H_5)_3P]_2NiX_2C_4H_9X$.

Einfluss, welcher das verschiedene Halogen auf die katalytische Fähigkeit von $(Ph_3P)_2NiX_2RX'$ ausübt

Im vorigen Paragraphen wurde der Vergleich der katalytischen Fähigkeit von $(Ph_3P)_2NiX_2RX'$, in dem X mit X' identisch war, gemacht. Im vorliegenden soll derselbe auch im Falle, dass X mit X' nicht identisch ist, gemacht werden.

Die Resultate sind in der Tabelle III gezeigt.

In allen Fällen war der Einführungssatz vom Gasgemisch 100% d. Th. Die Figur 2 illustriert die Reaktionsverläufe.

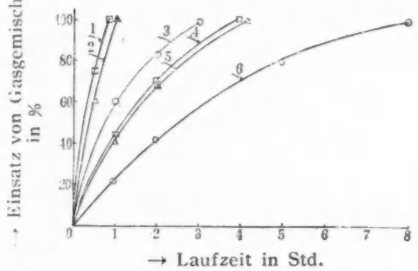

→ Laufzeit in Std.

1 $[(C_6H_5)_3P]_2NiJ_2C_4H_9J$
2 $[(C_6H_5)_3P]_2NiCl_2C_4H_9J$
3 $[(C_6H_5)_3P]_2NiBr_2C_4H_9Br$
4 $[(C_6H_5)_3P]_2NiCl_2C_4H_9Br$
5 $[(C_6H_5)_3P]_2NiBr_2C_4H_9Cl$
6 $[(C_6H_5)_3P]_2NiCl_2C_4H_9Cl$

Fig. 2. Katalytische Wirkungen von $[(C_6H_5)_3P]_2NiX_2C_4H_9X'$

Beobachtet man die Resultate, so werden die katalytischen Fähigkeiten der Komplex-

verbindungen hinsichtlich der Reaktionsgeschwindigkeit in drei Hauptklassen, d. h., Nr. 35 und Nr. 36, 51, 52 und Nr. 53, 37 eingeteilt. Wird das Halogen mit dem schweren Atomgewicht in die Komplexverbindung entweder als Nickel- oder als Alkylhalogenid, d. h., in welcher Form es auch sei, eingeführt, so ist eindeutig zu ersehen, dass deren katalytische Fähigkeit mit der katalytichen Fähigkeit der Verbindung, deren Halogenatome all das Schwere sind, identisch ist.

Diese Tatsache deutet an, dass alle Halogenatome die gleiche Stelle an Nicklatom einnehmen. Darüber hinaus gibt dies die wichtige Suggestion über die chemische Konstitution von diesem Typus Komplexverbindung und über den Mechanismus der Aktivierung des Kohlenoxyds bei der Acrylestersynthese.

Folglich kann man die regelmässige Ordnung über die katalytische Fähigkeit von der Komplexverbindung $(Ph_3P)_2NiX_2RX'$ wie folgt erwarten.

$(Ph_3P)_2NiJ_2RJ \fallingdotseq (Ph_3P)_2NiJ_2RBr \fallingdotseq$
$(Ph_3P)_2NiJ_2RCl \fallingdotseq (Ph_3P)_2NiBr_2RJ \fallingdotseq$
$(Ph_3P)_2NiCl_2RJ > (Ph_3P)_2NiBr_2RBr \fallingdotseq$
$(Ph_3)_2NiBr_2RCl \fallingdotseq (Ph_3P)_2NiCl_2RBr >$
$(Ph_3P)_2NiCl_2RCl.$

Beschleunigung der Reaktion bei der Äthylacrylatsynthese

Die Synthese von Äthylacrylat aus Acetylen, Kohlenoxyd und Äthanol in Anwesenheit von der Triphenylphosphin-Nickelkomplexverbindung ist im allgemeinen schwerer als die von Butylacrylat.

Dies soll gerade von den schon erwähnten zwei Erfahrungsgesetzen über die Beständigkeit der Komplexverbindung gegen Alkohol induziert werden. Das heisst, bei der Butylacrylatsynthese ist $(Ph_3P)_2NiX_2C_2H_5X$ als Katalysator zwar wirksam, aber bei der Äthylacrylatsynthese ist $(Ph_3P)_2NiX_2C_4H_9X$ nicht mehr zweckmässig. Während die genügende Reaktionsgeschwindigkeit bei derjenigen unter Anwendung von $(Ph_3P)_2NiBr_2C_4H_9Br$ (5% an Butanol) gefunden wird, kann dementgegen bei der anderen die gleiche Geschwindigkeit nicht gefunden werden, es sei denn, dass beinahe die zweifache Menge Katalysator $(Ph_3P)_2NiBr_2C_2H_5Br$ verwendet wird.

Wir haben auf Grund der vorigen Schlussfolgerung geplant, die Reaktionsgeschwindigkeit durch die Anwendung von Äthljodid und Bromid im verschiedenen Verhältnis zusammen mit $(Ph_3P)_2NiBr_2$, dessen Menge dem $(Ph_3P)_2NiBr_2C_2H_5Br$ 5% auf Basis von Äthanol entspricht, zunehmen zu lassen. Das Experiment wurde halbkontinuierlich unter den folgenden Bedingungen durchgeführt; Äthanol 50 g, $(Ph_3P)_2NiBr_2$ 2.2 g, Reaktionstemperatur 180°, Gesamtdruck von Gasgemisch 40 Atm.

Die zur Bildung von $(Ph_3P)_2NiBr_2C_2H_5X$, das den 2.2 g $(Ph_3P)_2NiBr_2$ entspricht, theoretisch erforderlichen Mengen von Äthylbromid und Jodid sind 0.3 und beziehungsweise 0.4 g. Die Figur 3 stellt die Resultate dar.

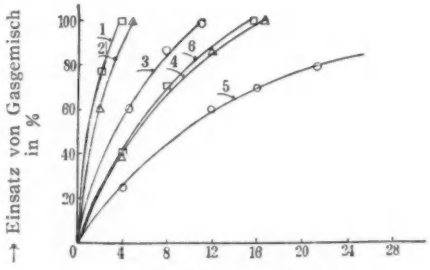

1	$[(C_6H_5)_3P]_2NiBr_2$ + (ÄtBr : ÄtJ = 0	: 1)	5%
2	,, + (,,	= 0.2 : 0.8)	5%
3	,, + (,,	= 0.5 : 0.5)	5%
4	,, + (,,	= 0.8 : 0.2)	5%
5	,, + (,,	= 1 : 0)	5%
6	,, + (,,	= 1 : 0)	10%

Fig. 3. Beschleunigungseffekt von Jodäthyl bei Äthylacrylatsynthese.

Wie man aus der Figur 3 ersehen kann, und man Äthylbromid und Jodid im Verhältnis von 8 : 2 verwendet, kann man die Geschwindigkeit, die mit der bei der Anwendung von 5 g (10%) $(Ph_3P)_2NiBr_2C_2H_5Br$ fast gleich ist, beobachten.

Über die Menge von RX

In den Experimenten im zweiten Paragraphen wurden die definierten Verbindungen $(Ph_3P)_2NiX_2RX'$ verwendet. Aber Reppe[3] hat angedeutet, dass die Anwesenheit von der überschüssigen Menge Alkylhalogenid zur Hemmung vom Auftreten des Katalysatorsabbruchs, insbesondere die Nickelcarbonylbildung, wirksam ist.

Jedoch mit der Zunahme der Menge Alkylhalogenid nimmt die Reaktionsgeschwindigkeit proportional nicht zu. Dies ist in der Figur 4 eindeutig gezeigt, die den Reaktionsverlauf bei der Butylacrylatsynthese unter der Veränderung von dem Molverhältnis von Butylbromid zu $(Ph_3P)_2NiBr_2$ illustriert.

3) W. Reppe, „Neue Entwicklungen auf dem Gebiet der Chemie des Acetylens und Kohlenoxyds", Springer Verlag (1949) S. 103.

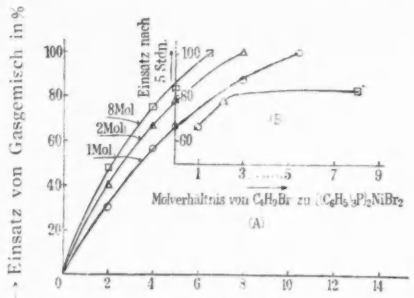

Fig. 4. Einfluss von Butylbromidmenge

Die Figur 4 (A) zeigt die Beziehung zwischen dem Einleitungssatz vom Gasgemisch und der Laufzeit und (B) die zwischen dem Einleitungssatz nach 5 Stunden und dem Molverhältnis von Butylbromid zu Bistriphenylphosphin-Nickelbromid. Aus der Figur 4 (B) scheint es, dass der bedeutende Unterschied zwischen 1 und 2 die Molverhältnisse des Bromids ist. (Arbeitungsmethode und Reaktionsbedingungen folgten denen wie im ersten Paragraphen beschrieben.)

Über die Art und Nummer von Halogenatom

Die Resultate voriges Paragraphen deuten die Möglichkeit des Seins der Komplexverbindung von Typus $(Ph_3P)_2NiX_2RX'$, wenn gleich deren Isolierung, falls R Alkylgruppe ist, ausserordentlich schwierig ist. Wir haben den Reaktionsverlauf hinsichtlich der Komplexverbindungen beobachtet, welche eine jede für sich verschiedene Nummer des Halogenatoms gleicher oder verschiedener Art enthalten, um diese Frage durchzuprüfen. Die verwendeten Komplexverbindungen sind folgende:

$(Ph_3P)_2NiBr_2C_4H_9Br$ und dasselbe$+C_4H_9Br$
$(Ph_3P)_2NiCl_2C_4H_9Br$ und dasselbe$+C_4H_9Br$
$(Ph_3P)_2Ni(OOCCH_2Cl)_2C_4H_9Br$ und dasselbe$+C_4H_9Br$

Die Komplexverbindung $(Ph_3P)_2Ni(OOCCH_2Cl)_2C_4H_9Br$, bisher die unbekannte mit Schmelzpunkt 157 bis 158°, wurde aus Triphenylphosphin, Monochloressigsäurenickel und Butylbromid hergestellt, gemäss dem Herstellungsverfahren von dementsprechendem Butylchloridkomplex von Reppe[4].

Die unter gleichen Bedingungen erhaltenen Resultate sind in der Figur 5 illustriert. Die Menge von der als Katalysator verwendeten Komplexverbindung war so gewählt, dass jede Komplexverbindung einen gleichen Nickelgehalt (0.67 g—2.5 g als $NiBr_2$—in 50 g Butanol) enthält.

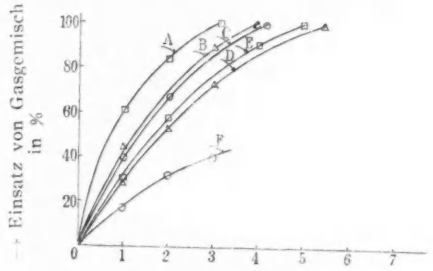

A $[(C_6H_5)_3P]_2NiBr_2C_4H_9Br$
B $[(C_6H_5)_3P]_2NiBr_2C_4H_9Br$
C $[(C_6H_5)_3P]_2NiCl_2C_4H_9Br$
D $[(C_6H_5)_3P]_2NiCl_2C_4H_9Br$
E $[(C_6H_5)_3P]_2Ni(OOCH_2Cl_2Cl)_2C_4H_9Br$
F $[(C_6H_5)_3P]_2Ni(OOCH_2Cl)_2C_4H_9Br$

Fig. 5. Art und Nummer von Halogenatomen in KKomplexverbindungen

Von diesen Resultaten werden die folgenden wichtigen Schlussfolgerungen erzielt:

1) Wenn selbst ein Halogenatom sich in der Komplexverbindung befindet, so hat die betreffende Komplexverbindung die katalytische Wirkung. (Das Chloratom im Monochloressigsäurerest wird dafür gehalten, dass es nicht unmittelbar an der Reaktion teilnimmt.)
2) Betreffs der Verbindungen mit den Halogenatomen der selben Art; je mehr Halogenatome in einer Komplexverbindung enthalten sind, desto grösser wird ihre katalytische Fähigkeit. F<E<B<A.
3) Betreffs der Verbindungen mit den verschiedenen Halogenatomen ist die katalytische Wirkung von der Nummer des schweren Halogenatoms abhängig. D<C.
4) Nicht, dass selbst ein leichtes Halogenatom keine Rolle spielt, sondern es ist von niedrigem Grade. F<D, E<C.
5) Das Sein der Komplexverbindung von Typus $(Ph_3P)_2NiX_2RX'$, worin R Alkyl ist, ist fast gewiss.

Die eingehende Erörterung über die obigen Schlussfolgerungen wollen wir anderweitig beschreiben.

Schlusswort

Die folgenden Resultaten wurden durch die Vergleichung von der katalytischen Fähigkeit der Komplexverbindungen erhalten.

1. In den Komplexverbindungen von Typus $(Ph_3P)_2NiX_2$ und $(Ph_3P)_2NiX_2RX$ nimmt die katalytische Fähigkeit in einer Reihe von Halogen Cl, Br, J stark zu.
2. Von dem Vergleich der katalytischen

4) W. Reppe, *D.B.P.*, 805, 641; *C.*, II, 2251 (1951).

Fähigkeit von $(Ph_3P)_2NiX_2RX'$ (wobei $X \neq X'$) wird erwartet, dass alle Halogenatome die gleiche Stelle an Nickel einnehmen.

3. Die Komplexverbindung $(Ph_3P)_2NiX_2 2RX'$, worin R Alkylrest ist, kann nicht isoliert werden. Das Sein ist aber fast unter den Reaktionsbedingungen gewiss.

4. Betreffs der Nummer und Art des Halogenatoms wurde eine Regelmässigkeit gefunden.

Herr Dr. K. Yoshikawa hat uns immer bei unseren Arbeiten geleitet und ermutigt. Wir sprechen dem Herrn Doktor und der Mitsui Chemical Industry Co., die uns diese Veröffentlichung unserer Arbeiten erlaubte, hierdurch unseren herzlichen Dank aus.

Mitsui Chemical Industry Co. Ltd., Miike Dyestuff and Chemical Works, Omuta, Fukuoka

Zur Kenntnis über die Hochdrucksynthese von Acrylester. V. Zur Kenntnis über die Triphenylphosphin-Nickel-Komplexverbindungen

Von Kazumi YAMAMOTO und Mitsuo OKU

(Eingegangen am 24. April 1954)

Einleitung[1]

Als Literatur betreffs der Eigenschaften des Triphenylphosphin-Nickelhalogenids gibt es nur eine Veröffentlichung von Reppe[2], die aber keine eingehende ist.

Was die Strukturen der bei der Acrylestersynthese wichtigen Komplexverbindungen, wie $(Ph_3P)_2NiX_2RX'$ und $(Ph_3P)_2NiX_2 2RX'$, worin Ph den Phenylrest, R den Alkyl- oder Arylrest ausdrückt und X und X' selbes oder verschiedenes Halogenatom bedeuten, anbetrifft, gibt es keine. Der von Copenhaver[3] zitierten Meinung von Schweckendiek nach, verbände Alkylhalogenid durch die Nebenvalenz mit Bistriphenylphosphin-Nickelhalogenid $(Ph_3P)_2NiX_2$ und auch seine Annahme über den Mechanismus der Aktivierung des Kohlenoxyds würde sich auf diese Meinung stützen.

Die Struktur oder die chemischen Verhalten von diesen Komplexverbindungen zu untersuchen ist sehr wichtig, um den betreffenden Mechanismus aufzuklären. Wir haben wohl neue Erkenntnisse über die chemischen und physikalischen Eigenschaften derjenigen Komplexverbindungen erworben, die stets Beziehung mit ihrer katalytischen Fähigkeit enthalten.

Thermisches Verhalten der Komplexverbindungen

Wir haben das thermische Verhalten der Komplexverbindungen durch die Thermanowaage beobachtet, um die Kenntnisse über die Konstitution und über den Zusammenhang zwischen der Konstitution und der katalytischen Fähigkeit bei der Acrylestersynthese zu erhalten.

Die Skizze des experimentellen Apparates ist aus der Figur 1 ersehen.

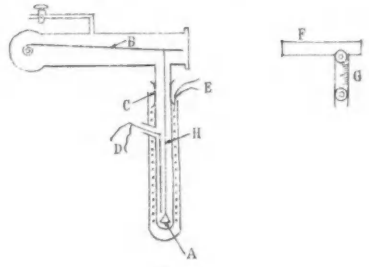

Fig. 1.

Die genau gewogene zirka 70 mg Probe wurde in das quarzige Tellerchen A, das mit dem dünnen Draht H von quarzigem Federhebel B hängt, eingesetzt und mit dem elektrischen Heizapparat E erhitzt. Der mit der Steigerung von der Temperatur zu begleitende Gewichtsverlust der Probe wird dadurch bestimmt, dass man den Aufgang von der Spitze des Hebels durch den mit dem Teleskop F gekuppelten, zuvor korrigierten Kathetometer G beobachtet. Die Geschwindigkeit der Temperatursteigerung, die durch das Thermoelement D gemessen wird, regelt sich in 2°/Min von der Raumtemperatur bis 200° und 1°/Min von 200° bis 250°, wobei die Temperatur konstant gehalten wird. Auf solche Weise wurde die Zersetzungsgeschwindigkeit mit den Gewichtsverlust—Temperatur und Gewichtsverlust-Laufzeit in Kurven dargestellt. Zuerst wurde der thermische

1) Vgl. K. Yamamoto und M. Oku, Dieses Bulletin, **27**, 505 (1954).
2) W. Reppe und R. J. Schweckendiek, *Ann.*, **560**, 104 (1948).
3) J. Copenhaver und M. Bigelow, „Acetylen and Carbonmonoxide Chemistry", Rheinhold Pub. Co. (1949), S. 262.

Abbau von $(Ph_3P)_2NiBr_2$ in der Luft beobachtet. Jedoch der Schmelzpunkt von dem Sublimat, das auf der oberen, inneren Mauer von C in der Figur 1 anklebte, war 153° unter dem Mikroskop. Dieser Schmelzpunkt stimmt gut mit dem des Triphenylphosphinoxyds (Smp. 152–3°[4]) überein. Dies zeigt, dass die Oxydation statt findet. Folglich wurde das nachfolgende Experiment in der Atmosphäre von Stickstoff durchgeführt. Die experimentellen Resultate sind aus den Figuren 2 und 3 zu ersehen.

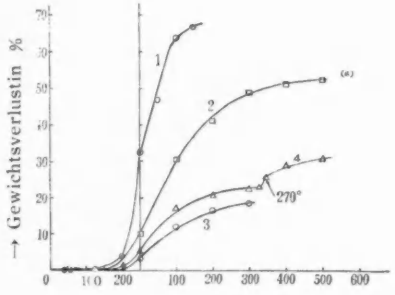

→°C

→ Laufzeit bei 250° in Min.

1 $[(C_3H_5)_3P]_2NiCl_2$
2 $[(C_3H_5)_3P]_2NiBr_2$
3 $[(C_3H_5)_3P]_2NiJ_2$
4 $[(C_3H_5)_3P]_2NiBr_2C_4H_9Br$

Fig. 2(a). Thermisches Verhalten von Komplexverbindungen.

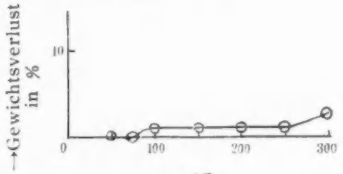

→ °C.

Fig. 2(b). $[(C_3H_5)_3P]_2NiBr_2 2C_3H_5Br$.

Aus der Figur 2(b) kann man ersehen, dass $(Ph_3P)_2NiBr_2 2C_3H_5Br$ ziemlich beständig gegen die Wärme ist. Die anderen Verbindungen zersetzen sich dementgegen schon bei 250°. In jedem Falle wurde das Sublimat, dessen Schmelzpunkt 79° mit dem des Triphenylphosphins völlig übereinstimmte, auf der oberen, inneren Mauer von C und auf dem Draht H in der Figur 1 erhalten. Betreffs einiger Beispiele, bei welchen der Grenzwert des Gewichtsverlustes für konstant gehalten wird, sind die theoretischen Triphenylphosphingehalte sowohl von $(Ph_3P)_2NiX_2$ als auch von $(Ph_3P)_2NiX_2C_4H_9X'$ und die beobachteten Gewichtsverluste, in denen das Gewicht des auf dem Draht H sublimierten Triphenylphosphins für solche nicht beobachtet wird, in der Tabelle I angegeben.

TABELLE I
VERGLEICH VON Ph_3P-GEHALT UND GEWICHTSVERLUST VON KOMPLEXVERBINDUNGEN

Komplex	Gew.-verlust. (%) (a)	Theor. Ph_3P-Gehalt (%) (b)	(a)/(b)
$(Ph_3P)_2NiCl_2$	66	80.0	0.88
$(Ph_3P)_2NiBr_2$	56	70.5	0.80
$(Ph_3P)_2NiBr_2C_4H_9Br$	30	59.5	0.50
$(Ph_3P)_2NiCl_2C_4H_9Cl$	33.3	72.0	0.46
$(Ph_3P)_2NiBr_2C_4H_9Cl$	26.4	62.8	0.43

Infolgedessen wird die thermische Zersetzung von der Komplexverbindung Typus $(Ph_3P)_2NiX_2$ wie folgt ausgedrückt werden.

$$(Ph_3P)_2NiX_2 \rightarrow 2Ph_3P + NiX_2$$

Bei dem Typus $(Ph_3P)_2NiX_2RX$ dementgegen wird man sich vorstellen können, dass das von der Zersetzung sublimierte Triphenylphosphin zwar nur ein Molekül ist, ein anderes aber sich in der Bindungsart ganz und gar unterscheidet. Unter der Berücksichtigung des Herstellungsverfahrens (vgl. III. Mitteilung[5]) könnte man diese Zersetzung im Endeffekt im Sinne der Gleichung erläutern.

$$(Ph_3P)_2NiX_2RX \rightarrow (Ph_3RP)X + NiX_2 + Ph_3P$$

In der Tat erhitzten wir die Verbindung $(Ph_3P)_2NiBr_2C_4H_9Br$ bei 250°, 6 Stunden lang unter der Anwendung vom Rose -Tiegel in der Atmosphäre des Stickstoffes und erhielten eine kristallinische Substanz aus dem Zersetzungsprodukt durch die Ausziehung mit heissem Wasser und die Umkristallisation. Die Substanz schmilzt bei 235°. Wir stellten wie unten beschrieben fest, dass sie das Triphenylbutylphosphoniumbromid ist.

Darüber hinaus beobachteten wir gegen alles Erwarten, dass die von dem Zersetzungsprodukt von $(Ph_3P)_2NiBr_2C_4H_9Cl$ erhaltene kristallinische Verbindung auch bei 235° schmilzt, und sie wie oben benannt, als Phosphoniumbromid angesehen werden soll.

Wir möchten über solche erstaunliche Umwandlung des Halogenatoms in dem nächsten Paragraphen auch eine andere Erscheinung erörtern.

Wenn das Alkylhalogenid sich dagegen mit Bistriphenylphosphin-Nickelhalogenid durch die Nebenvalenz verbände, sollte es zu

4) A. Kosolapoff, *J. Am. Chem. Soc.*, **64**, 2982 (1942).

5) K. Yamamoto, Dieses Bulletin, **27**, 503 (1954).

allererst beim Erhitzen verdünsten, wir aber haben Butylbromid bei der trockenen Destillation von $(Ph_3P)_2NiBr_2C_4H_9Br$ in der Atmosphäre des Stickstoffes nicht fangen können.

Auch die Tatsache, dass das $(Ph_3P)_2NiBr_2$-$2C_6H_5Br$ auch bei 300°C noch keinen bemerkenswerten Gewichtsverlust bietet, dürfte die Nebenvalenz-Theorie von Schweckendiek verneint werden.

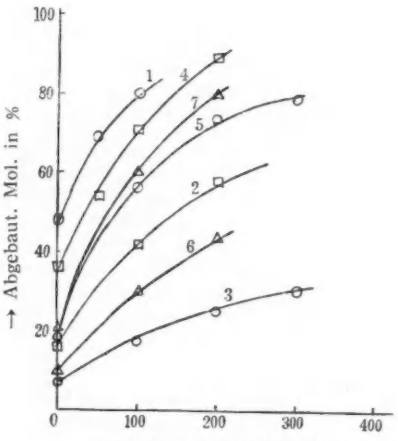

1 $[(C_6H_5)_3P]_2NiCl_2$
2 $[(C_6H_5)_3P]_2NiBr_2$
3 $[(C_6H_5)_3P]_2NiJ_2$
4 $[(C_6H_5)_3P]_2NiCl_2C_4H_9Cl$
5 $[(C_6H_5)_3P]_2NiBr_2C_4H_9Br$
6 $[(C_6H_5)_3P]_2NiJ_2C_4H_9J$
7 $[(C_6H_5)_3P]_2NiBr_2C_4H_9Cl$

Fig. 3. Thermische Zersetzung von Komplexverbindungen.

Die Figur 3 illustriert die Zersetzungsneigungen von $(Ph_3P)_2NiX_2$ und $(Ph_3P)_2NiX_2RX'$ mit dem Prozent vom abgebauten Molekül gegen die Laufzeit bei 250°. Davon wird man den Effekt, welcher das Halogen auf die Bindung zwischen dem Nickel und Triphenylphosphinrest ausübt, wissen können. Das heisst, betreffs der Komplexverbindung jedes Typuses, in der Reihenfolge Chlorid→Bromid →Jodid nimmt deren Stabilität zu. Unter Erinnerung der in der vorigen Mitteilung beschriebenen Reihenfolge der katalytischen Fähigkeit von den Komplexverbindungen, könnte man die wichtige Tatsache, dass die katalytische Fähigkeit mit deren Stabilität in der gleichen Ordnung steht begreifen.

Zersetzung von Komplexverbindungen in Methanol

Wir haben vorher zwei Erfahrungsgesetze über die Stabilität der Komplexverbindung $(Ph_3P)_2NiX_2RX'$ gegen Alkohol beschrieben. In Methanol jedoch zersetzt sich die Verbindung, welcher Typus es auch sei. Wir erforschten zuerst das Verhalten von $(Ph_3P)_2NiBr_2$, $(Ph_3P)_2NiBr_2C_4H_9Br$ und $(Ph_3P)_2$-$NiBr_22C_6H_5Br$ als Vertreter jedes Typus qualitativ.

Wird zirca 0.5 g der Probe mit 5 cm^3 Methanol bei Zimmertemperatur behandelt, so löst sich die Komplexverbindung unter Verlöschung der eigentümlichen Farbe und mit spontaner Verdampfung von Methanol kristallisiert das Zersetzungsprodukt aus.

1) Von $(Ph_3P)_2NiBr_2$ kristallisiert Triphenylphosphin (Smp. 79°) beinahe quantitativ aus.

2) Von $(Ph_3P)_2NiBr_2C_4H_9Br$ kristallisiert der wasserlösliche Kristall mit hohem Schmelzpunkt nebst dem Triphenylphosphin aus. Wenn man den ersteren daraus mit heissem Wasser extrahiert und ihn zweimal aus Wasser umkristallisiert, so kann man den farblosen, kubischen Kristall mit Schmelzpunkt 235° erhalten. (*Anal.* gef. P 7.71, C 67.5, H 5.80%)

Fügt man zur wässrigen Lösung von demjenigen die des Silbernitrats hinzu, so schlägt Silberbromid sofort nieder. Also kann man die Substanz für Triphenylbutylphosphoniumbromid erachten, das bisher nicht veröffentlicht wurde. Wir haben es aus Triphenylphosphin und Butylbromid im Butanol bei 180° hergestellt und beobachtet, dass dessen Schmelzpunkt auch bei 235° ist.

$[(C_6H_5)_3(C_4H_9)P]Br$

Gef.	P 7.73	C 65.98	H 5.99	Br 20.1%	
Ber.	7.77	66.20	6.02	20.0	

Dieses Präparat zeigte keine Schmelzpunktdepression bei der Mischprobe mit der aus Produkt sowohl der Methanolyse als der thermischen Zersetzung erhaltenen Probe.

Folglich wurde es festgestellt, dass auch die Zersetzung in Methanol, wie bei der thermischen, verläuft;

$$(Ph_3P)_2NiBr_2C_4H_9Br \rightarrow [Ph_3(C_4H_9)P]Br + NiBr_2 + Ph_3P$$

3) Von $(Ph_3P)_2NiBr_22PhBr$ scheidet Triphenylphosphin nicht mehr aus, sondern wird der wasserlösliche Kristall von Schmelzpunkt 287°, der mit dem des Tetraphenylphosphoniumbromids[6] überein-

6) J. Dodonov, *Ber.*, **61**, 907 (1928).

stimmt, gefunden. Folglich wird die Zersetzung mit der folgenden Gleichung ausgedrückt;

$(Ph_3P)_2NiBr_2 2PhBr \rightarrow 2(Ph_4P)Br + NiBr_2$

Nachher wurde die Zersetzung von $(Ph_3P)_2NiX_2RX'$ oder $(Ph_3P)_2NiX_2 2RX'$ untersucht, wobei X beziehungsweise X' verschiedenes Halogenatom bedeutet. In diesen Fällen haben wir eine wichtige Tatsache gefunden, dass als Halogenatom des Phosphoniumhalogenids, wie bei der thermischen Zersetzung, stets das mit schwerem Atomgewicht festgestellt wird. Zum Beispiel wird nur Triphenylbutylphosphoniumbromid (Smp. 235°) bei der Zersetzung sowohl von $(Ph_3P)_2NiBr_2C_4H_9Cl$ wie von $(Ph_3P)_2NiCl_2C_4H_9Br$ gefunden und nicht Triphenylbutylphosphoniumchlorid, das von uns aus Triphenylphosphin und Butylchlorid in Butanol hergestellt wurde, und dessen Schmelzpunkt 227–8° war. Also werden beide Zersetzungen wie folgt gezeigt;

$(Ph_3P)_2NiBr_2C_4H_9Cl \longrightarrow$
$[Ph_3(C_4H_9)P]Br + \frac{1}{2}NiBr_2 + \frac{1}{2}NiCl_2 + Ph_3P$
$(Ph_3P)_2NiCl_2C_4H_9Br \longrightarrow$
$[Ph_3(C_4H_9)P]Br + NiCl_2 + Ph_3P$

Auch bei der Zersetzung von $(Ph_3P)_2NiBr_2$ 2PhCl oder $(Ph_3P)_2NiCl_2$2PhBr wird die gleiche Erscheinung beobachtet, dass die Abbauprodukte jedenfalls Tetraphenylphosphoniumbromid und Nickelchlorid sind. Dies beseitigt die Zweifel, welche zwei derartige Komplexverbindungen, die gleiche Farbe und gleichen Schmelzpunkt[5] haben, jede für sich die Gemische der gleichen Menge von $(Ph_3P)_2$ $NiBr_2$2PhBr und $(Ph_3P)_2NiCl_2$2PhCl sein sollten und bringt dies vielmehr die Möglichkeit hervor, dass beide dieselben Verbindungen sind.

Diese Resultate stellen die in voriger Mitteilung beschriebene Schlussfolgerung „Alle Halogenatome nehmen gleiche Stelle an Nickel ein" dar und zwar verneinen grundsätzlich den Schweckendiekschen Gedanke, dass Alkylhaloganid sich an $(Ph_3P)_2$ NiX_2 nur durch Nebenvalenz verbände.

Als solche Strukturen, in denen die Halogenatome die gleiche Stelle an Nickel einnehmen, nehmen wir die folgenden an, abgesehen davon, dass entweder diejenigen die echten Elektrolyte sind oder Nichtelektrolyte;

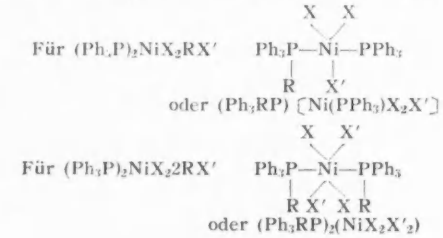

Unter der Annahme von diesen Strukturen wird man sowohl das thermische Verhalten als auch die Zersetzung von Komplexverbindungen in Methanol sowie die Möglichkeit, dass $(Ph_3P)_2NiBr_2$2PhCl und $(Ph_3P)_2NiCl_2$2PhBr die gleichen Verbindungen seien, gut verstehen können. Über das katalytische Verhalten von $(Ph_3P)_2NiX_2RX'$ möchten wir anderweit noch näher diskutieren.

Leitungsfahigkeit von Komplexverbindungen

Zuerst wurden die Leitungsfähigkeiten von $(Ph_3P)_2NiBr_2C_4H_9Br$ und $(Ph_3P)_2NiBr_2$2PhBr in Aceton, das ein gutes Lösungsmittel für dieselben ist, bestimmt. Wie in der Tabelle II Zeile I und II gezeigt, wurden die Resultate gefunden, dass diese Verbindungen die Elektrolyte sein könnten. Aber auch die Komplexverbindung $(Ph_3P)_2NiBr_2$, die von den Arbeiten von Jensen[7] über Bistriäthylphosphin-Nickelchlorid $[(C_2H_5)_3P]_2NiCl_2$ eindeutig als Nichtelektrolyt angesehen wird, zeigte die Leitungsfähigkeit wie in Zeile III. Dies erläutert, dass auch in Aceton das schon beschriebene Dissoziationsgleichgewicht vorhanden ist.

$(Ph_3P)_2NiBr_2 \rightleftarrows 2Ph_3P + NiBr_2$
$(Ph_3P)_2NiBr_2C_4H_9Br$
$\rightleftarrows (Ph_3C_4H_9P)Br + NiBr_2 + Ph_3P$
$(Ph_3P)_2NiBr_2$2PhBr $\rightleftarrows 2(Ph_4P)Br + NiBr_2$

Folglich gibt es eine Gefährlichkeit, dass die erhaltenen Leitungsfähigkeiten die der Komplexverbindungen für sich nicht bedeutsam sind, sondern die von Nickelbromid und Phosphoniumbromid.

TABELLE II
LEITUNGSFÄHIGKEIT VON KOMPLEXVERBINDUNGEN IN ACETON

Komplex	Temp. (°C)	Verdünungsgrad (cm^3.)	Mol. Leitungsfähigkeit (Ω^{-1})
$(Ph_3P)_2NiBr_2C_4H_9Br$	20	2.5×10^5	72.91
I.		5.0×10^5	84.53
		1.0×10^6	102.3
		2.0×10^6	108.8
$(Ph_3P)_2NiBr_2$2PhBr	20	1.9×10^6	210.6
II		3.8×10^6	231.4
		7.6×10^6	235.3
		1.5×10^7	242.9
$(Ph_3P)_2NiBr_2$	20	2.5×10^5	32.9
III.		5.0×10^5	39.08
		1.0×10^6	42.28
		4.0×10^6	45.47
		8.0×10^6	52.13
		1.6×10^7	62.52

9) K. A. Jensen, *Z. anorg. allg. Chem.*, **229**, 273 (1936).

Diese Erscheinung wurde auch in Butanol an $(Ph_3P)_2NiBr_2C_4H_9Br$, wenn der Umfang auch niedrig ist, beobachtet. Die Tabelle III zeigt diese Reultate und die eigentümlichen Leitungsfähigkeiten von Nickel- und Triphenylbutylphosphonium-bromid in den Zeilen I, II, und bzw III. Darüber hinaus stellt die Zeile IV die Leitungsfähigkeit der gleichen Komplexverbindung in Äthanol dar. Die höheren Werte im Äthanol geben das in der Mitteilung III[5] erwähnte zweite Erfahrungsgesetz über die Beständigkeit der Komplexverbindung in Alkohol quantitativer dar.

Tabelle III

Leitungsfähigkeit von Komplexverbindungen in Alkohol

	Komplex	Alkohol	Verdünnungsgrad (cm^3)	Mol. Leitungsfähigkeit (Ω^{-1}) 20°	50°
I.	$(Ph_3P)_2NiBr_2C_4H_9Br$	Butanol	5.0×10^4	6.70	11.05
			2.0×10^5	9.40	16.50
			5.0×10^5	10.36	20.55
			5.0×10^6	20.25	32.85
II.	$NiBr_2$	Butanol	1.9×10^4	1.85	2.39
			7.5×10^4	2.32	2.87
			1.9×10^5	3.25	4.15
			1.9×10^6	7.87	10.54
			1.9×10^7	17.30	23.08
III.	$(Ph_3C_4H_9P)Br$	Butanol	2.38×10^4	5.60	9.85
			9.52×10^4	7.50	13.08
			2.38×10^5	8.90	15.92
			2.38×10^6	13.60	26.40
			2.38×10^7	15.95	28.08
IV.	$(Ph_3P)_2NiBr_2C_4H_9Br$	Äthanol	2.8×10^4	27.6	38.6
			5.6×10^4	33.1	46.3
			2.8×10^5	46.2	65.5
			2.8×10^6	70.3	103.2

Die Tabelle III erläutert, dass die Dissoziation desto grösser wird, je höher die Temperatur ist. Aber unter Anwendung der eingeschlossenen Zelle zeigten die Leitungsfähigkeiten der bei erhöhter Temperatur stehenden Butanollösung von $(Ph_3P)_2NiBr_2C_4H_9Br$ durch den maximalen Wert bei 120° den Abfall (Tabelle IV.)

Tabelle IV

Leitungsfähigkeit der Butanollösung von $(Ph_3P)_2NiBr_2C_4H_9Br$ bei erhöhter Temperatur

($Verdünnungsgrad\ 3.1\times10^5\ cm.^3$ bei 20°)

Temperatur (°C)	70	100	110	120	130	140	150
Mol. Leitung. (Ω^{-1})	24.80	30.70	34.10	34.10	30.70	29.22	27.60

Unter Berücksichtigung von der Veränderung seiner Farbe bei der erhöhten Temperatur (vgl. III. Mitteilung) wird dies dadurch aufgeklärt, dass es auf die Verminderung vom Dissoziationsgrad zurückführt. Es ist jedoch eindeutig, dass die oben erhaltenen Data die Erkenntnis, die wir erhalten wollen gerade nicht ergeben. Wenn, demnach, Triphenylphosphin (Smp. 79°), das ein Dissoziationsprodukt ist, verwendet wird, wird man die Leitungsfähigkeit von Komplexverbindungen an und für sich selbst erhalten können, der Verstellung des Gleichgewichts nach links wegen. Das Resultat des von obigem Gesichtspunkt durchgeführten Experiments erläutert, wie in der Tabelle V gezeigt, $(Ph_3P)_2NiBr_2C_4H_9Br$ für sich gewiss ein Nichtelektrolyt zu sein.

Tabelle V

Leitungsfähigkeit von $(Ph_3P)_2NiBr_2C_4H_9Br$ in geschmolzenem Triphenylphosphin

Verdünnungs-* grad (cm^3.)	Temperatur (°C)	Mol. Leitungsfähigkeit (Ω^{-1})
4.03×10^4	200	**
4.03×10^3	200	**
4.03×10^2	200	**
4.03×10	200	1.43×10^{-4}
4.03×10	180	1.07×10^{-4}
"	160	7.55×10^{-5}
"	140	5.19×10^{-5}
"	120	3.21×10^{-5}
"	100	1.60×10^{-5}
"	80	3.78×10^{-6}

* Diese Werte sind auf der Dichte von Ph_3P d_4^{80} 1.0749[8] gründet, folglich bedeuten sie den Verdünnungsgrad bei 80°.

8) A. Walden, *Z. für phys. Chem.*, **79**, 714 (1912).

** Spezifische Leitungsfähigkeit ist zu gering, als dass sie gemessen werden könnte.

Auch in Bezug auf die Triphenylphosphinlösung von $(Ph_3P)_2NiBr_2$ und $(Ph_3P)_2NiBr_22PhBr$ wurden die Leitungsfähigkeiten bestimmt und die Resultate wurden erhalten, wie aus der Tabelle VI zu ersehen.

TABELLE VI

LEITUNGSFÄHIGKEITEN VON $(Ph_3P)_2NiBr_2$ UND $(Ph_3P)_2NiBr_22PhBr$ IN GESCHMOLZENEM Ph_3P

Komplex	Verdünnungsgrad (cm^3.)*	Temp. (°C)	Mol. Leitungsfähigkeit (Ω^{-1})
$(Ph_3P)_2NiBr_2$	4.06×10^4	200	**
Smp. 219–22°	4.06×10^3	200	**
	4.06×10^2	200	**
	4.06×10	200	4.76×10^{-6}
	„	180	2.75×10^{-6}
	„	160	9.51×10^{-7}
$(Ph_3P)_2NiBr_22PhBr$	3.99×10^4	250	**
Smp. 270°	3.99×10^3	250	**
	3.99×10^2	250	3.74×10^{-4}
	„	220	2.34×10^{-4}
	„	200	1.49×10^{-4}
	3.99×10	250	1.28×10^{-4}
	„	220	8.78×10^{-5}
	„	200	6.78×10^{-5}

*, ** Vgl. Tabelle V.

Struktur der Komplexverbindungen

Von den Resultaten der Leitungsfähigkeiten wurde es klar, dass alle drei Typen Komplexverbindungen als Nichtelektrolyte angesehen werden können. Betreffs des $(Ph_3P)_2NiX_2$ kommt es nicht in Betracht, da dessen Konfiguration, welche die das Nickel als Zentralatom enthaltene ebene Konfiguration nach dem Arbeiten von Jensen über den Triäthylphosphinabkömmling analogisch erwartet werden soll, durchaus als Nichtelektrolyt angesehen wird.

Was die anderen zwei Verbindungen betrifft, so steht das nun in Frage. Wir möchten unsere Meinung darüber qualitativ beschreiben, da zur Entscheidung der genauen Konfiguration man die X-Strahlen- oder mindestens magnetische Untersuchungen durchführen muss. Um deren Konfigurationen festzustellen, haben wir die Erkenntnisse über das Absorptionsspektrum oder Dipolmoment suchen wollen, aber die genauen Resultate wegen des Auftretens der Dissoziation in einer Lösung, wie schon beschrieben, nicht erhalten können.

Zum Beispiel, hinsichtlich des $(Ph_3P)_2NiX_2RX'$ kann man bloss von den Resultaten der Leitungsfähigkeit allein keinen Schluss darüber ziehen, denn der Grund ist noch schwach, um die Wesenheit von Ionkomplex $(Ph_3RP)[Ni(PPh_3)X_2X']$, wenn er auch in geschmolzenem Triphenylphosphin elektrolytisch nicht dissoziiert, abzulehnen. Auch bei $(Ph_3P)_2NiX_22RX'$ könnte man eine salzartige Struktur $(Ph_3RP)_2(NiX_2X'_2)$ gar nicht ausser acht lassen.

Aber alles zusammengenommen, ist es hinreichend möglich, dass man die Struktur der 5- bzw. 6-Koordinationskomplexverbindungen annimmt.

In jüngster Zeit haben Burstall und Nyholm[9] in ihren Arbeiten über [Ni(*o*-Phenylenbisdimethyl-Arsin)$_2$Cl$_2$]Cl veröffentlicht, dass dessen echte Struktur durch Resonanzhybride dargestellt werde, zu welcher die Struktur mit der einfachen Bindung und die mit der Doppelbindung (π-Bindung), die sich unter Anwendung von 3d-Elektronenpaar des Nickelatoms und der vakanten d-Bahn des Arsenatoms bildet, wie folgt beitragen;

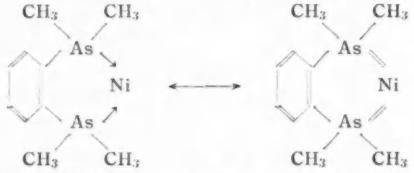

Bei $(Ph_3P)_2NiX_2$ möchten wir auch gleiche Erläuterung geben.

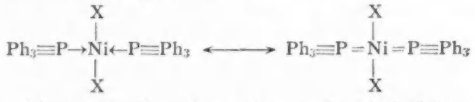

Unter der Annahme des wahrscheinlichen Doppelbindungscharakters der P-Ni Bindung kann man die Anlagerung von RX' zu der betreffenden Verbindung leicht erklären.

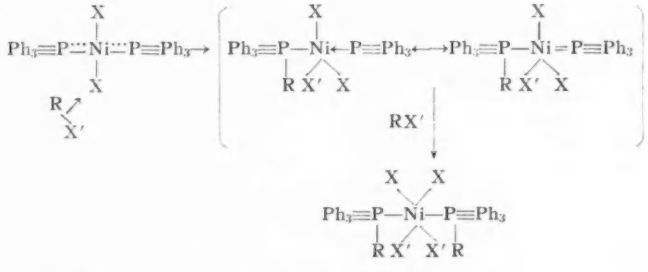

9) A. Burstall und R. Nyholm, *J. Chem. Soc.*, **1952**, 3570.

Auch die sekundäre Anlagerung von RX′ kann man ebenfalls dadurch so auffassen und die Resonanzhibride von $(Ph_3P)_2NiX_2RX'$ annehmen, wie oben gezeigt. Die leichte Umwandlung von Dialkylhalogenid zur Monoalkylhalogenidkomplexverbindung könnte man auch durch die verbesserte Beständigkeit von der letzteren aufgrund der Resonanz verstehen.

Ferner hinsichtlich der in der Mitteilung IV[1] beschriebenen Monochloressigsäuresnickel-Komplexverbindungen, wäre es vernünftiger, die 5- bzw. 6-koordinative Verbindung anzunehmen.

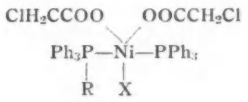

und

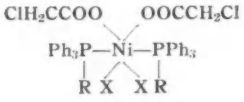

Von den obigen Meinungen und von den Werten der Leitungsfähigkeiten wagen wir die Behauptung, dass solche Komplexverbindungen jede für sich 5- bzw. 6-koordinative Verbindung sind.

Von nun an wollen wir sie bequemlichkeitshalber wie folgt bezeichnen.
(Ph_3RP)-$Ni(PPh_3)X_2X'$ für $(Ph_3P)_2NiX_2RX'$ und
$(Ph_3RP)_2 : NiX_2X'_2$ für $(Ph_3P)_2NiX_22RX'$.

Zusammenfassung

1. Von den Experimenten über das thermische Verhalten sowohl als auch über die Zersetzung der Komplexverbindungen in Methanol wurde gezeigt, dass RX′ in $(Ph_3P)_2$ NiX_2RX' oder $(Ph_3P)_2NiX_2RX'$ durch die Nebenvalenz an $(Ph_3P)_2NiX_2$ nicht verbunden ist. Beide Verbindungen sollen vielmehr mit den folgenden Formeln ausgedrückt werden:

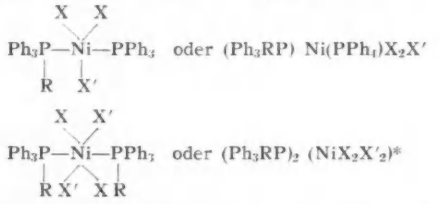

Unter der Annahme solcher Strukturen ist aufzuklären, dass alle Halogenatome die gleiche Stelle an Nickel einnehmen, und dass $(Ph_3P)_2NiBr_22PhCl$ und $(Ph_3P)_2NiCl_22PhBr$ eine gleiche Verbindung sind.

2. Es wurde bei der Zersetzung sowohl von $(Ph_3P)_2NiX_2RX'$ als von $(Ph_3P)_2NiX_22RX'$ in Methanol beobachtet, dass das Halogenatom mit schwerem Atomgewicht sich als Phosphoniumhalogenid stets von der Komplexverbindung trennt. Bei der thermischen Zersetzung von $(Ph_3P)_2NiX_2RX'$ ist auch die Lage der Dinge gleich.

3. Durch die Messung der Leitungsfähigkeit der Komplexverbindungen in geschmolzenem Triphenylphosphin erfolgt, dass $(Ph_3P)_2NiX_2$, $(Ph_3P)_2NiX_2RX'$ und $(Ph_3P)_2$ NiX_22RX' all die Nichtelektrolyte sind. Auf Grund dieser Resultate haben wir über ihre Strukturen betrachtet und die Behauptung gewagt, dass die letzten zwei Verbindungen jede für sich 5- bzw. 6- koordinative Verbindung seien.

Die Herren Dr. K. Yoshikawa und K. Ohga haben uns stets bei unseren Arbeiten leitend unterstützt und ermutigt. Wir sagen diesen Herren und der Mitsui Chemical Industry Co., die uns diese Veröffentlichung unserer Arbeiten erlaubte, hierdurch unseren herzlichen Dank.

Mitsui Chemical Industry Co. Ltd.,
Miike Dyestuff and Chemical
Works, Omuta, Fukuoka

* Reppe hat erst in seinen Vorträgen zum Andenken an das 75. Jubiläum der japanischen chemischen Gesellschaft veröffentlicht, dass Komplexverbindung $[(C_6H_5)_3P(C_4H_9)]_2NiBr_4$ bei der Butylacrylatsynthese als Katalysator verwendet wird.

Zur Kenntnis über die Hochdrucksynthese von Acrylester. VI. Mechanismus der Aktivierung des Kohlenoxyds an Triphenylphosphin-Nickelkomplexverbindungen

Von Kazumi YAMAMOTO

(Eingegangen am 21. April 1954)

Einleitung

In der vorigen Mitteilung[1] habe ich vorgeschlagen, die Triphenylphosphin-Nickelkomplexverbindungen von Typus $(Ph_3P)_2NiX_2RX'$ und $(Ph_3P)_2NiX_22RX'$, worin Ph den Phenylrest, R den Alkyl- oder Arylrest ausdrückt und X und X' selbes oder verschiedenes Halogenatom bedeuten, beziehungsweise als (Ph_3RP)-Ni (PPh_3) X_2X' und $(Ph_3RP)_2 : NiX_2X_2'$ zu bezeichnen. In dieser Mitteilung soll der Mechanismus der Aktivierung des Kohlenoxyds an Komplexverbindungen bei der Acrylestersynthese erörtert werden.

Über den betreffenden Mechanismus sind die $Ph_3PNi(CO)_3$-Theorie von McKinley[2] und die Hypothese von Schweckendiek, die in Copenhavers Buch[3] beschrieben ist, bekannt.

Um es kurz zu sagen, ist die Hypothese von McKinley wie folgt: Nickelcarbonyl mit der tetrahedrischen Struktur gibt unter der Umsetzung mit einem Molekül von Triphenylphosphin das wahrscheinlich verzogene Triphenylphosphin-Nickelcarbonyl $Ph_3PNi(CO)_3$, das durch das Nahekommen des Acetylens unter der Abgabe von einem Molekül Kohlenoxyd die Zwischenverbindung $Ph_3PNi(CO)_2(C_2H_2)$ liefert. Das $Ph_3PNi(CO)_3$ wird durch die Einwirkung von Kohlenoxyd auf solche instabile Zwischenverbindung wiedererzeugt, wobei das aktive Cyclopropenon sich bildet. Nach meinem Experiment jedoch hatte das $Ph_3PNi(CO)_3$ die katalytische Wirkung durchaus nicht.

Dementgegen scheine es, dass die Hypothese von Schweckendiek aus den drei verschiedenen Gedanken bestände. Das heisst;

1) $(Ph_3P)_2NiX_2$ gibt mit Kohlenoxyd unter der Abgabe von den Triphenylphosphinresten das sehr aktive $(CO)_2NiX_2$, das wieder mit Triphenylphosphin umsetzt und aktiviertes Kohlenoxyd abgibt.

$$(Ph_3P)_2NiX_2+2CO \rightleftarrows (CO)_2NiX_2+2Ph_3P$$

Dabei spielt Alkylhalogenid die Rolle, die Nebenreaktion vom Katalysator selbst zu hemmen.

2) Bei $(Ph_3P)_2NiX_2RX'$ (er behauptet, dass RX' sich durch die Nebenvalenz mit $(Ph_3P)_2NiX_2$ verbände) wird Alkylhalogenid reversibel durch Kohlenoxyd umgesetzt, wobei das Kohlenoxyd aktiviert wird

3) Der letzte Mechanismus wird nur schematisch dargestellt;

$$2(Ph_3P)_2NiBr_2RBr \xrightarrow{RBr} (Ph_3P)_3(NiBr_2)_2RBr + (Ph_3RP)Br$$

$$(Ph_3P)_3(NiBr_2)_2RBr + CO \rightarrow (Ph_3P)_3(CO)(NiBr_2)_2RBr$$

$$(Ph_3P)_3(CO)(NiBr_2)_2RBr + (Ph_3RP)Br \xrightarrow[C_2H_2]{R'OH} CH_2{:}\,CHCOOR' + 2(Ph_3P)_2NiBr_2RBr$$

Es scheint, dass es seinen Gedanken an der Folgerichtigkeit fehlt. Darüber hinaus wird von mir festgestellt, dass Alkylhalogenid sich nicht nur durch die Nebenvalenz mit $(Ph_3P)_2NiX_2$ verbindet.

Reaktion von Komplexverbindungen mit Kohlenoxyd

Als ein Mittel zur Forschung vom Mechanismus der Aktivierung des Kohlenoxyds am Komplexkatalysator wurden die Verhalten von den typischen Vertretern, wie $(Ph_3P)_2NiBr_2$, $[Ph_3(C_4H_9)P]$-$Ni(PPh_3)Br_3$ und $[Ph_3(C_4H_9)P]$-$Ni(PPh_3)Br_3+C_4H_9Br$ (anstatt des unisolierbaren $[Ph_3(C_4H_9)P]_2 : NiBr_4$), gegen das unter Druck stehende Kohlenoxyd in Anwesenheit von Butanol beobachtet. Ich verhinderte dadurch das Reaktionsgemisch mit der Gefässwand in Berührung zu kommen, indem ich in einem Autoklav 100 cm³ Inhalt ein geöffnetes Glasgefäss von zirca 50 cm³ Inhalt (Figur 1.) einsetzte, in welchem 20 cm³ Butanol und 5 g Komplexverbin-

Fig. 1.

1) K. Yamamoto und M. Oku, Dieses Bulletin, **27** 509, (1954).
2) C. McKinley, *Ind. Eng. Chem.*, **44**, 995 (1952).
3) J. Copenhaver und M. Bigelow, „Acetylene and Carbonmonoxide Chemistry", Rheinhold Publ. Co., (1949), S. 261

dung enthalten waren. Die Reaktionsbedingungen wurden wie folgt bestimmt: Anfangsdruck von Kohlenoxyd 15 Atm Reaktionstemperatur 180°, Laufzeit 1 Stunde.

1) **$(Ph_3P)_2NiBr_2$.** — Unter den Reaktionsbedingungen wurde einiger Druckabfall beobachtet. Nach der Abkühlung wurde die Bildung von Nickelcarbonyl durch die Rauchreaktion mit Bromdampf nachgewiesen. Das Reaktionsgemisch (hellgrün) liegen gelassen, schied sich der weisse Kristall ab' der bei 123° unter der Zersetzung schmilzt, und der als für $Ph_3PNi(CO)_3$ (vgl. Mitteilung III[4]) angesehen werden kann. Nach der Abscheidung vom Kristall die Mutterlauge unter dem Rückfluss gekocht, wurde der andere Kristall vom Schmelzpunkt 206° mit der Bildung des Nickelspiegels erhalten. Dies ist im Sinne folgenden Schemas zu erklären:

$$2Ph_3PNi(CO)_3 \longrightarrow Ni(CO)_4 + (Ph_3P)_2Ni(CO)_2 \text{ Smp. } 209°$$
$$\hookrightarrow Ni + 4\ CO$$

Wenn man die Mutterlauge nach der Beseitigung solch unlöslicher Substanzen noch einmal konzentriert, so kann man einen grünen Kristall (ca. 2g) nebst der kleinen Menge Triphenylphosphin (Smp. 79°C) erhalten. Der aus Butanol umkristallisierte schmilzt bei 178° und zeigt keinen Schmelzpunktabfall bei der Mischprobe mit $(Ph_3(C_4H_9)P)$-$Ni(PPh_3)Br_3$···d.h.,$(Ph_3P)_2NiBr_2C_4H_9Br$ ···(Smp 178°).. Das Erstaunliche ist, dass die ursprüngliche Substanz $(Ph_3P)_2NiBr_2$ gar nicht nachgewiesen wurde. Was die Bildung des $[Ph_3(C_4H_9)P]$-$Ni(PPh_3)Br_3$ betrifft, so kann man sich des Herstellungsverfahrens desselben aus $(Ph_3P)_2NiBr_2$ und Brom in Anwesenheit von Butanol erinnern[1]. Das heisst wird der Reaktionsverlauf den folgenden Gleichungen gemäss dargestellt;

$$(Ph_3P)_2NiBr_2 + 2CO \rightarrow (Ph_3P)_2Ni(CO)_2 + 2Br \text{ oder}$$
$$(Ph_3P)_2NiBr_2 + 3CO \rightarrow Ph_3PNi(CO)_3 + Ph_3P + 2Br$$
$$2(Ph_3P)_2NiBr_2 + 4C_4H_9OH + 2Br \rightarrow 2(Ph_3(C_4H_9)P)\text{-}Ni(PPh_3)Br_3 + C_3H_7COOC_4H_9 + 2H_2O$$

Auch bei der Acrylestersynthese unter der Anwendung vom gleichen Glasgefäss wurden die Bildungen von $(Ph_3P)\,Ni\,(CO)_3$ und $[Ph_3\,(C_4H_9)\,P]$-$Ni\,(PPh_3)\,Br_3$ festgestellt. Davon folglich wird die so wichtige Tatsache angedeutet, dass die katalytische Wirkung von der Komplexverbindung $(Ph_3P)_2NiX_2$ wirklich die von (Ph_3RP)-$Ni(PPh_3)X_3$ sei.

2) **$[Ph_3\,(C_4H_9)\,P]$-Ni $(PPh_3)\,Br_3$·····$[(Ph_3P)_2$-$NiBr_2C_4H_9Br]$.** — Unter den ganz gleichen Bedingungen reagiert diese Komplexverbindung mit Kohlenoxyd fast nicht. Sie wurde meistens ohne Veränderung zurückgewonnen.

3) **$[Ph_3\,(C_4H_9)\,P]_2$: $NiBr_4$···$[(Ph_3P)_2\ NiBr_2$-$2C_4H_9Br]$.** — Wie bisher wiederholt gesagt, wurde $[Ph_3\,(C_4H_9)\,P]$-$Ni\,(PPh_3)\,Br_3$ zusammen mit einem Molekül Butylbromid zur Probe angewandt, da die Komplexverbindung dieses Typus unisolierbar ist. In diesem Falle, wird nach der Reaktion Nickelcarbonyl im Abgase nachgewiesen und die erheblichen Mengen des wasserlöslichen Kristalls mit Smp. 235° und des Nickelbromids wurden vom Reaktionsgemisch aus erhalten. Der Kristall wird für Triphenylbutylphosphoniumbromid (Smp. 235°[1]) identifiziert. Es ist zwar schwierig, den Wiederspruch zwischen solchem Verhalten und der katalytischen Wirkung[5] dieses Typus aufzuklären. Jedoch kann man das Sein der Komplexverbindung dieses Typus und das Auftreten der folgenden Reaktion erwarten:

$$[Ph_3(C_4H_9)P]_2 : NiBr_4 + 4CO \rightarrow 2[Ph_3(C_4H_9)P]Br + \underset{\downarrow}{Ni(CO)_4} + \underset{\uparrow}{Br_2}$$
$$NiBr_2 + 4CO$$

Der Mechanismus der Aktivierung des Kohlenoxyds

1) **Mechanismus an $(Ph_3P)_2NiBr_2$.** — Wie in der Einleitung beschrieben, wird nach Schweckendiek der Mechanismus an $(Ph_3P)_2$-NiX_2 gemäss der Gleichung dargestellt:

$$(Ph_3P)_2NiX_2 + 2CO \rightleftarrows 2Ph_3P + (CO)_2NiX_2$$

Es wurde jedoch erklärt, dass die katalytische Wirkung dieser Komplexverbindung, wie in dem vorigen Paragraphen dargestellt, auf die von (Ph_3RP)-$Ni\,(PPh_3)\,X_3$ zurückzuführen ist. Die betreffende Gleichung wird wiedergegeben:

$$3(Ph_3P)_2NiX_2 + 3CO + 4ROH \rightarrow 2(Ph_3RP)\text{-}Ni(PPh_3)X_3 + Ph_3PNi(CO)_3 + Ph_3P + 2H_2O + R'COOR$$

Verläuft demnach diese Umsetzung quantitativ, so soll sich 2/3 Molekül (Ph_3RP)-$Ni(PPh_3)X$ aus einem Molekül $(Ph_3P)_2NiX_2$

4) K. Yamamote, Dieses Bulletin, **27**, 501 (1954).
5) K. Yamamoto und M. Oku, Dieses Bulletin, **27**, 505 (1954)

bilden. Die Wahrheit zu sagen, bleibt die Bildung von demselben wahrscheinlich zwischen 2/3 und 1/3 Molekül, wegen der Nebenreaktion wie Bildung von Nickelcarbonyl. Auf solche Weise begreift es sich, dass die katalytische Fähigkeit der ursprünglichen Komplexverbindung zwischen dem äquivalenten (Ph_3RP)-$Ni(PPh_3)X_3$ und NiX_2 steht.

2) Mechanismus an (Ph_3RP)-$Ni(PPh_3)X_2X'$.—Die wichtige Frage ist also der Mechanismus an der Komplexverbindung (Ph_3RP)-$Ni(PPh_3)X_3$.

Meine von bisher beschriebenen Tatsachen geschlossene Meinung über die betreffende Aufgabe wird schematisch augenscheinlich so dargestellt;

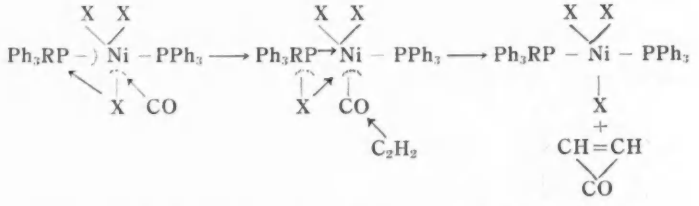

$$(Ph_3RP)\text{-}Ni(PPh_3)X_3 + CO \rightleftarrows (Ph_3RP)X + Ni(PPh_3)(CO)X_2$$

Das heisst, dieser Mechanismus ist so zu erklären, dass zuerst mit Kohlenoxyd das aktive, instabile 4-koordinative $Ni(PPh_3)$-$(CO)X_2$ unter der augenblicklichen Bildung von Phosphoniumhalogenid entsteht, das unter der Abgabe von aktiviertem Kohlenoxyd mit solchem Phosphoniumhalogenid die ursprüngliche Komplexverbindung wiedererzeugt. Der Grad, unter welchem die Bindung zwischen dem Nickel und Halogenatom unter dem Angriffe von Kohlenoxyd abgebrochen wird, ist desto grösser, je nichtionischer die betreffende Bindung ist, d.h., je schwerer das Atomgewicht des betreffenden Halogens ist, desto grösser wird die katalytische Wirkung der Mutterverbindung, wie bei dem anorganischen Nickelhalogenid[5].

Nach dieser Theorie ist das unter der Selektivität von schwerem Halogenatom zur Umsetzung mit Kohlenoxyd so zu erklären, dass die katalytische Wirkung der Komplexverbindung (Ph_3RP)-$Ni(PPh_3)X_2X'$ (wobei $X \neq X'$) beinahe mit der, der mit all demselben, schweren Halogenatom identisch ist.[5]

Auch die Erscheinung, welche bei der Zersetzung von solcher Mischhalogen-Komplexverbindung in Methanol nur Phosphoniumhalogenid mit schwerem Halogenatom stets nachgewiesen wird, trägt sicher gross zur Selektivität von Halogen-Kohlenoxyd-Umsetzung bei. Mit anderen Worten dürfte die Bindungsenergie zwischen dem Phosphoniumrest und Halogenatom sehr bedeutend sein. Auch der in Mitteilung IV[5] beschriebene Schluss über die Art und Nummer vom Halogenatom wird durch diese Theorie aufgeklärt werden. Das heisst, man kann die Zunahme von der katalytischen Fähigkeit mit der zunehmenden Nummer Halogenatom in der Komplexverbindung unter der Vergrösserung der Probabilität des Zusammenstosses vom Halogenatom mit Kohlenoxyd verstehen.

Solche Komplexverbindung, wie sie nur ein Halogenatom besitzt, das mit Nickel unmittelbar gebunden ist, z. B., $(Ph_3P)_2$-$Ni(OOCCH_2Cl)_2RX$ oder (Ph_3RP)-$Ni(PPh_3)$-$(OOCCH_2Cl)_2X$, soll die katalytische Fähigkeit haben[5], da diese Theorie wesentlich auf Grund der reversibelen Umsetzung von Kohlenoxyd mit einem Halogenatom ist.

3) Mechanismus an $(Ph_3RP)_2 : NiX_2X'_2$.—Es ist nun zweifellos, auch im Falle, dass R Alkyl ist, dass die Komplexverbindung $(Ph_3RP)_2 : NiX_2X'_2$ existiert, wenn gleich sie unisolierbar ist. Darüber hinaus drückt sich der Mechanismus der Aktivierung des Kohlenoxyds an dieser Komplexverbindung gemäss dem von (Ph_3RP)-$Ni(PPh_3)X_2X'$ schematisch aus;

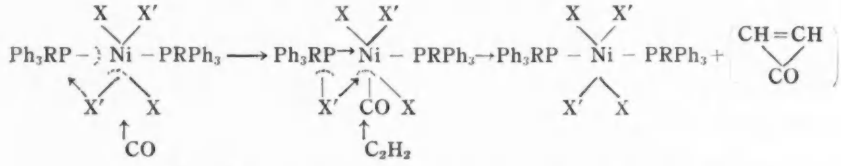

$$(Ph_3RP)_2 : NiX_2X'_2 + CO \rightleftarrows (Ph_3RP)X' + (Ph_3RP)\text{-}Ni(CO)X_2X'.$$

Die Erläuterung sowohl vom Schema, als von der Bedeutung von Halogenatom (insbesondere von dem mit schwerem Atomgewicht) ist ebenfalls zu erklären wie in dem vorigen Paragraphen beschrieben. Die Tatsache, dass die katalytische Fähigkeit der Komplexverbindung dieses Typus grösser als die der entsprechenden Verbindung (Ph_3RP)-$Ni(PPh_3)X_2X'$ ist[5], wird man unter der Vergrösserung der Probabilität des Zusammenstosses sowohl von Halogenatom mit dem Phosphoniumrest, der als Halogenakzeptor wirkt, wie von Halogenatom mit Kohlenoxyd mit der zunehmenden Nummer von Halogenatom und Phosphoniumrest verstehen können. Nach meiner Theorie spielt überschüssiges Alkylhalogenid eine wichtige Rolle zur Erhaltung der Komplexverbindung dieses Typus, $(Ph_3RP)_2 : NiX_2X'_2$.

Die in vorigem Paragraphen beschriebene Tatsache, dass das $[Ph_3(C_4H_9)P]$ Br sich durch die Umsetzung von $[Ph_3(C_4H_9)P]_2 : NiBr_4$ mit dem unter Druck stehenden Kohlenoxyd in Abwesenheit von Acetylen als Akzeptor vom aktiven Kohlenoxyd bildete, bestätigt die Gültigkeit der oben erwähnten Theorie.

Um es kurz zu sagen, kann die zur Bildung von Cyclopropenon benötigte Aktivierungsenergie durch die Bildung der intermediären Kohlenoxyd-Komplexverbindung erniedrigt werden.

4) Mechanismus an NiX_2.—Vormals habe ich[6] mit meinem Mitarbeiter über die Acrylestersynthese in Anwesenheit vom Nickelhalogenidkatalysator und über das Verhalten des Kohlenoxyds mitgeteilt.

Ich möchte auf Grund der Erkenntnisse zum Mechanismus der Aktivierung des Kohlenoxyds am Komplexkatalysator wiederum über den betreffenden Mechanismus an NiX_2 Betrachtungen anstellen.

Wie schon mitgeteilt, hätte man von den verschiedenen experimentellen Tatsachen erwarten können, dass die Erniedrigung der zur Bildung des Cyclopropenons erforderlichen Aktivierungsenergie, durch die Bildung irgendeines intermediären Zwischenproduktes, das sich durch die Umsetzung von Kohlenoxyd und Nickelhalogenid, bevor das Nickelcarbonyl zusammengesetzt wird, bildet, erreicht wird.

Folgert man diese Annahme aus dem oben erwähnten Mechanismus am Komplexkatalysator, so dürfte man die Analogie zwischen den beiden Mechanismen finden. Bei der einfachen halogenhaltigen Nickelverbindung existiert nicht eine solche günstige Verbindung wie NiYX, wobei Y den Rest wie $ClCH_2COO$- ausdrückt. Es ist also zwar schwierig, diese Annahme experimentell darzutun, aber der Mechanismus an NiX_2 könnte nach Analogie von demselben am Komplexkatalysator dargestellt werden, wie folgt:

$$NiX_2 + CO \rightleftarrows NiX(CO) + X$$

Dies ist so zu erklären, dass das Nickelhalogenid mit einem Molekül Kohlenoxyd zunächst das unisolierbare, sicher sehr instabile NiX(CO) liefert, das unter Abgabe von aktiviertem Kohlenoxyd mit Halogenatom das Nickelhalogenid wieder erzeugt. Die meisten Halogenatome könnten sich auf solche Weise reversibel verlaufen, aber sie migrieren zum Teil zu unwirksamen Verbindungen. Und dies geht zum Schlusse die wirkliche Konzentration des Nickelhalogenids nieder. Die Hilfskatalysatorwirkung des metallischen Nickels könnte sich daraus erklären, dass das Nickel hauptsächlich die Rolle als Akzeptor dieser migrierenden Halogenatome unter dem Beitrag zur Erhaltung der wirklichen Konzentration des Nickelhalogenids spielt.

Auf solche Weise ist der Mechanismus an der Komplexverbindung mit dem an dem anorganischen Nickelhalogenid-Katalysator im wesentlichen nicht zu unterscheiden. Worauf beruht die Vorzüglichkeit des Komplexkatalysators, wenn das der Fall ist? Meine Antwort für die obige Aufgabe ist wie folgt:

1) Der Zusammenbruch vom Katalysator auf Grund der Migrierung des Halogens ist sehr wenig, da er in eigenem Molekül den mächtigen Akzeptor "Phosphoniumrest" für solches Halogenatom enthalten ist.

2) Die Bindung zwischen Nickel- und Halogenatom nimmt im nichtionischen Charakter durch die Koordination von Triphenylphosphin oder Phosphoniumrest an Nickelatom zu.

Ausserdem soll angegeben werden, d.h., die ausserordentliche Kristallisierbarkeit oder grosse Löslichkeit gegen ein organisches Lösungsmittel auf Grund des zunehmenden organischen Charakters der Nickelverbindung.

Zusammenfassung

Auf Grund der bisher erwähnten Tatsachen habe ich über den Mechanismus der Aktivierung des Kohlenoxyds an Triphenylphosphin-Nickelkomplexverbindungen die folgenden Schlüsse erhalten.

1) Die katalytische Wirkung von $(Ph_3P)_2$-NiX_2 Typus Komplexverbindung ist auf die von (Ph_3RP)-$Ni(PPh_3)X_3$ – $(Ph_3P)_2NiX_2RX$ –

6) K. Yamamoto und K. Sato, Dieses Bulletin, **27**, 496 (1954).

zurückzuführen.

2) Der Mechanismus an (Ph_3RP)-$Ni(PPh_3)$-X_2X' Komplexverbindung ist wie folgt zu formulieren:

$$(Ph_3RP)\text{-}Ni(PPh_3)X_2X' + CO \rightleftarrows (Ph_3RP)X' + Ni(PPh_3)(CO)X_2$$

Das heisst, dieser Mechanismus ist so zu erklären, dass zuerst mit Kohlenoxyd das aktive, instabile 4-koordinative $Ni(PPh_3)(CO)X_2$ unter der augenblicklichen Bildung von Phosphoniumhalogenid entsteht, das unter der Abgabe von aktivem Kohlenoxyd mit solchem Phosphoniumhalogenid die ursprüngliche Komplexverbindung wiedergibt.

3) Der Mechanismus an $(Ph_3RP)_2 : NiX_2X'_2 - (Ph_3P)_2NiX_2 2RX'$ – ist ebenso auch wie folgt zu formulieren;

$$(Ph_3RP)_2 : NiX_2X'_2 + CO \rightleftarrows (Ph_3RP)X' + (Ph_3RP)\text{-}Ni(CO)X_2X'$$

4) Der Mechanismus an Nickelhalogenid ist nach Analogie von dem an Komplexverbindungen zweckmässiger wie folgt, zu illustrieren

$$NiX_2 + CO \rightleftarrows NiX(CO) + X$$

5) Die Vorzüglichkeit der Komplexkatalysatoren wird wie folgt dargestellt:

a) Die Komplexverbindungen sind in eigenem Molekül den mächtigen Akzeptors "Phosphoniumrest" für Halogenatom enthalten.

b) Die Zunahme vom nichtionischen Charakter der Bindung Ni-Halogen auf Grund der Koordination von dem Triphenylphosphin oder Phosphoniumrest an Nickelatom.

Herr Dr. K. Yoshikawa hat mich stets bei meinen Arbeiten leitend unterstützt und ermutigt. Die Herren M. Oku und K. Sato haben mit mir eifrig mitgearbeitet und Beistand durch lebhafte Diskussion über diesen Gegenstand geleistet. Ich sage diesen Herren und der Mitsui Chemical Industry Co., die mir diese Veröffentlichung meiner Arbeiten erlaubte, hierdurch meinen herzlichen Dank.

Mitsui Chemical Industry Co. Ltd.
Miike Dyestuff and Chemical
Works, Omuta, Fukuoka

Radiochemical Studies on Ultra-Micro Quantities of Organometallic Compounds. II. On the Composition of Polonium Dithizonate

By Tomitaro ISHIMORI

(Received November 11, 1953)

Previously the author[1] has reported on the formation of polonium dithizonate which is extracted into a carbon tetrachloride solution of dithizone (diphenylthiocarbazone) from an aqueous solution under some appropriate chemical circumstances. Further there is a literature[2] which shows that the complex salt can be used in the purification of polonium; however, the present author could not find out any report on the composition of polonium dithizonate.

In the present paper, the composition of polonium dithizonate (formed in a solution acidified with nitric acid) is determined according to the method described in the first paper[3] of this series and the author estimates that two anions of dithizone are bound to one atom of polonium in polonium dithizonate.

(A) Preparation of the Polonium Solution. —The polonium solution used is a solution of radium F which is prepared as follows:

1.5 g. powdered pitchblende are dissolved in nitric acid. The undissolved residue is filtered off after the solution is diluted with water. The filtrate is treated with hydrogen sulfide to precipitate polonium (radium F) with lead and some other elements of the hydrogen sulfide group which may occur in the starting material. The precipitate is dissolved in nitric acid, and the residue containing sulfur is filtered off. The filtrate is diluted until the content of nitric acid becomes about 2.5% (vol.), and then extracted successively with some portions of the chloroform solution of dithizone. The combined chloroform solution is shaken with 10 cc. of (1:1) nitric acid to obtain an aqueous solution of polonium. The aqueous solution is separated, diluted to about 20 cc. with water, and preserved as the stock solution.

1) T. Ishimori and H. Sakaguchi, *J. Chem. Soc. Japan*, **71**, 327 (1950).
2) G. Bouissieres and C. Ferrandini, *Anal. Chim. Acta*, **4**, 610 (1950).
3) T. Ishimori, This Bulletin, **27**, 139 (1954).

The resultant solution contains about 25% (vol.) nitric acid and about 10^{-2} curie radium F (about 10^{-12} g. P_0) per 1 cc. The radioactivity due to the alpha emission of the evaporated residue of the solution is measured by an electroscope (gold leaf type) made by the Scientific Research Institute, Tokyo. The decay of the radioactivity shows that the half-life is about 140 days (Fig. 1). On the other hand, the extremely weak beta-rays are detected by a Geiger-Müller counter. Therefore, this solution seems to contain slight contaminations of radium E and other isotopes.

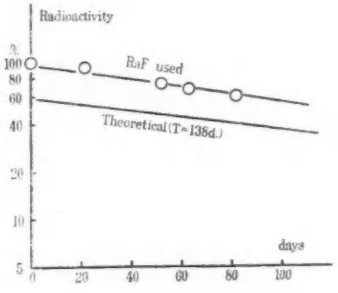

Fig. 1. Decay of RaF

(B) Determination of the Composition of Polonium Dithizonate.—In the first paper[3] of this series, the author gave a method for the determination of the composition of an organo-metallic compound in an ultra-micro amount, basing his conclusions on the following relation:

$$E^{-1}=A+B(HR)^{-n}$$

where, E is extractability, the ratio of the radioactivity due to the total amount of the radioactive metallic cation taken into the system and that extracted into the organic phase, n, the ratio between the number of organic anions and that of the metallic cation, and A and B are constants.

According to the method, the composition of polonium dithizonate is determined by repeating the measurement of extractability for various amounts of dithizone, (HDz), plotting the results in $E^{-1}-(HDz)^{-1,2,3}$ diagrams, and finding out $(HDz)^{-n}$ which is almost linear to E^{-1}. In these experiments, all experimental conditions such as pH and volume of the aqueous phase or volume of the organic phase, must be kept constant. Otherwise the above equation can not be used as the theoretical basis.

(1) Series of Experiments I.—10 cc. of distilled water and 1.0 cc. of the stock solution of polonium are respectively added to six small separating funnels. Though the solutions are not buffered, the pH values are supposed to be fairly constant as they contain about 2.2% (vol.) of nitric acid. Therefore, the necessary condition for a constant pH value[3] is almost satisfied in this case.

5.0 cc. of the dithizone chloroform solutions with various concentrations are prepared by diluting the stock solution of dithizone in chloroform (about 0.4×10^{-3} mol./l.)[4] and added to each separating funnel which contains the diluted aqueous solution of polonium. The funnels are shaken vigorously for a minute.

The separated chloroform layers are evaporated up in glass dishes to measure the radioactivities due to the fractions of radium F which are extracted into the chloroform solution.

The measured intensities[5] are compared with that of the standard specimen which is prepared by evaporating 1 cc. of the stock solution of polonium in a glass dish, and the extractability, E, is calculated.

The results obtained are shown in Table I and Fig. 2(a,b,c).

TABLE I

RESULTS OF (E, 1)

No.	(HDz)	$(HDz)^{-1}$	$(HDz)^{-2}$	$(HDz)^{-3}$	d/m $P_{0\,extd.}$	E^{-1}
1	0.96	1.04	1.09	1.13	11.75	1.31
2	0.42	2.38	5.66	13.5	10.33	1.49
3	0.080	12.5	156	1.95×10^{3}	3.43	4.48
4	0.032	31.2	974	3.04×10^{4}	0.87	17.7
5	0.024	41.7	1740	6.97×10^{4}	0.55	28.0
6	0.000	∞	∞	∞	−0.03	—

E: Extractability; The ratio of radioactivities due to radium F taken (15.39 d/m) and radium F extracted.

(HDz): Amount of dithizone denoted in an arbitrary unit in which $(HDz)=1$ corresponds to about 10^{-6} gram mol. dithizone.

4) The concentration of the chloroform solution of dithizone is determined by titrating known quantities of silver nitrate.

5) The radioactivity is measured by the electroscope mentioned above. The absorption of alpha-particles is checked by adding the stock solution of dithizone on the specimen of polonium and drying it up. The following table shows that the effect of the absorption is negligible.

ml. dithizone solution (added)	0	1	2
radioactivity measured (d/m)	18.8	19.2	19.4

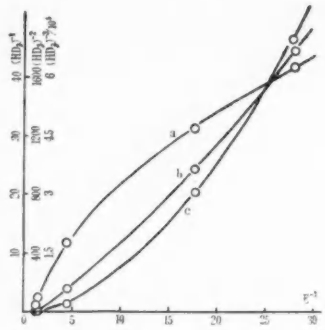

Fig. 2(a, b, c). $(HDz)^{-n}-E^{-1}$ diagram
a: $(HDz)^{-1}-E^{-1}$
b: $(HDz)^{-2}-E^{-1}$
c: $(HDz)^{-3}-E^{-1}$

(2) Series of Experiments II.—Almost the same experiments are repeated, but the procedures are slightly different from that of (1) in the following point: The aqueous solution of polonium is prepared by pipetting 4 cc. of the stock solution of polonium into a 50 cc. volumetric flask, and then adding water to the mark. After mixing thoroughly, 10 cc. of the diluted solution of polonium are taken to each separating funnel respectively. Therefore, the acidity of the aqueous solution is weaker than that of (1).

The results are shown in Table II as well as Fig. 3(a,b,c).

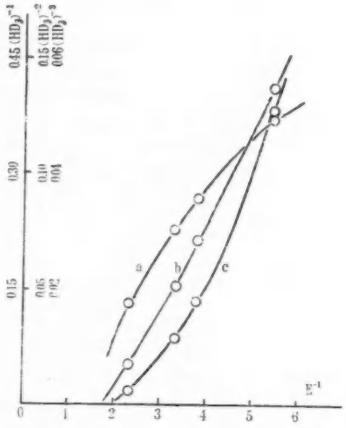

Fig. 3(a, b, c). $(HDz)^{-n}-E^{-1}$ diagram
a: $(HDz)^{-1}-E^{-1}$
b: $(HDz)^{-2}-E^{-1}$
c: $(HDz)^{-3}-E^{-1}$

TABLE II
RESULTS OF (B, 2)

No.	(HDz)	$(HDz)^{-1}$	$(HDz)^{-2}$	$(HDz)^{-3}$	d/m $P_{0\,extd.}$	E^{-1}
1	7.50	0.133	0.0176	0.0024	6.01	2.33
2	4.38	0.228	0.0519	0.0118	4.20	3.34
3	3.75	0.267	0.0713	0.0181	3.44	3.79
4	2.70	0.371	0.137	0.0509	2.39	5.45

E: Extractability; The ratio of radioactivities due to radium F taken (13.00 d/m) and radium F extracted.

(HDz): Amount of dithizone denoted in an arbitrary unit in which $(HDz)=1$ corresponds to about 10^{-8} gram mol. dithizone.

In these two series of experiments, the acidity of the aqueous solution is different. So the values of extractability given by both series do not coincide for a value of (HDz). However, the results of both series agree in the facts that almost linear relation is found between $(HDz)^{-2}$ and E^{-1} (cf. Fig. 2b and 3b), while the curve of $(HDz)^{-1}-E^{-1}$ is convex (cf. Fig. 2a and 3a) and that of $(HDz)^{-3}-E^{-1}$ is concave. Therefore according to the method described in the first paper of this study,[3] polonium dithizonate is supposed to have two anions of dithizone for one atom of polonium.

So far there is no generally accepted knowledge about the form in which polonium is dissolved in aqueous solutions. However G. v. Hevesy et al.[5] reported bivalent cation Po^{++} in hydrochloric acid solution. On the other hand M. Haissinsky[5] reported that PoO_3^{--} or PoO^{++} is prevailing in dilute nitric acid solution. So we can guess that polonium dithizonate will correspond to the chemical formula $PoDz_2$ or $PoODz_2$.

The author wishes to express has hearty thanks to Prof. Iwaji Iwasaki, Tokyo Institute of Technology, who was kind enough to send him some pitchblende for the preparation of radium F.

Department of Chemistry,
Faculty of Science,
Kyushu University,
Fukuoka

6) Gmelins Handbuch d. Anorganischen Chemie, 8 Auflage, System Nr. 12 (1941), Verlag Chemie, Berlin, S. 103-104.

Polarographic Diffusion Current Observed with Square Wave Voltage. I. Effect Produced by the Sudden Change of Electrode Potential

By Tomihito KAMBARA

(Received February 26, 1954)

In recent years several polarographic electrolyses with rectangular voltage have been reported, providing us many attractive findings. Therefore the present author intends to clear up at first the effects due to the sudden change of electrode potential and then the essential feature of electrolysis with square wave voltage theoretically and further elucidate some experimental results.

Note on the Boundary Condition

In order to discuss the diffusion current observed in the polarographic electrolysis, we must solve the system of differential equations for the diffusions of two materials, i.e. the oxydant (suffix O) and the reductant (suffix R), given by

$$\frac{\partial C_0}{\partial t}=D_0\frac{\partial^2 C_0}{\partial x^2}\ ;\quad \frac{\partial C_R}{\partial t}=D_R\frac{\partial^2 C_R}{\partial x^2}. \tag{1}$$

Since before the electrolysis, the initial uniform concentrations $^*C_0$ and $^*C_R$ govern the system, the initial condition is shown by

$$t=0,\ 0\leqq x\leqq\infty,\ C_0={}^*C_0,\ C_R={}^*C_R. \tag{2}$$

The boundary condition, on the other hand, depends on the experimental condition. In the case that the electrolysis is carried out under the application of a constant voltage, it is imagined that each of the concentrations of oxidant and reductant at the electrode surface takes a constant value immediately after the beginning of electrolysis. Such a conception has been given by Cottrel[1] and Ilkovic.[2] We have treated this problem while taking the rates of forward and reverse reactions of the electrode process into consideration[3]; the analogous treatments are also given by Meiman,[4] Smutek[5] and Delahay.[6] In this article, however, let us suppose that the ratio of the concentrations of both forms at the electrode surface is given by the Nernst formula, i.e. the velocities of the electrode processes in two directions are so great that an equilibrium state is always attained thereat. Therefore it is seen that

$$x=0,\ t>0,\ C_R=K_1\cdot C_0, \tag{3}$$

where the equilibrium constant K_1 depends on the electrode potential E_1 and is given by

$$K_1=\exp\frac{-nF(E_1-E_0)}{RT}. \tag{4}$$

In this equation the symbols n, F, R, T and E_0 are used in their usual significances. On the other hand, as for the flows of the diffusing oxidant and reductant, it is obvious that the material flow must be continuous everywhere, provided that there is no accumulation or disappearance at the electrode surface. Accordingly it is found that

$$x=0,\ t>0,\ D_0\frac{\partial C_0}{\partial x}=-D_R\frac{\partial C_R}{\partial x} \tag{5}$$

This condition can be rigorously obtained, as shown by Sevcik,[7] when the amount of oxydant disappearing in unit time is considered to be equal to the amount of reductant produced newly by the electrode reaction in unit time.

As is well known, the general integrals of Eqs. (1) are given by

$$C_0=a_0+b_0\cdot\mathrm{erf}\frac{x}{2\sqrt{D_0t}};$$

$$C_R=a_R+b_R\cdot\mathrm{erf}\frac{x}{2\sqrt{D_Rt}}. \tag{6}$$

From the above cited conditions, it is seen that among four integral constants, a_0, b_0, a_R and b_R, the following relationships hold.

$$\left.\begin{aligned} &a_0+b_0={}^*C_0;\quad a_R+b_R={}^*C_R;\\ &a_R=K_1a_0;\quad \sigma b_0=-b_R;\end{aligned}\right\}, \tag{7}$$

where

$$\sigma=\sqrt{D_0/D_R}\ .$$

Whence

$$\left.\begin{aligned} &a_0=\frac{\sigma{}^*C_0+{}^*C_R}{\sigma+K_1}={}^\infty_1C_0;\quad a_R=K_1\cdot a_0={}^\infty_1C_R;\\ &b_0={}^*C_0-{}^\infty_1C_0;\quad b_R={}^*C_R-{}^\infty_1C_R;\end{aligned}\right\} \tag{9}$$

where ${}^\infty_1C_0$ and ${}^\infty_1C_R$ are the respective interfacial concentrations corresponding to the constant potential E_1. Therefore, it follows that

$$\left.\begin{aligned} &C_0={}^\infty_1C_0+({}^*C_0-{}^\infty_1C_0)\cdot\mathrm{erf}\frac{x}{2\sqrt{D_0t}};\\ &C_R={}^\infty_1C_R+({}^*C_R-{}^\infty_1C_R)\cdot\mathrm{erf}\frac{x}{2\sqrt{D_Rt}}\end{aligned}\right\}. \tag{10}$$

Accordingly it is seen that in the integration of linear diffusion equation, upon supposing that the continuity of fluxes and an equilibrium state between the concentrations of two forms hold at the electrode surface, we have the result that

1) F. G. Cottrel, *Z. phys. Chem.*, **42**, 385 (1903).
2) D. Ilkovic, *Collection Czech. Chem. Communs.*, **6**, 498 (1934); *J. chim. physique*, **35**, 129 (1938).
3) T. Kambara and I. Tachi, This Bulletin, **25**, 135 (1952); T. Kambara, ibid., 281.
4) N. Meiman, *J. Phys. Chem. USSR*, **22**, 1454 (1948).
5) M. Smutek, *Chem. Listy*, **45**, 241 (1951); *Collection Czech. Chem. Communs.*, **18**, 171 (1953).
6) P. Delahay, *J. Am. Chem. Soc.*, **75**, 1430 (1953).
7) A. Sevcik, *Collection Czech. Chem. Communs.*, **13**, 349 (1948).

both interfacial concentrations have constant values.

This conclusion is identical with that given by Ilkovic,[2] by whose theory it is supposed that the boundary condition is given by

$$x=0,\ t>0,\ C_0={}^{i}C_0,\ C_R={}^{i}C_R. \tag{11}$$

It must be mentioned here, however, that there is no rational reason for the constancies of ${}^{i}C_0$ and ${}^{i}C_R$, as pointed out by MacGillavry.[3] It is seen, for example, that even if ${}^{i}C_0$ and ${}^{i}C_R$ are both certain functions of time t, it is possible that the ratio ${}^{i}C_0/{}^{i}C_R$ might be independent of time. And it is obvious that merely from the condition of an equilibrium state at the surface, the conclusion that the concentrations ${}^{i}C_0$ and ${}^{i}C_R$ are constant, respectively, can not result, while their ratio is readily seen to be constant. Nevertheless it is clear that by employing Eq. (5) the identity of the conclusions derived from the above two theories is confirmed. Further it must be remembered that although the same conclusion is attained by employing the two different boundary conditions, such an accordance can not be derived when the solution does not stretch to infinity in one dimension, or the electrode shows not a flat surface but a spherical one.

Discontinuous Change of the Electrode Potential

Now, let us consider the case when the potential of the observation electrode is discontinuously and abruptly changed as shown in Fig. 1; i.e. from $t=0$ the electrolysis begins under the application of potential E_1 and at $t=T$ the potential jumps from E_1 to E_2 discontinuously.

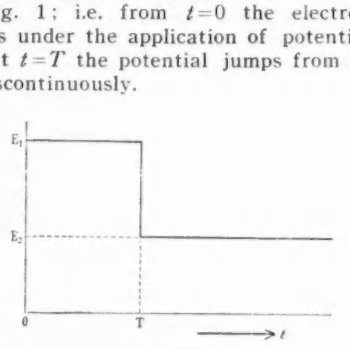

Fig. 1.

(1) Solution by Means of Laplace Transformation.—Let τ be the time elapsed after the potential was abruptly changed from E_1 to E_2; then it is clear that

$$\tau=t-T. \tag{12}$$

Hence our problem comes to integrate the equations:

$$\frac{\partial C_0}{\partial \tau}=D_0\frac{\partial^2 C_0}{\partial x^2}\ ;\quad \frac{\partial C_R}{\partial \tau}=D_R\frac{\partial^2 C_R}{\partial x^2} \tag{13}$$

with the initial condition shown by

$$\tau=0,\ x>0,$$
$$C_0=a_0+b_0\cdot\operatorname{erf}\frac{x}{2\sqrt{D_0T}}=C_0^{\pm}(x),$$
$$C_R=a_R+b_R\cdot\operatorname{erf}\frac{x}{2\sqrt{D_RT}}=C_R^{\pm}(x). \tag{14}$$

This condition is required by the above discussions. The boundary condition is, on the other hand, demonstrated by

$$x=0,\ \tau>0,\ D_0\frac{\partial C_0}{\partial x}=-D_R\frac{\partial C_R}{\partial x},\ C_R=K_2\cdot C_0, \tag{15}$$

where

$$K_2=\exp\frac{-nF(E_2-E_0)}{RT}. \tag{16}$$

This condition results from the principle of continuity of fluxes and the assumption of a state of equilibrium between the concentrations of the two forms at the interface.

By means of the Laplace transformation defined by

$$\mathfrak{L}C(x,\tau)=p\int_0^{\infty}e^{-p\tau}\cdot C\cdot d\tau=u(x,p),$$

we can finally obtain the formulae for u_0 and u_R; i.e. they can be written in the form

$$u=A\cdot e^{mx}+B\cdot e^{-mx}$$
$$+b\cdot\operatorname{erf}\frac{x}{2\sqrt{DT}}+2a\cdot\sinh\frac{mx}{2}$$
$$-\frac{b}{2}\cdot e^{mx+pT}\left\{\operatorname{erf}\left(\frac{x}{2\sqrt{DT}}+\sqrt{pT}\right)-\operatorname{erf}\sqrt{pT}\right\} \tag{17}$$
$$-\frac{b}{2}\cdot e^{-mx+pT}\left\{\operatorname{erf}\left(\frac{x}{2\sqrt{DT}}-\sqrt{pT}\right)+\operatorname{erf}\sqrt{pT}\right\},$$

where the subscripts O and R are omitted and the m's are shown by

$$m_0=\sqrt{p/D_0};\ m_R=\sqrt{p/D_R}. \tag{18}$$

Next the four integral constants A_0, B_0, A_R and B_R, can be determined by Eqs. (15) and (16). Then it can be readily seen that the transformations of the interfacial concentrations are given by

$${}^{\circ}u_0=A_0+B_0=\frac{\sigma^{*}C_0+{}^{*}C_R}{K_2+\sigma}=\mathfrak{L}_2^{\circ}C_0;$$
$${}^{\circ}u_R=A_R+B_R=K_2(A_0+B_0)=\mathfrak{L}_2^{\circ}C_R. \tag{19}$$

There is no doubt that these equations imply that the interfacial concentrations are independent of time τ and that they are equal to the equilibrium interfacial concentrations which are to be observed when the constant potential E_2 is applied throughout from $t=0$ continuously [Cf. Eq. (9)].

Next we will evaluate the current intensity. From Eq. (17) it follows that

$$\left(\frac{\partial u_0}{\partial x}\right)_{x=0}=\sqrt{\frac{p}{D_0}}(A_0-B_0)=\frac{\sqrt{p}}{(K_2+\sigma)\sqrt{D_0}}\cdot$$
$$\{(K_2a_0-a_R)+(K_2b_0-b_R)\cdot e^{pT}\cdot\operatorname{erfc}\sqrt{pT}\}. \tag{20}$$

8) D. MacGillavry, *Rec. trav. chim. Pays-Bas*, **57**, 53 (1938).

9) Cf. Table of transformations given in R. V. Churchill: "Modern Operational Mathematics in Engineering." (1944).

Further it is found that

$$\frac{K_2a_0-a_R}{K_2+\sigma}={}^{\circ}_{1}C_0-{}^{\circ}_{2}C_0;\quad \frac{K_2b_0-b_R}{K_2+\sigma}=b_0={}^{*}C_0-{}^{\circ}_{1}C_0. \tag{21}$$

Now, for the execution of inverse transformation, the following theorems are useful.

$$\mathfrak{L}^{-1}\sqrt{p}=\frac{1}{\sqrt{\pi\tau}};$$

$$\mathfrak{L}^{-1}\sqrt{p}\cdot e^{pT}\cdot\operatorname{erfc}\sqrt{pT}=\frac{1}{\sqrt{\pi(T+\tau)}}. \tag{22}$$

Hence it is manifest that

$$\left(\frac{\partial C_0}{\partial x}\right)_{x=0}=\frac{{}^{*}C_0-{}^{\circ}_{1}C_0}{\sqrt{\pi D_0(T+\tau)}}+\frac{{}^{\circ}_{1}C_0-{}^{\circ}_{2}C_0}{\sqrt{\pi D_0\tau}}. \tag{23}$$

(2) Solution by Means of the Principle of Superposition.—It is obvious from the above deduction that when the voltage as shown in Fig. 1 is applied, it can be assumed that the interfacial concentrations in a state of equilibrium take constant values according to the electrode potential, provided that the rate of the electrode process is rapid enough. Accordingly our problem is now to solve the Eq. (1) with the initial condition given by Eq. (2) and with the boundary condition given by

$$x=0,\quad \begin{cases} T>t>0, & C_0={}^{\circ}_{1}C_0; \\ t>T, & C_0={}^{\circ}_{2}C_0. \end{cases} \tag{24}$$

Further it is clear that the applied voltage shown in Fig. 1 is equivalent to the superposition of the two constant voltages, as given by

$$\begin{array}{ll} E=E_I+E_{II} & (t>0); \\ E_I=E_1 & (t>0); \\ E_{II}=\begin{cases} E_2-E_1 \\ 0 \end{cases} & \begin{matrix} (t>T); \\ (T>t>0). \end{matrix} \end{array} \tag{25}$$

This relation is illustrated in Fig. 2(a) and (b). It may be supposed analogously that as for the interfacial concentration the superposition of two concentrations as shown in Fig. 3(a) and (b) is also effective. Then we can divide the function $C_0(x, t)$ into two parts; namely

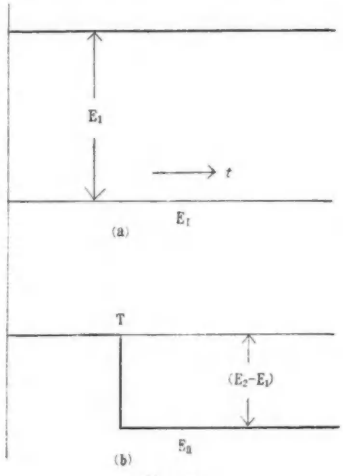

Fig. 2.

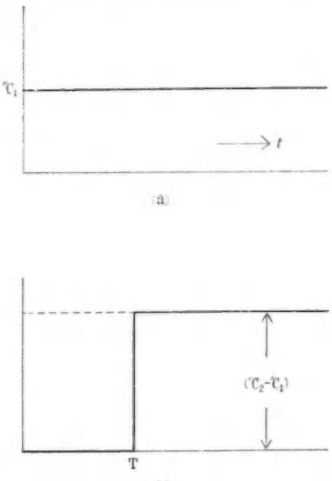

Fig. 3.

$$C_0=C_0(\mathrm{I})+C_0(\mathrm{II}), \tag{26}$$

and we have to integrate the following two equations.

$$\frac{\partial C_0(\mathrm{I})}{\partial t}=D_0\frac{\partial^2 C_0(\mathrm{I})}{\partial x^2};\quad \frac{\partial C_0(\mathrm{II})}{\partial t}=D_0\frac{\partial^2 C_0(\mathrm{II})}{\partial x^2}. \tag{27}$$

The conditions for $C_0(\mathrm{I})$ are shown by

$$\begin{array}{lll} t=0, & 0\leq x\leq\infty, & C_0(\mathrm{I})={}^{*}C_0; \\ t>0, & x=0, & C_0(\mathrm{I})={}^{\circ}_{1}C_0. \end{array} \tag{28}$$

and as for the function $C_0(\mathrm{II})$, the following conditions are valid.

$$\begin{array}{lll} t\leq T, & 0\leq x\leq\infty, & C_0(\mathrm{II})=0; \\ t>T, & x=0, & C_0(\mathrm{II})={}^{\circ}_{2}C_0-{}^{\circ}_{1}C_0. \end{array} \tag{29}$$

The solutions thereof are clearly given by

$$C_0(\mathrm{I})={}^{*}C_0-({}^{*}C_0-{}^{\circ}_{1}C_0)\cdot\operatorname{erfc}\frac{x}{2\sqrt{D_0t}};$$

$$C_0(\mathrm{II})=\begin{cases} 0; & (T\geq t) \\ ({}^{\circ}_{2}C_0-{}^{\circ}_{1}C_0)\cdot\operatorname{erfc}\dfrac{x}{2\sqrt{D_0(t-T)}}, & (t>T) \end{cases} \tag{30}$$

and there is no doubt that by the sum of these two functions the desired solution is shown as given by Eq. (26). Thus the concentration gradient at the electrode surface is shown by

$$\left(\frac{\partial C_0}{\partial x}\right)_{x=0}=\frac{{}^{*}C_0-{}^{\circ}_{1}C_0}{\sqrt{\pi D_0t}}+\frac{{}^{\circ}_{1}C_0-{}^{\circ}_{2}C_0}{\sqrt{\pi D_0(t-T)}}, \tag{31}$$

where the second term in the right hand side of the equation should disappear for $t<T$. Eq. (31) is clearly identical with the conclusion of the preceding discussion shown by Eq. (23), since the relationship $\tau=t-T$ holds.

Indeed the solution given by Eqs. (26) and (30)

is obtained only with the assumption that the interfacial concentration has a constant value according to the electrode potential. However, the fact that the solution satisfies the two conditions, i.e. the concentrations of both forms are in an equilibrium state at the electrode surface and also that the fluxes of both forms are continuous at the surface, can be easily verified. Further no discussion may be needed about the facts that for the reductant also a similar relation holds.

Discussion of the Result

In Fig. 4 is shown an example of the variation of concentration distribution near the electrode surface with time. The

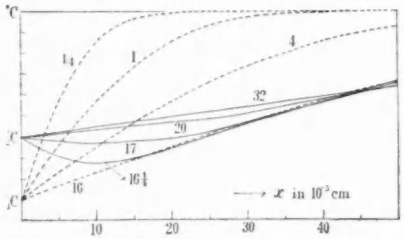

Fig. 4. Theoretical curves representing the variation of concentration distribution of depolarizer with time, drawn with the values: ${}^{1}_{2}C = \frac{1}{10}{}^{*}C$; ${}^{0}_{2}C = \frac{4}{10}{}^{*}C$; $D = 10^{-6}\,\mathrm{cm^2.\,sec^{-1}}$. Figures show the times elapsed after the electrolysis in the unit of 1/100 sec., and the potential is converted from E_1 to E_2 at $T = 16/100$ sec.

legitimacy of the above discussion can be rationally comprehensible from the consideration of special cases. Namely, when the discontinuous jump of the electrode potential at $t=T$ is zero, it follows that

$$E_1 = E_2\,;\ {}^{0}_{1}C_0 = {}^{1}_{2}C_0\,;\ \left(\frac{\partial C_0}{\partial x}\right)_{x=0} = \frac{{}^{*}C_0 - {}^{0}_{1}C_0}{\sqrt{\pi D_0 t}}. \quad (32)$$

This conclusion is, of course, quite in harmony with the Cottrel-Ilkovic theory for the current at a stationary plane electrode. Further, when the condition given by $t \gg T$ is satisfied, viz. when a considerable long time has elapsed after the change of voltage from E_1 to E_2, the hysterisis of the diffusion layer produced by the electrolysis with the application of voltage E_1 during the time interval from $t=0$ to $t=T$ should be ignored, compared with the long history of electrolysis performed after that. This can be well demonstrated by the following equation.

$$\left(\frac{\partial C_0}{\partial x}\right)_{x=0} \approx \frac{{}^{*}C_0 - {}^{0}_{2}C_0}{\sqrt{\pi D_0 (t-T)}} \approx \frac{{}^{*}C_0 - {}^{0}_{2}C_0}{\sqrt{\pi D_0 t}}. \quad (33)$$

According to the above theoretical treatment, however, it is required that the current intensities at $t=0$ and $t=T$ become infinite. This is clearly irrational; but in order to surmount this difficulty, it is necessary to take the rates of the electrode processes into consideration. As reported in the above quoted papers[3,6]; the mathematical treatment thereof, however, seems to be much more complicated.

Summary

Change of the structure of diffusion layer with time and the course of diffusion current at a stationary and reversible electrode due to the sudden change of the applied voltage are discussed mathematically.

The author wishes to express his sincere thanks to Professor I. Tachi for his kind encouragement.

Department of Agricultural Chemistry, Faculty of Agriculture, Kyoto University, Kyoto

Polarographic Diffusion Current Observed with Square Wave Voltage. II. Basic Theory for a Reversible Electrode

By Tomihito KAMBARA

(Received February 26, 1954)

In the preceding paper[1] the diffusion current, observed when the voltage applied to a reversible electrode is suddenly changed, is discussed theoretically. The theory is so easily to be extended that the electrolysis with a square wave voltage as shown in Fig. 1(a) can be elucidated as follows.

Our problem is now to solve the differential equation:

$$\partial C/\partial t = D \cdot \partial^2 C/\partial x^2 \tag{1}$$

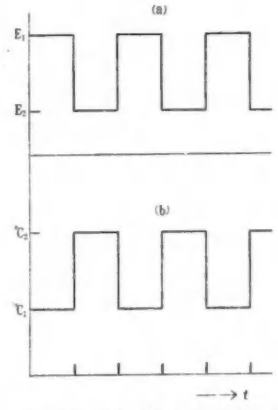

Fig. 1. Changes of electrode potential and interfacial concentration of depolarizer.

with the proper conditions which hold when the square wave voltage $E(t)$ of the period $2T$ shown by

$$\begin{aligned} E(t) &= \begin{cases} E_1 & (0<t<T) \\ E_2 & (T<t<2T) \end{cases} \\ E(t) &= E(t+2T) \end{aligned} \tag{2}$$

is applied. Since the concentration of depolarizer shows everywhere the constant value $^*C$ before the electrolysis, the initial condition is given by

$$t=0,\ 0\leq x\leq \infty,\ C=^*C. \tag{3}$$

Next as for the interfacial concentration, it is shown in the previous paper that the conception that the concentrations of the oxidized and reduced forms are at a state of equilibrium at the electrode surface leads to a simplified supposition that each interfacial concentration shows a constant value according to the applied potential. Thus it is seen that the boundary condition is given by

$x=0,\ t>0,$

$$C = \left\{ \begin{array}{l} {}^{\mathrm{i}}_{1}C(E=E_1;\ 2nT<t<(2n+1)T) \\ {}^{\mathrm{i}}_{2}C(E=E_2;\ (2n+1)T<t<(2n+2)T) \end{array} \right\} \tag{4}$$

where n is an integer. This relationship is illustrated in Fig. 1(b).

(1) Solution by Means of the Principle of Superposition.—Let the function $C(x,\ t)$ be an algebraic sum of the functions $C(\mathrm{I})$, $C(\mathrm{II})$,……, etc.; namely

$$C=C(\mathrm{I})+C(\mathrm{II})+C(\mathrm{III})+C(\mathrm{IV})+\cdots\cdots, \tag{5}$$

and it is supposed that each function is governed by Fick's law of diffusion. As shown in Part I of this study, the following relations hold for the function $C(\mathrm{I})$.

$$\begin{aligned} &t=0,\ 0\leq x\leq \infty,\quad C(\mathrm{I})=^*C; \\ &t>0,\ x=0,\qquad C(\mathrm{I})={}^{\mathrm{i}}_{1}C; \\ &C(\mathrm{I})={}^{\mathrm{i}}_{1}C+(^*C-{}^{\mathrm{i}}_{1}C)\cdot\mathrm{erf}\frac{x}{2\sqrt{Dt}} \end{aligned} \tag{6}$$

Further, as for the function $C(\mathrm{II})$, the following relations hold.

$$\begin{aligned} &t-T\leq 0,\ 0\leq x\leq \infty,\ C(\mathrm{II})=0; \\ &t-T>0,\ x=0,\ C(\mathrm{II})={}^{\mathrm{i}}_{2}C-{}^{\mathrm{i}}_{1}C; \\ &C(\mathrm{II})=({}^{\mathrm{i}}_{2}C-{}^{\mathrm{i}}_{1}C)\cdot\mathrm{erfc}\ \frac{x}{2\sqrt{D(t-T)}}. \end{aligned} \tag{7}$$

When such a calculation is carried out repeatedly, next it is found that $C(\mathrm{III})$ is shown by

$$\begin{aligned} &t-2T\leq 0,\ 0\leq x\leq \infty,\ C(\mathrm{III})=0; \\ &t-2T>0,\ x=0,\ C(\mathrm{III})={}^{\mathrm{i}}_{1}C-{}^{\mathrm{i}}_{2}C; \\ &C(\mathrm{III})=({}^{\mathrm{i}}_{1}C-{}^{\mathrm{i}}_{2}C)\cdot\mathrm{erfc}\frac{x}{2\sqrt{D(t-2T)}} \end{aligned} \tag{8}$$

Upon generalizing this procedure, it is found that the concentration of depolarizer $C(x,\ t)$ is demonstrated by

$$C={}^{\mathrm{i}}_{1}C+(^*C-{}^{\mathrm{i}}_{1}C)\cdot\mathrm{erf}\frac{x}{2\sqrt{Dt}}+$$

$$+\sum_{n=1}^{n}(-1)^n({}^{\mathrm{i}}_{1}C-{}^{\mathrm{i}}_{2}C)\cdot\mathrm{erfc}\frac{x}{2\sqrt{D(t-nT)}}, \tag{9}$$

which holds at the time interval given by

$$nT<t<(n+1)T$$

That this expression can satisfy the conditions shown by the Eqs. (1), (3) and (4), is

1) T. Kambara, This Bulletin, **27**, 523 (1954).

to be easily verified; and it is comprehensible that the interfacial concentrations are at a state of equilibrium and that the fluxes of oxidant and reductant are continuous at the electrode surface, when the above developed theoretical treatment is applied both to oxidant and reductant.

(2) Solution by Means of the Laplace-Transformation.—Next the above deduced conclusion will be derived by the aid of the Laplace-transformation. Upon applying the Laplace-transformation defined by

$$\mathfrak{L}C(x,\ t)=p\int_0^\infty e^{-pt}\cdot C(x,\ t)\cdot dt=u(x,\ p),$$

the differential equation (1) with the initial condition shown by Eq. (3) is converted into

$$p(u-{}^*C)=D\cdot\partial^2u/\partial x^2. \tag{10}$$

The general solution of this equation is given by

$$u={}^*C+A\cdot\exp\sqrt{\frac{p}{D}}x+B\cdot\exp\left(-\sqrt{\frac{p}{D}}x\right).$$

Since the relationship $u={}^*C$ must always hold for $x=\infty$, the integral constant A is clearly zero. Next the remaining constant B must be determined. Eq. (4), showing the boundary condition, can be written in the form:

$$x=0,\ t>0,\ C=\frac{1}{2}({}^\circ_{\mathrm{i}}C+{}^\circ_{2}C)+\frac{1}{2}({}^\circ_{\mathrm{i}}C-{}^\circ_{2}C)\cdot M(T,\ t), \tag{11}$$

where the function $M(T,\ t)$ is the "square wave" or "meander" function shown in Fig. 2 and is defined as follows.

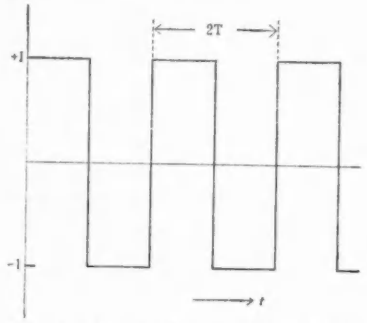

Fig. 2. Schematic representation of square wave function shown by Eq. (12).

$$M(T,\ t)=\begin{cases}+1 & (0<t<T);\\ -1 & (T<t<2T);\end{cases}\qquad M(T,\ t+2T)=M(T,\ t). \tag{12}$$

Furthermore it can be shown that the function $M(T,\ t)$ has the following transformation.

$$\mathfrak{L}M(T,\ t)=\tanh\frac{pT}{2} \tag{13}$$

If the interfacial concentration is represented by

$$C(0,\ t)={}^\circ C=\mathfrak{L}^{-1}\,{}^\circ u,$$

it is found that

$${}^\circ u=B+{}^*C={}^\circ_{2}C+\frac{1}{2}({}^\circ_{\mathrm{i}}C-{}^\circ_{2}C)\cdot\left(1+\tanh\frac{pT}{2}\right)$$

$$={}^\circ_{2}C+({}^\circ_{\mathrm{i}}C-{}^\circ_{2}C)\cdot\{1+\exp(-pT)\}^{-1};$$

thus the constant B is determined, and it follows that

$$u(x,\ p)={}^*C+({}^\circ_{2}C-{}^*C)\cdot\exp\left(-\sqrt{\frac{p}{D}}x\right)+({}^\circ_{\mathrm{i}}C-{}^\circ_{2}C)\cdot\exp\left(-\sqrt{\frac{p}{D}}x\right)\cdot\{1+\exp(-pT)\}^{-1} \tag{14}$$

Upon utilizing the expansion:

$$\frac{1}{1+\exp(-pT)}=1-\exp(-pT)+\exp(-2pT)-\ \cdots\cdots,$$

Eq. (14) can be transformed into

$$u(x,\ p)={}^*C+({}^\circ_{2}C-{}^*C)\cdot\exp\left(-\sqrt{\frac{p}{D}}x\right)+({}^\circ_{\mathrm{i}}C-{}^\circ_{2}C)\sum_{n=0}^{n}{}'(-1)^n\cdot\exp\left(\sqrt{\frac{p}{D}}x\right)\cdot\exp(-np\,T). \tag{14a}$$

In order to execute the inverse transformation, we can legitimately employ the following theorems; i. e.

$$\mathfrak{L}^{-1}\exp\left(-\sqrt{\frac{p}{D}}x\right)=\operatorname{erfc}\frac{x}{2\sqrt{Dt}};$$

and if we have (15)

$$\mathfrak{L}^{-1}f(p)=A(t),$$

then it is found that

$$\mathfrak{L}^{-1}[e^{-kp}\cdot f(p)]=A(t-k).$$

It must be noticed here that $A(t-k)=0$ for $t<k$ and that $A(t-k)$ implies the "translated function". There is no doubt that by means of the Eqs. (15) the expression for $u(x,\ p)$ shown by Eq. (14a) can be inversely transformed into Eq. (9).

Thus the basic expression for the concentration distribution in the case that a square wave voltage is applied upon a reversible electrode is theoretically obtained by means of the two mathematically different methods. It follows immediately from the above conclusion that the concentration gradient at the electrode surface is manifested by

$$\left(\frac{\partial C}{\partial x}\right)_{x=0}=\frac{{}^*C-{}^\circ_{\mathrm{i}}C}{\sqrt{\pi Dt}}+\sum_{n=1}^{n}{}'(-1)^{n+1}\frac{{}^\circ_{\mathrm{i}}C-{}^\circ_{2}C}{\sqrt{\pi D(t-nT)}} \tag{16}$$

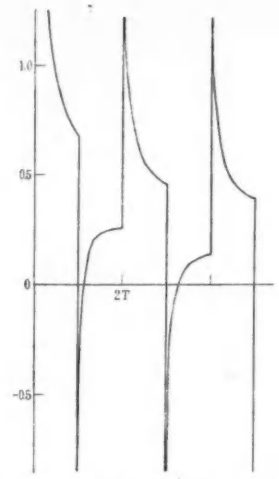

Fig. 3. Schematic representation of the course of instantaneous currents intensity due to the application of a square wave voltage. Curve shows the equation by

$$I=\frac{\alpha}{\sqrt{t}}+\sum_{n=1}^{n}(-1)^n\frac{\beta}{\sqrt{t-nT}},$$

The numerical values employed are as follows:

$$\alpha=3;\quad \beta=1;\quad T=20.$$

The instantaneous current intensity is readily obtainable from this equation, and in Fig. 3 is illustrated an example of the function given by Eq. (16). In our laboratory Dr. Suzuki[2] has investigated the electrolysis with square wave voltage by the aid of a rotating switch and the electro-magnetic oscillograph, and the recordings thereof are, in the case of reversible electrode reactions, quite in harmony with the present theoretical consideration. The validity of the above developed mathematical treatment will be amply and convincingly shown in the following article, in which many experimental facts will be rationally elucidated.

Summary

By means of the principle of superposition and of the Laplace transformation, the differential equation of diffusion is integrated, and the result thus obtained gives the fundamental theoretical expression for the electrolysis with a square wave voltage.

The author wishes to express his sincere thanks to Prof. I. Tachi for his kind guidance. The author's thanks are also due to Dr. M. Suzuki, who helped the author with many oscillographic data.

Department of Agricultural Chemistry, Faculty of Agriculture, Kyoto University, Kyoto

2) M. Suzuki, *J. Electrochem. Soc. Japan*, **22**, 63, 112, 162, 221 (1954); *Memoirs College Agr., Kyoto Univ.*, No. 67 (1954).

Polarographic Diffusion Current Observed with Square Wave Voltage. III. Applications of the Theory

By Tomihito KAMBARA

(Received February 26, 1954)

In Part I of this study,[1] the change of diffusion current produced by the discontinuous change of the electrode potential is discussed, and further in Part II the theory for the electrolysis with a square wave voltage is developed.[1] The conclusion thereof is, employing the same symbols as in the previous studies, that the concentration gradient of the depolarizer at the electrode surface is demonstrated by

$$\left(\frac{\partial C}{\partial x}\right)_{x=0}=\frac{{}^{*}C-{}^{0}_{1}C}{\sqrt{\pi Dt}}+\sum_{n=1}^{n}(-1)^{n+1}\frac{{}^{0}_{1}C-{}^{0}_{2}C}{\sqrt{\pi D(t-nT)}} \tag{1}$$

1) T. Kambara, This Bulletin, **27**, 523, 527 (1554).

The instantaneous current intensity i, on the other hand, is shown by

$$i=nFqD(\partial C/\partial x)_{x=0}. \tag{2}$$

Now, writing

$$\alpha={}^{*}C-{}^{0}_{1}C;\quad \beta={}^{0}_{2}C-{}^{0}_{1}C; \tag{3}$$

$$k=nFq\sqrt{D/\pi}; \tag{4}$$

it is seen that

$$I=\frac{i}{k}=\frac{\alpha}{\sqrt{t}}+\sum_{n=1}^{n}(-1)^n\frac{\alpha}{\sqrt{t-nT}}. \tag{5}$$

Further, for the sake of convenience in the following discussions, some quantities will be introduced as follows. Let i_1 be the diffusion current observed when the electrolysis is

continuously executed with the constant voltage E_1; then it is seen that

$$i_1=\frac{nFq\sqrt{D}}{\sqrt{\pi t}}\,({}^{*}C-{}_{1}^{\circ}C)=\frac{k\alpha}{\sqrt{t}}, \tag{6}$$

where ${}_{1}^{\circ}C$ is the equilibrium interfacial concentration of depolarizer corresponding to the voltage E_1. Therefore the mean value of the current intensity in the time interval from $t=0$ to $t=t_1$ is shown by

$$\bar{i}_1=\frac{1}{t_1}\int_0^{t_1} i_1\cdot dt=\frac{2k\alpha}{\sqrt{t_1}}. \tag{7}$$

An analogous discussion holds also for the electrolysis with the steady voltage E_2, where it is found that

$$i_2=\frac{k(\alpha-\beta)}{\sqrt{t}}; \tag{8}$$

$$\bar{i}_2=\frac{1}{t_1}\int_0^{t_1} i_2\cdot dt=\frac{2k(\alpha-\beta)}{\sqrt{t_1}}. \tag{9}$$

These can be readily seen, since ${}_{2}^{\circ}C$ implies the equilibrium interfacial concentration corresponding to the constant voltage E_2. Thus from these equations it follows that

$$\beta=\frac{\sqrt{t_1}}{2k}(\bar{i}_1-\bar{i}_2)=\frac{\sqrt{t}}{k}(i_1-i_2). \tag{10}$$

Next, some conclusions derived from the theory will be compared with several experimental findings in the section below.

Experiment of Madame Fournier

In the recording of polarographic current-voltage curve, Fournier[2] has experimented while a suitable alternating voltage is superposed onto the constant voltage, which increases negatively as is usual in polarography. The result of her experiment is well understood when the superposed sine-wave voltage is regarded to be equivalent to a square wave voltage of suitable amplitude and frequency. Now, we will compute the mean current which flows during the time interval shown by

$$t_1=2mT, \quad (m: \text{an integer}) \tag{11}$$

where T represents, as in the previous papers, the half-period, and in the case of the dropping mercury electrode t_1 corresponds to the drop time. Eq. (5) can be written as

$$I=\frac{\alpha}{\sqrt{t}}+\beta\left(\frac{-1}{\sqrt{t-T}}+\frac{1}{\sqrt{t-2T}}+\frac{-1}{\sqrt{t-3T}}+\cdots\cdots+\frac{1}{\sqrt{t-(2m-2)T}}+\frac{-1}{\sqrt{t-(2m-1)T}}\right)$$

Thus the integrated value of I is given by

$$\int_0^{t_1} I\cdot dt=\int_0^{t_1}\frac{\alpha}{\sqrt{t}}dt+\beta\left(\int_T^{t_1}\frac{-dt}{\sqrt{t-T}}+\int_{2T}^{t_1}\frac{dt}{\sqrt{t-2T}}+\cdots\cdots+\int_{(2m-2)T}^{t_1}\frac{dt}{\sqrt{t-(2m-2)T}}+\int_{(2m-1)T}^{t_1}\frac{-dt}{\sqrt{t-(2m-1)T}}\right).$$

where the lower limits of the integrals take the values: 0, T, $2T$, ……, etc., because each term containing $(t-nT)^{-1/2}$ in the summation in Eq. (5) must vanish away for $t<nt$ owing to the property of the translated function. Upon executing the integrations, it is found that

$$\int_0^{t_1} I\cdot dt=2\alpha\sqrt{2mT}-2\beta\sqrt{T}\,(\sqrt{2m-1}+\sqrt{2m-3}+\cdots\cdots+\sqrt{3}+\sqrt{1})+2\beta\sqrt{T}\,(\sqrt{2m-2}+\sqrt{2m-4}+\cdots\cdots+\sqrt{4}+\sqrt{2}).$$

For the large value of m, the approximate values of the series appearing in this equation can be estimated by performing integration instead of the summation as follows.

$$\sum_{m=1}^{m}\sqrt{2m-1}\simeq\int_1^m\sqrt{2}\left(m-\frac{1}{2}\right)^{1/2}\cdot dm=\frac{2\sqrt{2}}{3}\left\{\left(m-\frac{1}{2}\right)^{3/2}-\left(\frac{1}{2}\right)^{3/2}\right\};$$

$$\sum_{m=2}^{m}\sqrt{2m-2}\simeq\int_2^m\sqrt{2}\,(m-1)^{1/2}\cdot dm=\frac{2\sqrt{2}}{3}\left\{(m-1)^{3/2}-1\right\}.$$

Hence we obtain

$$\int_0^{2mT} I\cdot dt\simeq 2\alpha\sqrt{2mT}-2\beta\sqrt{T}\cdot\frac{2\sqrt{2}}{3}\left\{\left(m-\frac{1}{2}\right)^{3/2}-(m-1)^{3/2}+1-\left(\frac{1}{2}\right)^{3/2}\right\}.$$

Therefore, upon regarding m to be very large and applying the familiar binomial theorem, the mean value of Fournier current is shown by

$$\bar{i}_F=\frac{k}{2mT}\int_0^{2mT} I\cdot dt=\frac{2k\alpha}{\sqrt{2mT}}-\frac{4k\beta}{3}\cdot\frac{\sqrt{2T}}{2mT}\left(\frac{3\sqrt{m}}{4}+\frac{\sqrt{8}-1}{\sqrt{8}}\right). \tag{12}$$

Inserting Eqs. (7), (10) and (11) into (12) gives

$$\bar{i}_F=\bar{i}_1-\frac{2}{3}(\bar{i}_1-\bar{i}_2)\left\{\frac{3}{4}+\frac{\sqrt{8}-1}{\sqrt{8m}}\right\},$$

which, again owing to the large value of m, can be simplified into

$$\bar{i}_F=\frac{1}{2}(\bar{i}_1+\bar{i}_2). \tag{13}$$

On the other hand, the equation for the polarographic wave due to the reversible electrode reaction is, upon employing the usual notations, demonstrated by

$$\left.\begin{aligned}\bar{i}&=\frac{\bar{i}_d}{2}(1+\tanh\xi);\\ \xi&=\frac{1}{2}\cdot\frac{nF}{RT}(-E+E_{1/2}).\end{aligned}\right\} \tag{14}$$

In the Fournier's investigation, it can be written that

$$E_1=E-\Delta E; \quad E_2=E+\Delta E; \quad (\Delta E>0) \tag{15}$$

i. e.

2) M. Fournier, *Compt. rend.*, **232**, 1673 (1951).

$$\left.\begin{aligned}&\xi_1=\xi-\Delta\xi\ ;\quad \xi_2=\xi+\Delta\xi\ ;\\ &\Delta\xi=\frac{1}{2}\cdot\frac{nF}{RT}\cdot\Delta E.\end{aligned}\right\} \tag{16}$$

Accordingly the Fournier's current-voltage curve is manifested by

$$\bar{i}_F=\frac{\bar{i}_d}{4}\{2+\tanh(\xi-\Delta\xi)+\tanh(\xi+\Delta\xi)\}. \tag{17}$$

Then, since we have

$$\tanh\xi=-\tanh(-\xi),$$

it is found that the curve:

$$\bar{i}_F=\frac{\bar{i}_d}{2}=\frac{\bar{i}_d}{4}\{\tanh(\xi-\Delta\xi)+\tanh(\xi+\Delta\xi)\}$$

$$=-\frac{\bar{i}_d}{4}\{\tanh(-\xi-\Delta\xi)+\tanh(-\xi+\Delta\xi)\}$$

has a point of symmetry shown by

$$\bar{i}_F=\bar{i}_{d/2}\ ;\quad \xi=0\ ;\quad E=E_{1/2}\ ; \tag{18}$$

which is, of course, identical with the usual half-wave point.

Further the following relations are also found:

$$\left.\begin{aligned}&i_F=i_d\quad \text{for}\quad E=-\infty\ ;\ \xi=\infty\ ;\\ &i_F=0\quad \text{for}\quad E=\infty\ ;\quad \xi=-\infty\ ;\end{aligned}\right\} \tag{19}$$

Next the inclination of the Fournier's polarogram at the half-wave potential is given by

$$-\left(\frac{d\bar{i}_F}{dE}\right)_{E=E_{1/2}}=\frac{\bar{i}_d nF}{4RT}\cdot\frac{1}{\cosh^2\Delta\xi}\ ; \tag{20}$$

whereas that of the ordinary polarogram is, as is well known, given by

$$-\left(\frac{d\bar{i}}{dE}\right)_{E=E_{1/2}}=\frac{\bar{i}_d nF}{4RT}. \tag{21}$$

Thus it can be concluded that the inclination is made less steep by the superposition of an alternating voltage. The above derived theoretical conclusions have all been confirmed experimentally by Fournier in the case of reversible electrode reaction, e. g. the cathodic reduction of monovalent metal ion; the general aspect of Fournier current is illustrated in Fig. 1.

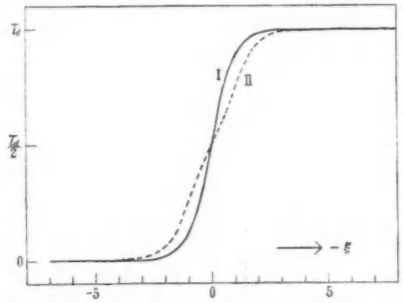

Fig. 1. Curve I shows the ordinary polarogram, and curve II shows the Fournier's polarogram drawn theoretically with the value $\Delta\xi=2$ [Cf. Eqs. (14)–(17)].

Kalousek Apparatus

In the apparatus designed by Kalousek,[3] the electrolysis is performed by applying a square wave voltage; viz. at first the electrolysis is carried out with the potential E_1 for T sec. and then the potential is discontinuously changed to a more positive value E_2; i. e.

$$E_2>E_1, \tag{22}$$

and it may be supposed that the reversibility of the electrode process is to be judged by the intensity of the oxidation current. And thus in this apparatus, it is so designed that only the current flowing during the application of the more positive potential E_2 is recorded by the galvanometer. In order to clear up the observations obtained with this apparatus, at first, we must compute the integrated value of the current, which flows in the half-period shown by

$$E=E_2\ ;\ (2m+1)T<t<(2m+2)T\ \ (m:\ \text{integer}) \tag{23}$$

It follows from Eq. (5) that

$$\int_{(2m+1)T}^{(2m+2)T} I\cdot dt=\int_{(2m+1)T}^{(2m+2)T}\frac{\alpha}{\sqrt{t}}\cdot dt$$

$$+\sum_{n=1}^{2m+1}\int_{(2m+1)T}^{(2m+2)T}(-1)^n\cdot\frac{\beta}{\sqrt{t-nT}}\cdot dt$$

$$=2\alpha(\sqrt{2m+2}-\sqrt{2m-1})\sqrt{T}$$
$$+2\beta\sqrt{T}(\sqrt{2m}+\sqrt{2m-2}+\cdots\cdots+\sqrt{2})$$
$$-2\beta\sqrt{T}(\sqrt{2m-1}+\sqrt{2m-3}+\cdots\cdots$$
$$+\sqrt{3}+\sqrt{1})$$
$$-2\beta\sqrt{T}(\sqrt{2m+1}+\sqrt{2m-1}+\cdots\cdots$$
$$+\sqrt{3}+\sqrt{1}).$$
$$+2\beta\sqrt{T}(\sqrt{2m}+\sqrt{2m-2}+\cdots\cdots+\sqrt{2})$$

As shown in the preceding section, for the large value of m, it can be written that

$$\sum_{m=1}^{m}m^{1/2}\simeq\int_1^m m^{1/2}\cdot dm=\frac{2}{3}(m^{3/2}-1);$$

$$\sum_{m=1}^{m}(2m-1)^{1/2}\simeq\int_1^m(2m-1)^{1/2}\cdot dm=\frac{1}{3}\{(2m-1)^{3/2}-1\};$$

$$\sum_{m=1}^{m}(2m+1)^{1/2}\simeq\int_1^{m+1}(2m+1)^{1/2}\cdot dm=\frac{1}{3}\{(2m+1)^{3/2}-1\};$$

i. e. the summation is replaced approximately by integration. Thus with the aid of binomial theorem, it is seen that

$$\int_{(2m+1)T}^{(2m+2)T} I\cdot dt=2\alpha\sqrt{T}(\sqrt{2m+2}-\sqrt{2m+1})$$
$$+\frac{4\beta\sqrt{2T}}{3}\left\{2m^{3/2}-2-\left(m-\frac{1}{2}\right)^{3/2}-\left(m+\frac{1}{2}\right)^{3/2}\right.$$
$$\left.+\frac{1}{\sqrt{2}}\right\}\simeq 2\alpha\sqrt{T}(\sqrt{2m+2}-\sqrt{2m+1})$$
$$+\frac{4\beta\sqrt{2T}}{3}\left(\frac{1}{\sqrt{2}}-2\right). \tag{23}$$

Now we must evaluate the integrated value of the total current which flows under the application of potential E_2 during the time interval given by

$$t_1=2(m+1)T. \tag{24}$$

Then it is seen that

3) M. Kalousek, *Collection Czech. Chem. Communs.*, **13**, 105 (1948).

$$\sum_{m=0}^{m}\int_{(2m+1)T}^{(2m+2)T} I\cdot dt=\sum_{m=0}^{m}2\alpha\sqrt{T}\,(\sqrt{2m+2}-\sqrt{2m+1}$$
$$+(m+1)\frac{4\beta}{3}\sqrt{2T}\left(\frac{1}{\sqrt{2}}-2\right),$$

where it can be shown approximately that

$$\sum_{m=0}^{m}(\sqrt{2m+2}-\sqrt{2m+1})$$
$$\simeq\frac{2\sqrt{2}}{3}\left(\frac{3}{4}m^{1/2}-\frac{\sqrt{8}-1}{\sqrt{8}}\right)\simeq\left(\frac{m}{2}\right)^{1/2},$$

in which the summation is again replaced by integration. Therefore the Kalousek's mean current which flows during the half periods, in which the potential E_2 is applied, is demonstrated by

$$\bar{i}_K=k\sum_{m=0}^{m}\int_{(2m+1)T}^{(2m+2)T} I\cdot dt\Big/t_1$$
$$=\frac{k\alpha}{\sqrt{t_1}}\left(\frac{m}{m+1}\right)^{1/2}-\frac{4k\beta}{3}\left(2-\frac{1}{\sqrt{2}}\right)\frac{1}{\sqrt{2t_1}T}. \quad (25)$$

where the quantity $\sqrt{m/m+1}$ can be regarded to be nearly unity for the large value of m. Hence, upon inserting Eqs. (7) and (10) into this equation, it is seen that

$$\left.\begin{aligned}\bar{i}_K&=\frac{1}{2}\bar{i}_1=\frac{s}{\sqrt{2T}}(\bar{i}_1-\bar{i}_2);\\ s&=\frac{2}{3}\left(2-\frac{1}{\sqrt{2}}\right)=1.195\end{aligned}\right\} \quad (26)$$

Eurther the frequency of applied square wave voltage will be introduced according to

$$f=1/2T, \quad (27)$$

which is equal to the number of revolutions of rotating switch per second. Then it is manifest that

$$\bar{i}_K=\frac{1}{2}\bar{i}_1-s\sqrt{f}\,(\bar{i}_1-\bar{i}_2), \quad (28)$$

which is the fundamental equation for the Kalousek current provided that the electrode reaction proceeds reversibly.

The changes of the cathode potential with time due to the employment of Kalousek apparatus Ia, II and III are schematically illustrated in Fig. 2. In the case of apparatus I, it is so designed that the potential E_2 is always kept more positive by a constant value ΔE than the potential E_1; i. e.

$$E_2=E_1+\Delta E. \quad (29)$$

Accordingly it can be readily found that

$$\bar{i}_1-\bar{i}_2=\Delta\bar{i}=(d\bar{i}/dE)\cdot(-\Delta E), \quad (30)$$

and further it is clear that the potential E_1 is increased negatively with time, as is usual in polarography. Thus i_1 is shown by Eq. (14) demonstrating the ordinary polarographic wave. Therefore, it can be readily seen that

$$\bar{i}_K(I\alpha)=\frac{1}{2}\bar{i}-s\sqrt{f}\left(\frac{d\bar{i}}{dE}\right)\cdot(-\Delta E); \quad (31)$$

viz. the curve observed with the apparatus Ia is the superposition of two currents, namely (1) the current-voltage curve registered with the half decreased sensitivity of a galvanometer, and (2) the derivative curve thereof multiplied by the factor $(-s\sqrt{f})$. It is derived from Eq. (31) that a deep valley due to the oxidation current should be observed near the half-wave potential, which is in complete accordance with Kalousek's findings. Further it is seen that at a sufficiently negative potential, the Kalousek current is just one half the limiting diffusion current (cf. Fig. 3).

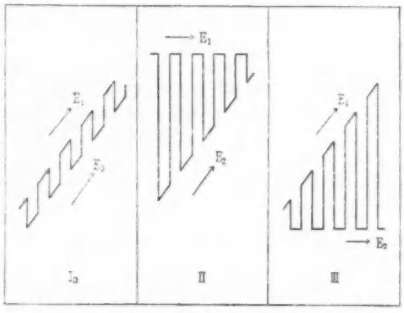

Fig. 2. Changes of the electrode potential with time in the Kalousek's apparatus.

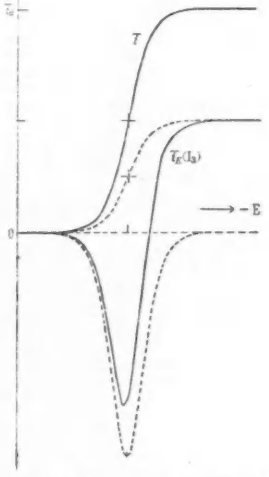

Fig. 3. Kalousek polarogram Ia.

Next in the apparatus II, the potential E_1 is fixed at such a negative value that the limiting current i_d is observable, whereas E_2 is increased negatively. Thus from Eq. (28) it follows that

$$\bar{i}_K(\mathrm{II})=\left(\frac{1}{2}-s\sqrt{f}\right)\bar{i}_d+s\sqrt{f}\,\bar{i}. \quad (32)$$

This conclusion shown in Fig. 4 is quite in harmony with the experiment.

Eurther, in the apparatus III, the potential E_2 is fixed at such a positive value that no appreciable reduction occurs, i. e.

$$\bar{i}_2=0,$$

whereas E_1 is increased negatively. Thus it is seen that

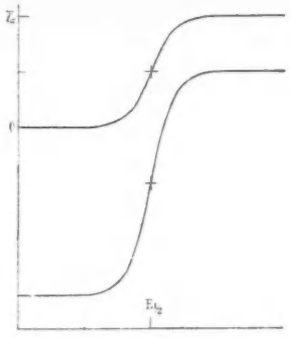

Fig. 4. Kalousek polarogram II.

$$\bar{i}_K(\mathrm{III}) = -\left(s\sqrt{f} - \frac{1}{2}\right)\bar{i}. \tag{33}$$

This equation also agrees well with the Kalousek's observation, and is illustrated in Fig. 5.

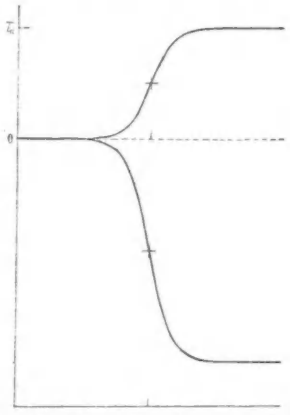

Fig. 5. Kalousek polarogram III.

Ishibashi-Fujinaga Apparatus

In I–F apparatus[4] aiming at the differential polarography and the increased sensitivity, a square wave voltage is applied by means of a rotating switch as in the Kalousek apparatus; furthermore, the rotating current alternator makes the current, flowing under the application of potential E_2, run through the galvanometer in the reverse direction, which is opposite ta the direction of the current flowing while the potential is E_1. This is, as it were, a full-wave rectification of the electrolytic current observed with a square wave voltage. Thus, in order to treat this problem theoretically, it is needed to compute the mean current which flows in the half-period shown by

$$E = E_1;\ 2mT < t < (2m+1)T\ (m;\ \text{integer}) \tag{34}$$

Therefore, at first, we must evaluate the quantity:

$$\sum_{m=0}^{n} \int_{2mT}^{(2m+1)T} I \cdot dt.$$

This calculation is to be executed as is seen in Eqs. (23) and (25); but this is much more simply performable as shown below. When the time interval given by

$$t_1 = (2m+2)T$$

is considerably long, it is already seen that (cf. Eq. (13))

$$\frac{1}{t_1}\int_0^{t_1} i \cdot dt = \bar{i}_F = \frac{1}{2}(\bar{i}_1 + \bar{i}_2).$$

On the other hand, there is no doubt that the following relationship holds.

$$\bar{i}_F = \frac{1}{t_1}\sum_{m=0}^{n}\left\{\int_{2mT}^{(2m+1)T} i \cdot dt + \int_{(2m+1)T}^{(2m+2)T} i \cdot dt\right\}. \tag{35}$$

Thus it follows from the Eqs. (13), (26) and (35) that

$$\frac{1}{t_1}\sum_{m=0}^{n}\int_{2mT}^{(2m+1)T} i \cdot dt = \bar{i}_F - \bar{i}_K$$

$$= \frac{1}{2}\bar{i}_2 + s\sqrt{f}\,(\bar{i}_1 - \bar{i}_2). \tag{36}$$

Hence the mean current observed with I–F apparatus is clearly given by

$$\bar{i}_{IF} = \frac{1}{t_1}\sum_{m=0}^{n}\left\{\int_{2mT}^{(2m+1)T} i \cdot dt - \int_{(2m+1)T}^{(2m+2)T} i \cdot dt\right\}$$

$$= \left(2s\sqrt{f} - \frac{1}{2}\right)(\bar{i}_1 - \bar{i}_2). \tag{37}$$

In the differential apparatus, it is so arranged that

$$\Delta E = E_2 - E_1 = \text{const.}$$

Therefore, from Eq. (30) it follows that

$$\bar{i}_{IF}(\mathrm{diff.}) = \left(2s\sqrt{f} - \frac{1}{2}\right)\cdot\left(\frac{d\bar{i}}{dE}\right)\cdot(-\Delta E). \tag{38}$$

Thus the sensitivity of the derivative curve increases, when the revolution number of a rotating switch is elevated and when a large ΔE is chosen. It is seen that if $f = 16$ c./sec. the height of the peak of the derivative curve is about ten times greater than $-i$ corresponding to the given value of ΔE. Next in the I–F apparatus for the increased sensitivity, the potential E_2 is so chosen that no appreciable cathodic current flows; i.e.

$$i_2 = 0. \tag{39}$$

On the other hand, i_1 is the current intensity corresponding to the ordinary polarographic wave and is given by Eq. (14). Hence it follows that

$$\bar{i}_{IF}(\mathrm{incr.}) = \left(2s\sqrt{f} - \frac{1}{2}\right)\cdot\bar{i}; \tag{40}$$

i. e. the observed polarogram exhibits the same effect, that is to be seen with the increased sensitivity of the galvanometer employed; such an effect of increasing the sensitivity, however, depends clearly on the reversibility of the electrode process.

Note—In the above discussions, in which the current intensities under several experimental conditions are well comprehensible from the present theoretical considerations, the reversibility

4) M. Ishibashi and T Fujinaga, This Bulletin, **25**, 68, 238 (1952).

of electrode reaction is always assumed. Accordingly deviations of experimental results from the theoretical conclusion are obviously due to the irreversible character of the process concerned; and hence the degree of such a deviation may be a rational measure of the irreversibility.

The above theory is developed based on the assumption that a stationary plane electrode is employed; thus it may not be quite adequate to apply the theory to the phenomenon obtained with a dropping electrode. But, since the equation for the diffusion current at a plane electrode differs from the Ilkovic equation only by a numerical factor, the present theory seems to be approximately correct. Were it possible to perform the calculation taking the effects due to the curvature and expansion of mercury drop into consideration, although mathematically very hard, it would be a strictly correct.

When in the above treatment the changes of the mercury drop surface given by

$$q=0.85\cdot m^{2/3}\cdot t^{2/3}$$

is employed, then we have the definite integral of the form:

$$\int_{nT}^{t}\frac{t^{2/3}\cdot dt}{\sqrt{t-nT}}=\int_{0}^{t}\frac{(t'+nT)^{2/3}}{\sqrt{t'}}\cdot dt',$$

which can not be evaluated rationally. But in this integral the effect of the denominator is far greater than that of numerator, so that the error produced by the assumption that the surface area is independent of time may not be very serious.

Summary

The theoretical treatment given in the previous works on the electrolysis with square wave voltage is here applied to the elucidation of experimental results. Thus the experiment by Madame Fournier is satisfactorily explained, and further the findings obtained with Kalousek's and Ishibashi-Fujinaga's apparatus are also rationally clarified.

The author wishes to express his sincere thanks to Professor Tachi for his interest to this study. The author's thanks are also due to Professors J. Heyrovsky, M. Kalousek and J. Koutecky in the Polarographic Institute of the Czechoslovak Academy of Sciences, who helped him with constructive criticism and kind encouragement.

Department of Agricultural Chemistry, Faculty of Agriculture, Kyoto University, Kyoto

---

On the Reactions Between Some Organic Sulfur Compounds and Silver Ions with Potentiometric Titrations

By Shinichi KIKUCHI, Yoshikata SAKAGUCHI* and Kazumi AKIBA

(Received May 6, 1954)

Introduction

Reactions between organic photographic fog-inhibitors and silver ions were measured by means of silver potentiometric titration in this laboratory. The senior authors, Kikuchi and Sakaguchi reported those on the pyrimidine derivatives[1,2,3] and Kikuchi, Sakaguchi, and Murobushi on the benzimidazoles and rhodanines[4]. The present report intends to clarify the reactions between some organic compounds other than cited before and the silver ion by the same method with an improved device. The substances chosen in this report are as follows:

potassium thiocyanate (I)
thiourea (II)
thiosemicarbazide (III)
benzaldehyde thiosemicarbazone (IV)
piperonal thiosemicarbazone (V)
p-dimetylamino benzaldehyde thiosemicarbazone (VI)
p-acetamide benzaldehyde thiosemicarbazone (VII)
o-nitrobanzaldehyde thiosemicarbazone (VIII)
m-nitrobenzaldehyde thiosemicarbazone (IX)
p-nitrobenzaldehyde thiosemicarbazone (X)
phenyl thiosemicarbazide (XI)
benzaldehyde phenyl thiosemicarbazone (XII)

Some other substance not containing sulfur

* Y. Sakaguchi has been in Fuji Photo. Film Co., since April, 1952.

1) S. Kikuchi and Y. Sakaguchi, *Journ. Sci. Phot. Japan* (in Japanese) **12**, No. 4, 3-7 (1950); abstracted in *Sci. et industr. Phot.*, **23** (2) 307 (1952).

2) Y. Sakaguchi and S. Kikuchi, ibid., **13** No. 4, 126-131 (1951); abstracted in *Sci. et industr. Phot.*, **23** (2) 178(1952).

3) S. Kikuchi and Y. Sakaguchi, *Sci. et Industr. Phot.*, **23A** 248-260 (1952).

4) S. Kikuchi, Y. Sakaguchi and K. Murobushi, *Bull. Soc. Scient. Photo. Japan* (in English), No. 2, 10-19 (1952).

are also chosen:

hydrazine (XIII)
urea (XIV)
guanidine (XV)
diphenyl guanidine (XVI)

These sulfur compounds are mainly chain compounds and some of these are apparently photographic sensitizers or even fogging agents. The authors wished to know the effect of the substitution of amino group of thiourea in connection of this reaction.

Experimental Part

(a) Pen-recording System of Potential—The silver potential of substances is measured potentiometrically. The voltage difference of a cell which is set up with the calomel and the silver electrode is amplified and read on a pen-writing recorder described in the previous paper[3,5]

(b) Automatic Titrator[1] — The addition of silver nitrate solution to the reagent is done with the automatic titrator designed in this laboratory (Fig. I). A syringe plunger is driven by the system of synchronous motor, gears, belt, and travelling nut. The change of gears enables four steps of the travelling nut's speed (50, 10, 2.5, and 0.625 mm/min.). Besides changes of the connection of belt and pulley make seven stages which are 2, 1.5, 1.25, 1 (standard), 0.75, 0.625, and 0.5. The nut's speed should be changed in 28 steps between 100–0.3125 mm/min. But the combinations of gears and belt make two pairs of the same speed, so 26 steps in total are interchangeable. The size of the syringe may be changeable from 1 to 10 cc also. The present experiment took place under conditions of about 5 cc. syringe and 1.25 mm/min. speed which corresponded to 0.67 cc./5 min.

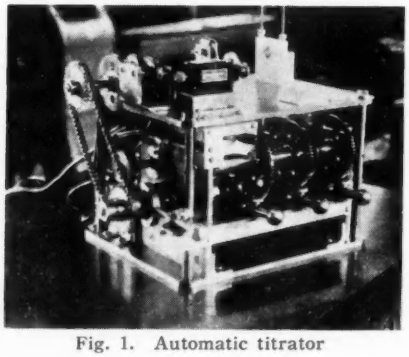

Fig. 1. Automatic titrator

(c) Procedure—0.075 N solution of silver nitrate is added to 50 cc. of 0.001 M/l buffered solution of organic compound in the rate of 0.67 cc./5 min. i.e. 0.00005 M/5 min. under vigorous agitation. In this concentration ratio, five minutes are necessary for an equivalence of Ag. On the other hand, the chart speed of the recorder can be changeable in 5, 10, 20, 60, 120, and 240 mm/min. or mm/hr. Throughout this experiment, the speed 10mm/min. was used, so 50 mm. on the chart corresponds to an equivalent.

If the compound is salted out in buffer solution, it is dissolved in organic solvent as methyl alcohol, then diluted with the buffer solution to the above concentration. A cleaned silver electrode is dipped in the solution and titration is started, and then its potential refered to the saturated calomel electrode is recorded as described above at 50°C.

(d) Buffer Solutions—As buffer solutions, the Walpole's acetate buffers are used for pH 4 and 5, the Sörensen's phosphate buffers for pH 6, 7, and 8, the Sörensen's borate buffers for pH 9, 10, and 11. The formulae for these were given in our previous report[1]. In phosphate buffers, some substances need more silver ions than expected and this showed that the phosphate buffers were inadequate for these substances. So the authors used the citrate buffers for pH 6 and 7, and the modified Sörensen's buffer for pH 8. The formulae of the buffers are given in Table 1.

TABLE I

FORMULAE OF BUFFERS

Sörensen's citrate buffer at 50°C
Solution A
(citric acid 21.008g+I N NaOH 200cc)/1.
Solution B 0.I N NaOH
*p*H 6.0 solution A 52.5 vol% solution B 47.5%
6.8 ,, 61.8 ,, 38.2
Sörensen's glycine buffer at 50°C
Solution A (glycine 7.505g+$NaNO_3$ 8.501g)/1.
Solution B 0.1 N NaOH
*p*H 8.0 solution A 93.5% solution B 6.5%

The sodium chloride of Sörensen's original formula is replaced by a gram equivalent of sodium nitrate to avoid the precipitation of silver chloride. In order to compare the buffering efficiency of the original and modified formulae, the *p*H change at 50°C. is shown in Table 2 when 0.05 N $AgNO_3$ is added to 50 cc. of the buffering solution.

TABLE II

BUFFERING POWER OF TWO BUFFER SOLUTIONS BY ADDITION OF $AgNO_3$

Kind of buffer	0.05N $AgNO_3$cc	0.00	1.00	2.00	3.00	4.00	5.00
glycine	pH	7.97	7.88	7.70	7.50	7.38	7.22
phosphate	pH	7.93	7.90	7.88	7.82	7.80	7.78

The phosphate buffer has a far better buffering power than the glycine buffer.

Results of Experiment

(a) Significance of Silver Potentiometric Titration Curves—As the significance of curves was fully discussed in the previous papers[2,3], the authors intend here to remind the readers of the following.

5) S. Kikuchi and Y. Sakaguchi, *Seisan Ke-kyū* (in Japanese) published by Univ. of To yo, **3** No. 4, 161 (1951).
6) J. J. Lingane, *Anal. Chem.*, **20** No. 4, 285-292 (1948).

i. The silver potential is likely to be less noble when the silver salt of organic compound is hard-soluble and the compound adheres to silver halide as sensitizer, fog-inhibitor or desensitizer.

ii. One can discriminate the quality of compounds with their colors of precipitates. Black, brown or grey colors shows the production of silver or silver sulfide which are the reason of sensitization or fogging action. Yellow, yellowish orange, and white colors which are their silver salts are generally the sign for good fog-inhibitors.

iii. The sawteeth form of curve shows the reduction of Ag^+.

iv. The curve of the ineffective substance is same as that of buffer solution.

(b) Potassium Thiocyanate (I) — Potassium thiocyanate gives constant silver thiocyante potentials curves at any pH. The thiocyanate ion is similar to inorganic halogen ions although it contains a sulfur atom.

(c) Urea (XIV), Guanidine (XV) and Diphenyl guanidine (XVI) — From Fig. 2 it may be seen that urea does not react with Ag^+. Guanidine and diphenyl guanidine resemble urea.

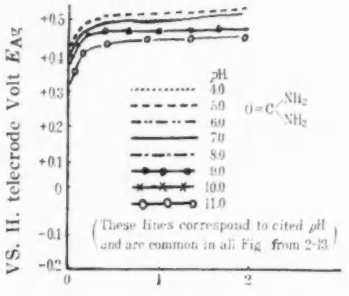

Abbreviations

B	black
Br	brown
D	dirty
G	grey
O	orange
P	precipitate
W	white
Y	yellow

Fig. 2. Urea.

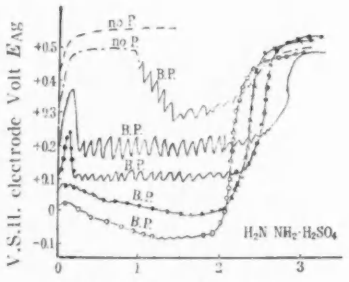

Fig. 3. Hydrazine sulfate.

(d) Hydrazine — The solution of hydrazine sulphate gives, as generally accepted, the curve of reduction of 2 mol. Ag^+ ion in the region more alkaline than pH 6 (Fig. 3).

(e) Thiourea and Thiosemicarbazide—From Fig. 4 the thiourea shows the reduction of 2 mols. of Ag^+ ion in the acid region, while in the neutral and alkaline regions, the curves indicate the decomposition of compound to give black silver sulfide up to 2 mols. equivalent of $AgNO_3$ and the yellow residue with more silver ions. The former is produced by means of $=S$ and the latter by $-NH_2$. The authors suppose that the electronegativity of NH_2 in thiosemicarbazide affects less than thiourea owing to the long distance from the carbon atom attached to $=S$, so the first gives the silver sulfide more easily than thiourea. (Fig. 4, 5)

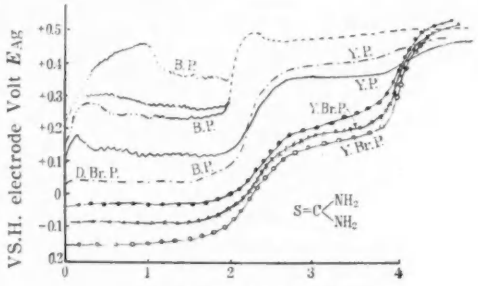

Fig. 4. Thiourea.

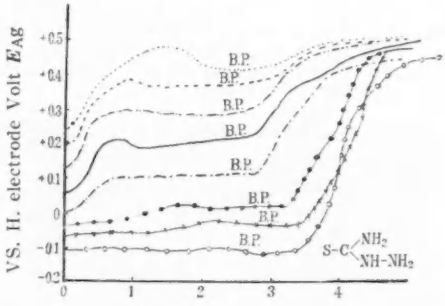

Fig. 5. Thiosemicarbazide.

(f) Benzaldehyde Thiosemicarbazone (IV)— Fig. 6 and 7 are obtained for (IV). In Fig. 6 Sörensen's phosphate buffers were used, the equivalence to Ag^+ becomes larger with pH increase up to 8. The silver equivalent at pH 6, 7, and 8 are 2, 2.5, and 3.5 respectively. Suddenly it turns back to 1 at pH 9. In Fig. 7 where the citrate and the glycine buffers are used, then (IV) gives unit silver equivalent at pH range from 4 to 10, in other word it does not give silver sulfide. In fact, (IV) is the good fog-inhibitor. Perhaps the benzaldehyde group lessons the electronegativity of NH_2 group.

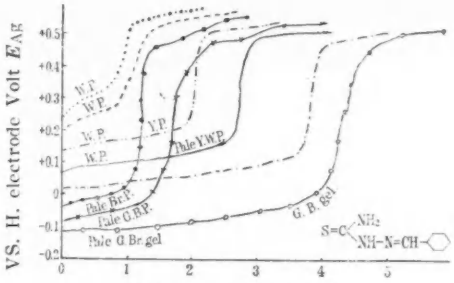

Fig. 6. Benzaldehyde thiosemicarbazone.

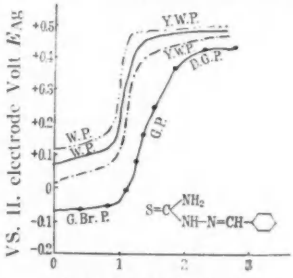

Fig. 7. Case of benzaldehyde thiosemicarbazone with new type of buffer solution.

(g) o-, m-, p- Nitrobenzaldehyde Thiosemicarbazones. (VIII, IX, X)—The curves for three isomers (VIII), (IX), (X) are given respectively in Fig. 8, 9, and 10. At pH 6, 7, and 8 (IX) and (X) they need too much silver ion and at pH 9 the equivalence turns back to unity. New buffers reveal that even at these pH the substances need one Ag^+. The substance (VIII) shows, contrary to (IX) and (X), the unit equivalent even with phosphate buffers. This fact makes us to suppose that silver atom, phosphate ion and some organic substance from the complex form and meta and para forms are more suitable for this complex formation than ortho form.

The colors of precipitates show that these compounds are probably good fog-inhibitors. Indeed the emulsion test with these substances done by Konishiroku Photo Co. reveals that these are good fog-inhibitors though a little desensitizing[7].

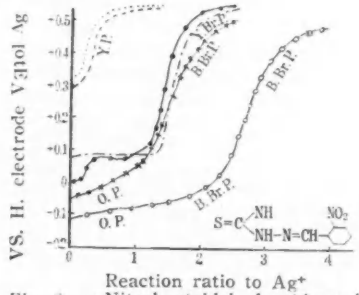

Fig. 8. o-Nitrobentaldehyde thiosemicarbazone.

7) Konishiroku Photo Co., *Report of the Committee of addition agent*, (1952).

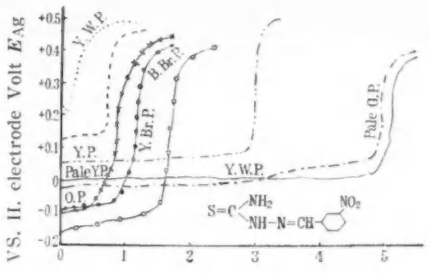

Fig. 9. m-Nitrobenzaldehyde thiosemicarbazone

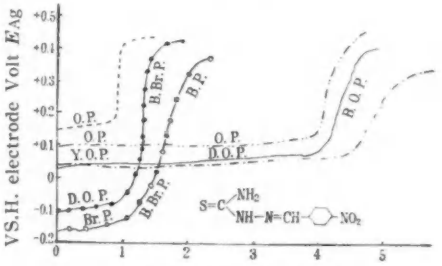

Fig. 10. p-Nitrobenzoldehyde thiosemicarbazone.

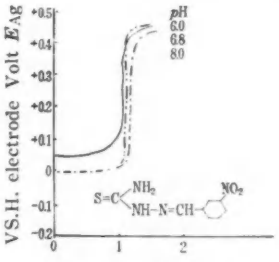

Fig. 11. Case of m-nitrobenzaldehyde thiosemicarbazone with new type of buffer solution.

(h) p-Dimethylamino Benzaldehyde Thiosemicarbazone (VI) and Phenyl Thiosemicarbazide (XI)—The silver potentiometric titration curves are also obtained for (VI) and (XI). The substance (VI) as predicated from its similar structure with (IV) has no tendency to produce Ag_2S, while substance (XI) has this tendency stronger than thiosemicarbazide (III).

(i) Piperonal Thiosemicarbazone (V) and p-Acetamide Benzaldehyde Thiosemicarbazone (VII) and Benzaldehyde Phenyl Thiosemicarbazone (XII)—These compounds have qualities between (IV) and (XI).

(j) The color of the precipitates and the free energy change are shown in Table III when the substances are titrated with Ag^+. To see easily all characters of the tested substances, Table III is dressed in which the symbol $-\Delta F^{\circ}_{323}$ (standard free energy change at 50°C.) is as previous reports[2,3].

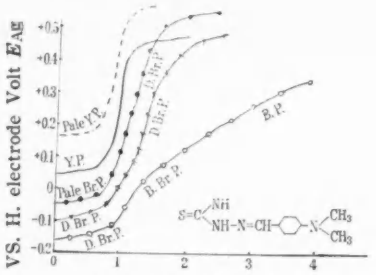

Fig. 12. *p*-Dimethylamino thiosemicarbazone.

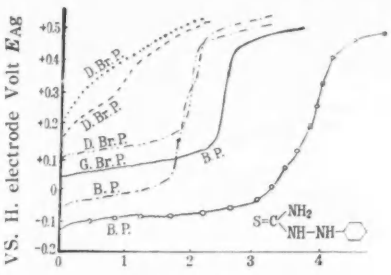

Fig. 13. Phenyl thiosemicarbazide.

TABLE III

PROPERTIES OF SUBSTANCES OBTAINED BY THE REACTION OF ORGANIC SULFUR COMPOUNDS AND THE SILVER ION

Substances	*p*H 5.0		7.0		9.0	
	$-\Delta F^\circ_{323}$ kcal/M	Colors of precipitate	$-\Delta F^\circ_{323}$	Colors	$-\Delta F^\circ_{323}$	Colors
Potassium thiocyanate (I)	15.4	white	15.4	white	15.4	white
urea (XIV)	—	no	—	no	—	no
guanidine (XV)	—	no	—	no	—	no
diphenyl guanidine (XVI)	—	no	—	no	—	no
hydrazine (XIII)	—	no	17–18	silver black ppt.	20	silver black ppt.
thiourea (II)	16	brown, black	19	dirty brown black	22.7	dirty brown, black
thiosemicarbazone (III)	14	brown, black	18	brown, black	22.5	black
benzaldehyde thiosemicarbazone (IV)	17.7	white	20.6	white	22.9	pale greyish brown
piperonal thiosemicarbazone (V)	18.7	white	21.1	white	23.2	pale brown
p-acetamide benzaldehyde thiosemicarbazone (VII)	17.5	white	20	white	22.5	brown black
p-dimethylamino benzaldehyde thiosemicarbazone (VI)	18.9	pale yellow	21.7	yellow	23.5	pale brown
m-nitrobenzaldehyde thiosemicarbazone (VIII)	18.3	yellow	20.8	yellow	23.0	pale brown
phenyl thiosemicarbazide (XI)	18.8	dark brown	20.7	greyish brown	23.5	black
benzaldehyde phenyl thiosemicarbazone (XII)	19	pale yellow	21.5	yellow	22.9	yellow brown

Conclusion

From the silver potentiometric titration of some organic sulfur compounds and their related compounds, the following facts are revealed.

1. In the phosphate buffer, some compounds (IV, V, VIII, X, XII) need too much silver ion because of the complex from of silver and phosphate and these compounds. Then the citrate and glycine buffers were used in order to avoid the complex formation from these compounds.

2. SCN^- radical gives an inorganic silver salt which is not affected with the *p*H change.

3. Hydrazine reduces Ag^+ although it does not give sulfur compound, because of the reducibility of NH_2.

4. Phenyl thiosemicarbazide (XI) gives sulfur most easily, next is thiosemicarbazide (III) and then thiourea (II).

5. We concluded that the sulphur atom is necessary to make good fog-inhibitors, and thiosemicarbazone derivatives which have long chain structure are excellent for the decrease of the electronegativity of NH_2. Thiosemicarbazide derivatives give sulfur compounds and thiocyanate gives silver thiocyanate only.

The authors wish to acknowledge the gift of thiosemicarbazone and thiosemicarbazide derivatives by K. Murobushi (Konishiroku Photo. Ind. Co.) and the suggestions by Y. Koseki (Fuji Photo Film. Co.).

Institute of Industrial Science, Tokyo University, Chiba

*Two Uncommon Amino Acids obtained from Roseothricin**

By Koji NAKANISHI, Toshiko ITO, Mamoru OHASHI, Ichiro MORIMOTO and Yoshimasa HIRATA

(Received May 17, 1954)

Roseothricin is a complex antibiotic comprised from several components and produced by *Streptomyces roseochromogenus*. It was formerly designated H-277 and isolated by Hosoya et al.[1] from the soil of suburban Tokyo during the course of investigations on the production of antibiotics from various molds. Although of rather limited clinical importance due to its somewhat high toxicity, it possesses a high and broad antibacterial spectrum[2]; furthermore, the acid hydrolysis of either roseothricin complex or of the separated components afforded two amino acids, neither of them belonging to the common natural amino acids. Hence chemical investigations have been undertaken on these hydrolysates, and one has been identified as β, ε-diaminocaproic acid (I) (β-lysine)[3]*** or isolysine[4]. The other substance, for which the trivial name of "roseonine" is proposed, has now been shown to be 2-amino-4 (or 5)-(1-carboxy-1-hydroxy-2-amino)-ethyl-2-imidazoline (II), a totally new β-amino acid.****

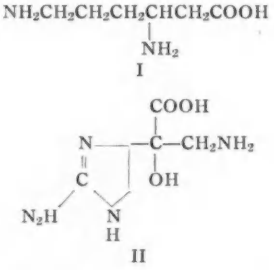

I

II

The separation of the components of roseothricin complex was accomplished by submitting the substance to paper chromatography, utilizing butanol-ammonia-*p*-toluenesulfonic acid mixture as solvent and *B. subtilis* test plate for location of the active agents.[5] Three substances were obtained, which were designated roseothricin A, B and C, in order of their decreasing flow distance; a fourth component was obtained occasionally. Filter paper cataphoresis (100 v., 4 hrs.) at pH 4.6[5] separated the complex into two fractions, A and B-C. Separation of the complex by means of paper chromatography and filter paper cataphoresis under slightly different conditions have also been reported.[6] Ion exchange chromatography was found to be effective[5] for the separation of A and B-C in fairly large quantities; the complex was absorbed on a column of Amb. IRC-50 (Na-form) column at pH 7, and when eluted with citric acid-HCl buffer at pH 4.6 and gradually lowering the pH by 0.2 units, the following three fractions were obtained: pure A, A-B-C mixture and finally B-C mixture. The separation of B and C has as yet not been accomplished. The toxicity against mice (ID_{50}) weighing 14.4-15.6 g. (intravenous injection) was as follows: A, 155 mg./kg.; B-C, 1 mg./kg.; complex, 14 mg./kg. The respective fractions were active against gram-positive, -negative and acid-fast bacteria, the activity against *Myco. tuberculosis* 607 being of the same order as that of streptomycin; the activity of A was 1/2-1/100 that of B-C and the complex, depending on the species of the strain[1,2,5].

Roseothricin gave a crystalline helianthate (decomp 215–8°, N, 15.51%); reineckate (decomp. 185–190°, N, 22.18%) and picrolonate (decomp. 225–230°, C, 48.23; H, 5.63; N, 20.34%). The ninhydrin, biuret and Fehling reactions were positive, whereas the Pauly, Tollens, maltol, Sakaguchi, Trommer, Nylander, Molisch, Folins, Hopkins-Cole, Millon and Bial reactions were negative[1]. The acid hydrolysis of reseothricin complex and of roseothricin A both afforded two ninhydrin positive products, I and II, which were separated by the solubility differences of the

* Reported at the 6th Annual Meeting, Chem. Soc. Japan, (Kyoto), April, 1953 and at the 7th Annual Meeting, Chem. Soc. Japan, (Tokyo), April, 1954. A communication has appeared in *J. Am. Chem. Soc.* **76**, 2845 (1954).

1) S. Hosoya, M. Soeda, N. Komatsu, S. Imamura, M. Iwasaki, Y. Sonoda and K. Okada, *Jap. J. Exp. Med.*, **20**, 121 (1949); *J. Antibiotics*, **3** (4), 217 (1950).

2) S. Hosoya, M. Soeda, N. Komatsu and S. Imamura, *Jap. J. Exp. Med.*, **20**, 481 (1950); *J. Antibiotics*, **4**, (2), 79 (1951).

3) H. E. Carter, W. R, Hearn, E. M. Lansford, Jr., A. C. Page, Jr., N. P. Salzman, D. Shapiro and W, R. Taylor, *J. Am. Chem. Soc.*, **74**, 304 (1952).

4) E. E. van Tamelen and E. E. Smissman, ibid., 3714.

5) Y. Saburi, *J. Antibiotics*, **6** (8), 402 (1953).

6) S. Hosoya, M. Soeda, N. Komatsu, N. Hara, Y. Sonoda and R. Arai, *Jap. J. Exp. Med.*, **20**, 683 (1950); *J. Antibiotics*, **4** (6), 314 (1951).

picrates. Compound I, $C_6H_{14}N_2O_2$, $[\alpha]_D^{21}$ +19.0° (dihydrochloride in water) was ninhydrin positive, but did not respond normally to the action of the reagent (*vide infra*, Experimental) and therefore it is probably not an α-amino acid. The Van Slyke amino nitrogen determination gave values of one mole of nitrogen after five minutes and another mole after thirty minutes (Table I). The Kuhn-Roth C-CH_3 determination and periodate test were negative. No absorption maximum was seen in the ultraviolet spectrum, and the infrared spectrum of the hydrochloride in nujol also suggested a simple amino acid structure, i.e., 3.6–4.2 μ (broad), 5.81 μ (sharp and strong) 6.25 μ (medium), 6.7 μ (weak). The pK'_a values, 3.20, 9.47 and 10.82 (10°C), indicted that one carboxyl and two amino groups were present, and that probably a β-amino acid grouping was involved, the other amino group occupying the terminal position. The data allowed only two possible structures, viz., β, ε-diaminocaproic acid and α-aminomethyl-δ-amino valeric acid. Two papers by American workers[3,4] on the elucidation of the structure of an amino acid which had been obtained from streptothricin[7], streptolin[7,8] and viomycin[7,9] appeared at this point, and it was found that compound I was identical with the new amino acid, i.e., β, ε-diaminocaproic acid (β-lysine or isolysine).

The infrared spectrum of roseonine (II), $C_6H_{12}O_3N_4$, $[\alpha]_D^{13}$ +51.0° (dihydrochloride in water) (Fig. 1) showed besides bands expected for regular amino acid hydrochlorides, sharp

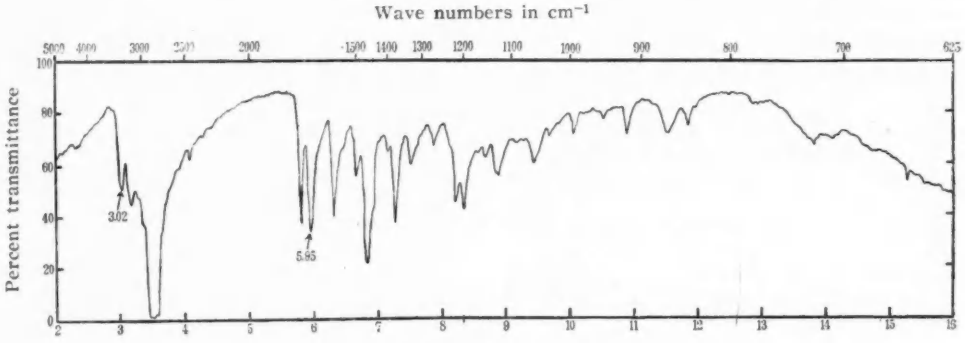

Fig. 1. Roseonine dihydrochloride (Nujol).

absorptions at 3.02 μ and 5.95 μ; the ultraviolet spectrum had an end absorption and a low broad maximum at 262–3 mμ (log ε: 1.22, dihydrochloride in water). Titration of the hydrochloride in aqueous solution gave pK'_a values of 2.4, 9.3 and 11.9 (17°C), the first constant apparently arising from the carboxyl group, and the second and third from nitrogen functions. The 11.9 acidic constant and the 5.95 μ infrared band suggested the possible existence of a guanido group and the low ultraviolet maximum was also comparable with that of guanidine hydrochloride, 265 mμ (log ε: 1.26, in water).

Permanganate oxidation of roseonine at room temperature gave guanidine and a small amount of glycine. When treated with periodate, it consumed one mol. of oxygen in 15 minutes with the formation of one mole each of ammonia and formaldehyde, which meant that one of the two adjacent carbon atoms bearing the hydroxyl and amino groups is at the end of a chain. Coupling this with the formation of glycine and the absence of a strong band in the region 9–10 μ (infrared spectrum) usually associated with primary alcoholic groups, the presence of the grouping $>C(OH)CH_2NH_2$ was clearly indicated. The Van Slyke amino nitrogen determination revealed the existence of two amino groups, one of them being liberated somewhat slowly (*vide infra*, Table I–II). The seresults may be summarized in the following expression III:

$$\left.\begin{array}{l} NH_2—C—N< \\ \quad\quad\quad\quad \| \\ \quad\quad\quad\quad N \\ >C(OH)CH_2NH_2 \\ —COOH \end{array}\right\} C_2H_4 \qquad \text{(No C—CH}_3\text{, N—CH}_3\text{)}$$

III

7) H. E. Carter, W. R. Hearn and W. R. Taylor, "Abstracts of Papers" 120th Meeting, Am. Chem. Soc., New York, N. Y. September, 1951, p. 3L.
8) E. E. Smissmann, R. W. Sharpe and E. E. van Tamelen, "Abstracts of Papers" 121st Meeting, *Am. Chem. Soc.*, Milwaukee, Wisconsin, April 1952, p. 80.
9) T. H. Haskell, S. A. Fusar, R. P. Frohardt and Q. R. Bartz, *J. Am. Chem. Soc.*, **74**, 599 (1952).

It was found at this point that the action of silver nitrite and subsequently hydroiodic acid—red phosphorous brought forth the remarkable conversion of reseonine into an imidazole derivative. Thus silver nitrite reacted normally to convert one amino group into a hydroxyl; the product IV consumed one mole of periodate with the formation of one mole of formaldehyde and it was natural to adopt the view (which received further confirmation, Table I–IV) that the non-guanido amino group had been replaced to give a vic-diol. Heating IV with hydroiodic acid and red phosphorous in a sealed tube gave a substance analyzing as $C_5H_9N_3$ (V); this coupled with *p*-diazobenzenesulfonic acid to give an orange-red color, a reaction which is typical for imidazoles possessing a free imino group and a hydrogen atom (or carboxyl) in positions 2,4 or 5 (Pauly reaction). The bromine decoloration test which is negative for 2-imidazolines but positive for imidazoles containing a free nuclear methine group was also positive. The Kuhn-Roth determination corresponded to one C—CH_3 whereas the N—CH_3 (or N—C_2H_5) determination was negative. Hence V must be 2-amino-4 (or 5)-ethylimidazole. Amongst the conceivable structures for a compound possessing the partial structure III, those represented by II or VI, i.e., 2-

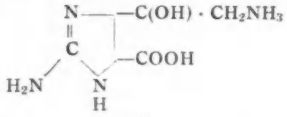

VI

amino-2-imidazoline derivatives, were the only two which could afford V. The possibility of an open chain structure, and hence the formula $C_6H_{14}O_3N_4$ instead of $C_6H_{12}O_3N_4$ was also considered, but all were excluded on grounds of apparent inconsistencies with data hitherto mentioned. The reaction sequences then may be formulated as follows:

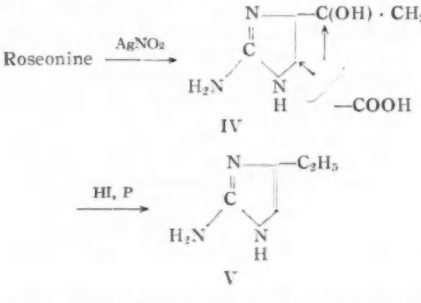

The conversion of IV into V could take place by dehydration of the side chain hydroxyl group, and rearrangement of the double bond to the more stable aromatic system and decarboxylation.

Interesting supporting evidences for the presence of a ring system in roseonine and V were obtained from comparative studies on the Van Slyke amino nitrogen determination (Table I). Comparing 7 with 6 and 8

TABLE I

VAN SLYKE AMINO NITROGEN

Compound	Moles of N liberated in 7 min.	Moles of N liberated in 30 min.
1. α,ε-Diaminocaproic acid (I) dipicrate	1.06	2.13
2. Roseonine (II) dihydrochloride	1.02	1.84
3. Roseonine (II) methyl ester dipicrate	1.04	2.00
4. *vic*-Diol (IV) from roseonine	0.09	0.71
5. Compound V monopicrate		0.23
6. 2-Amino-2-imidazoline (VII) monopicrate	0.14	0.86
7. Arginine monopicrate	1.01	1.04
8. 2-Amino-4,6-dihydroxypteridine (VIII)	0	0.29

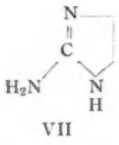

VII

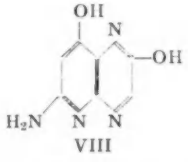

VIII

respectively, it may be noted that incorporation of the guanido group into either a non-aromatic or aromatic ring exerts a labilizing effect on the guanido amino group. Thus the presence of a 2-imidazoline ring in roseonine was strengthened by the fact that the response of the guanido amino group of roseonine and products (2, 3 and 4) was similar to that of 2-amino-2-imidazoline, namely, about 0.8 mol. in 30 minutes; furthermore, comparison of 5 (0.23 mol.) and 8 (0.29 mol.) also reveal a striking similarity between the two compounds and hence the probable incorporation of the guanido group of V into an aromatic nuclei.

Of the remaining alternative structures II and VI, the latter was excluded on the following grounds: (i) Roseonine is remarkably stable towards dilute and concentrated hydrochloric acid and thus the functional groups are probably not disposed in space so as to permit easy dehydration leading to formation of γ-lactone, -lactam or hydantoin-imide-(2) rings. These relations are satisfied in struc-

ture II: it may also be noted that normal acid dehydration involving the tertiary hydroxyl group would be hindered due to the presence of the carboxyl and an adjacent positive ammonium (NH_3^+) group. (ii) In the periodate treatment, a second mole of the reagent was consumed after 20 hours, a behavior conforming to that of serine, and hence apparently to that of isoserine.

Structure II is also consonant with the fact that the Sakaguchi and biacetyl reactions were negative since it has been reported that N, N'-disubstituted guanidines do not respond to these color tests[10].

Experimental**

I. Hydrolysis of Roseothricin.—A solution of 5 g. of roseothricin (complex or A) in 50 cc. of 20% HCl was heated in a sealed tube for 48 hours at 100°C. and the reaction mixture was evaporated to dryness in vacuo. After addition of 20–30 cc. of water and filtration to remove some tarry product, two spoonfuls of Amberlite IR-4B (OH-form) was added and left overnight when the *p*H was 7–8. The resin was removed and to this there was added 6 g. of picric acid under slight heating upon which a mixture of two picrates and a small amount of resinous product was deposited. The mixture was warmed to bring the picrates into solution, and the resinous material was removed by filtration through cotton. The cooled filtrate containing yellow and orange-yellow picrates was gently rewarmed, when the former dissolved more rapidly. The supernatant was decanted and the separation of the two picrates was effected by repeating the process of dissolution, cooling, warming and separation in the conventional triangular scheme of fractional crystallization. The yellow and orange-yellow picrates corresponded to that of β,ε-diaminocaproic acid and roseonine, respectively. Upon recrystallization from water, each picrate weighed about 2 g. When submitted to paper chromatography using butanol-acetic Acid-water (4:1:5) as solvent, the picrates dissociated and each gave a single spot with ninhydrin, Rf 0.15 (β,ε-diaminocaproic acid) and Rf 0.08 (roseonine).

II. β,ε-Diaminocaproic Acid (I). *Dipicrate*: m.p. 200–1° (water). Found: C, 35.55; H, 3.27; N, 18.19; M.W.[11] 596. Calcd. for $C_{18}H_{20}O_{15}N_8$ (604.40): C, 35.76; H, 3.31; N, 18.54. *Dihydrochloride*: The picrate was dissolved in a small quantity of hot water and the picric acid which precipitated upon acidification with hydrochloric acid was extracted thrice with ether and the solution was concentrated in vacuo. The addition of ethanol gave the hydrochloride which was recrystallized by adding alcohol to the hot aqueous solution, hygroscopic needles, m.p. 146–7° (water and alcohol). Haskell et al. report 153–5° for this derivative.[9] Found: C, 33.60; H, 7.66; N, 12.96; Cl, 31.61. Calcd. for $C_6H_{16}O_2N_2Cl_2$: C, 32.88; H, 7.36; N, 12.79; Cl, 32.36. *N, N-Dibenzoate* (neutral derivative)[3]: The dihydrochloride was benzoylated through the Schotten-Baumann procedure, and the product recrystallized from ethanol, m.p. 159–60°. *p-Hydroxyazobenzene-p'-sulfonate*[3,4] m.p. 243–5° (water).

α-Amino acid test: (*vide infra*).

III. Roseonine (II). *Dipicrate*: decomp. 237° (water). Found: C, 33.48; H, 3.17; N, 22.09; M. W. 654[11]. Calcd. for $C_{18}H_{18}O_{17}N_{10}$ (646.40): C, 33.45; H, 2.81; N, 22.09. *Dihydrochloride*: From the dipicrate by conventional methods, m.p. 215° (water and alcohol). Found: C, 27.51; H, 5.40; N, 21.55; Cl, 27.97. Calcd. for $C_6H_{14}O_3N_4Cl_2$: C, 27.65; H, 5.41; N, 21.46; Cl, 27.16. *Methyl ester dipicrate*: To a suspension of 20 mg. of the dihydrochloride in 3 cc. of methanol, there was added 0.12 cc. of BF_3 etherate (4 mol. equiv.) and the mixture was refluxed gently for 5 hours. After the addition of 3 cc. of water and picric acid, methanol was removed by boiling and the solution was left at room temperature; the formation of the picrate was slow but the yield was good (35 mg.), m.p. 202° (water). However, there were occasions when the preparation of the ester failed; the cause for this uncertainty was not fully investigated. The ester gave a positive ninhydrin coloration. It was very susceptible to acid hydrolysis. Found: C, 34.66; H, 3.40; N, 21.39. Calcd. for $C_{19}H_{20}O_{17}N_{10}$ (660.43): C, 34.56; H, 3.05; N, 21.22. *α-Amino acid test*—Reaction with ninhydrin: A solution of 33 mg. ninhydrin (2 mol. equiv.) in 5 cc. of water was added to a solution of 26 mg. of the dihydrochloride in 2 cc. of water and heated at 100°. Contrary to the behavior of usual α-amino acids (formation of purple precipitate), no reaction occurred. Hence the mixture was heated in a sealed tube for 3 hours at 150°, upon which ca. 10 mg. of purple brown precipitate was obtained; when 2, 4-dinitrophenylhydrazine was added to the colorless solution a small amount of hydrazone, decomp. 110° resulted. However, the same two substances were also produced when ninhydrin alone was treated in a similar manner. A small amount of roseonine picrate was recovered after addition of picric acid to the filtrate of the hydrazone. The behavior of β,ε-diaminocaproic acid was also exactly similar.

Action of periodate: Sodium metaperiodate oxidized II-dihydrochloride at room temperature to give one mole each of formaldehyde (dimedone) and ammonia (titration) after 15 minutes. The consumption of the reagent was 1.01 mol. (15 min.), 1.05 mol. (1 hr.), 2.32 mol. (20 hrs.) for roseonine dihydrochloride, and 1.15 mol. (10 min.), 1.13 mol. (1 hr.), 1.94 mol. (30 hrs.) for serine. Standard techniques were employed for these analyses. Similar results were obtained with periodic acid.

Permanganate oxidation: 100 mg. of II-dihydrochloride and 250 mg. of KOH were dissolved in 5 cc. of water, and 120 mg. of $KMnO_4$ in 5cc. of water

** All melting points were determined on a micro hot stage, and are uncorrected.

10) J. D. Mold, J. M. Ladino and E. J. Schantz, *J. Am. Chem. Soc.*, **75**, 6321 (1953).

11) Obtained from the extinction coefficient by the method of K. G. Cunningham, W. Dawson and F. S. Spring. *J. Chem. Soc.*, 2305 (1951).

was added dropwise with stirring over a period of 2 hours at 30°. After leaving for 2 hours, the mixture was filtered and the brown precipitate washed thoroughly with boiling water. The filtrate and wash solution were combined, and after acidification, taken up to dryness in vacuo. The residue was extracted repeatedly with boiling ether, and the ether extract was left overnight to evaporate when a minute amount of colorless crystals, m.p. 126–31° (with partial sublimation; m.p. depression with malonic acid) was obtained. Though the amount was insufficient to permit further purification, paper chromatography gave only a single spot corresponding to oxalic acid; a simultaneous run showed that neither malonic, succinic nor malic acid was present. The residue from ether extraction was extracted with boiling ethanol, leaving a white inorganic salt. Removal of alcohol gave a hydroscopic crystalline residue. An aqueous solution of picric acid was added; the crystals were first washed with ether and then recrystallized several times from water with addition of active charcoal; 3 mg. of yellow plates, m.p. 315°. No depression observed when mixed with authentic guanidine picrate. Found: C, 29.65; H, 3.13; N, 28.81. Calcd. for $C_7H_8O_7N_6$ (288.18): C, 29.17; H, 2.80; N, 29.17.

The filtrate from the guanidine picrate was acidified and, after extraction of excess reagent with ether, was concentrated in vacuo to give a syrupy mass. This was paper-chromatographed with the following solvents and in each case gave only a single ninhydrin positive spot undistinguishable from glycine. BuOH: AcOH: H_2O 4:1:1 (Rf 0.12). BuOH: AcOH: H_2O=4:1:5 (Rf 0.21). Lutidine: collidine: H_2O=1:1:1 (Rf. 0.15). 40% aq. acetone (Rf 0.45). Phenol: 1% ammonia= 85:15 (Rf 0.38).

Oxidation with $Ba(MnO_4)_2$ also afforded similar results.

vic—Diol (IV): A solution of 130 mg. of II-dihydrochloride was treated with 154 mg. of $AgNO_2$ (2 mol. equiv.) at room temperature for 15 hours, and after filtration of AgCl and concentration in vacuo, a syrupy mass was obtained. White crystals were isolated by the addition of alcohol and filtration; m.p. 190° (water and alcohol), yield 50 mg. Periodate oxidation for 20 minutes produced 0.62 mol. of formaldehyde. Found: C, 37.77; H, 5.62; N, 21.96. Calcd. for $C_6H_{11}O_4N_3$ (189.17): C, 38.09; H, 5.86; N, 22.21. When only one mole of $AgNO_2$ was added the yield of IV was poor, and upon addition of picric acid, unchanged starting material was obtained in good yield. Thus removal of both molecules of hydrochloric acid as AgCl seemed to be necessary for the satisfactory action of $AgNO_2$. Incidentally, $AgNO_2$ is presumably a weaker reagent than HNO_2 as could be seen from the fact that the β-amino group of histamine was converted into a hydroxyl by the latter but not by the former.

Compound V: II-Dihydrochloride (130 mg) was treated with 2 mol. of $AgNO_2$ and the product was worked up to give the syrupy mass as mentioned above. To this there was added 0.48 cc. of HI (b.p. 126°) and 24 mg. of red phosphorus, and the mixture was heated in a sealed tube for 8 hours at 150°. The clear colorless solution was separated from some tarry precipitate and after evaporating to dryness, water was added and the solution was concentrated again; the processes of concentration were carried out under nitrogen. A syrupy residue containing white crystals resulted. The crystals were separated by filtration and analyzed but were not further investigated, m.p. 168°, yield 30 mg. Found: C, 1.24; H, 5.26; N, 9.52; ash, 30.72. The acidic syrup was neutralized with Amberlite IR-4B when addition of picric acid afforded 30 mg. of a yellow picrate, m.p. 182° (water). The syrup as well as the free compound obtained from the picrate gave an orange-red Pauly test. The same picrate was obtained from the reaction product of one mole of $AgNO_2$, but the yield was even lower. Found: C, 39.05; H, 3.72; N, 23.91; M.W. 356[11] Calcd. for monopicrate, $C_{11}H_{12}O_7N_6$(340.25); C, 38.83; H, 3.56; N, 24.70.

Acid treatment: Roseonine is remarkably stable towards acid, and was recovered unchanged after heating 50 mg. of the dihydrochloride with 0.6 cc. HCl in a sealed tube for 8 hours at 150°.

Summary

Roseothricin has been hydrolysed to give two uncommon amino acids, *viz.*, β,ε-diaminocapric acid (I, β-lysine), and 2-amino-4(or 5)-(1-carboxy-1-hydroxy-2-amino)-ethyl-2-imidazoline (II, roseonine) as the sole ninhydrin positive products.

Acknowledgement

The present work was undertaken in collaboration with Prof. S. Hosoya and his associates, Institute for Infectious Diseases, University of Tokyo, to whom the authors are greatly indebted for their continuous support in the problem and generous supply of roseothricin.

Most of the analyses and infrared determinations were carried out by the microanalytical staff at the Institute of Polytechnics, Osaka City University, and the authors wish to make grateful acknowledgements to Mr. S. Senoh and Mr. M. Yamaguchi for their exceedingly generous cooperation.

They also wish to thank Professor F. Egami for his interest and counsel during the course of this study, and the Sanyo Pharmaceutical Co. for preparing a portion of roseothricin.

Department of Chemistry, Faculty of Science, Nagoya University, Nagoya

*** We are very grateful to Professor Carter for information give us on β-lysine.

**** It has been seown by direct comparison that roseonine is identical with streptolidine, a hydrolysis product of streptolin (Communication from Professor E. E. van Jamelen, September 10 (1954).

Heterogeneous Structure of Rayon. IV. Effect of Stretching on the Heterogeneous Structure (1)

By Saburo OKAJIMA and Shigeru HAYAMA

(Received September 16, 1953)

In the previous papers[1] the authors determined the conditions of the peeling-off of rayons by the fibre-heterogeneous acetylation and studied the properties of the skins and cores of some rayons on the market. Now the method has been applied to a series of viscose rayons prepared by a two-bath process in order to study the effect of the stretching of the rayon fiber in the second bath upon its heterogeneous structure.

Experiment

(1) Rayon samples.—The samples used were a series of viscose rayons prepared from an ordinary factory viscose by a two-bath process in the laboratory of the Teikoku Jinken Co. The spinning was carried out as shown diagramatically in Fig. 1, in which the first bath A was composed of 9.70% H_2SO_4 and 0.4% Zn besides some Na_2SO_4, its specific gravity being 1.25. The temperature was kept at 50±1°C and the immersion length was 23 cm.

The second bath B was hot water of 80°C, the immersion length being 35 cm.

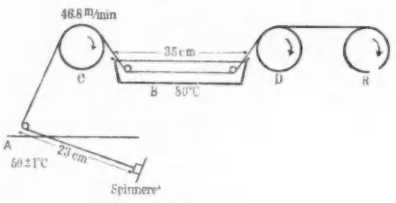

Fig. 1.

The peripheral velocity of the first godet C was fixed to 46.8 m./min. and that of the second one, D, was so controlled as to be able to stretch the yarn in the second bath to various degrees as given in Table I. The yarn collected on a bobbin R was, after being removed from R washed thoroughly, desulfured and bleached as usual. This process was carefully carried out so that the yarn was not stretched during the spinning between D and R. The details of the conditions and some of the properties of the yarns obtained are summarized in Tab. I.

TABLE I

Yarn No	Periph. speed of D, m./min.	Degree of stretch	Denier of the single filament	r	Dry stg., g./den	Dry elong., %
IIa	46.8	1.00	6.37	1.000	1.54±0.06	43.4±1.1
IIb	55.2	1.25	5.09	0.892	2.08±0.08	24.7±0.9
IIc	65.1	1.54	4.15	0.807	2.68±0.12	14.1±0.8
IId	73.0	1.87	3.41	0.753	3.26±0.11	11.1±0.3

The mechanical properties given in the above table were obtained by a test at 20°C and 65% R.H. and the values were estimated stochastically, the confidence coefficient being 95%.

The yarn was extracted with ether for several hours, washed repeatedly with hot water (60°C) and stored after air-drying. This sample was vacuum-dried immediately before use (the weight is W) and the heterogeneous acetylation was carried out for 3~300 hours at 60°C. The composition of the acetylation bath was as follows:

Acetic anhydride	5 g.	} per 0.5 g. sample.
Benzene	15 g.	
Sulfuric acid (1.84)	0.05 g.	

After acetylating the sample to the desired degree it was taken out of the acetylation bath, washed twice with benzol and further with hot water (60°C). It was then vacuum-dried and weighed (W_A). A half of it was peeled-off by pouring into chloroform and keeping over-night at 50°C, washed with water, vacuum-dried and weighed again (W'). From W, W' and W_A, L_2 and L_T are calculated as described in the previous paper.

The other half was used for the determination of the acetic acid content (A%). L_1 is then calculated from A, W and W_A.

The amount of the peeled-off cellulose is therefore $(L_1+L_2)/W$ or directly L_T/W, but the latter is smaller than the former by about 1.5% as was shown in the previous paper and also the present data show the same fact. Then the percentages of the peeled-off shell (P_r) and the layer dissolved during acetylation (P_s), are obtained from the above data as follows:

$$P_r=1-\left(1-\frac{L_T}{W}-0.015\right)^{\frac{1}{3}}=1-\left(1-\frac{L_1+L_2}{W}\right)^{\frac{1}{3}}$$

and

1) S. Okajima, S. Hayama and K. Kobayashi, This Bulletin **25**, 2/1, 275 (1952).

$$P_s = 1 - \left(1 - \frac{L_1}{W}\right)^{\frac{1}{3}}.$$

Of course P_r and P_s are given on the base of the original radius of the filament.

As to the details of the experimental methods and the notation used refer to the previous papers.

Experimental Results

The results are summarized in Figs. 2–6.

(1) Structural Difference between the Skin and the Core.—In the previous paper it was described that the acetylated shell of the fiber so degradated that it partly dispersed into the acetylation bath and that this rate of dispersion of the skin part was smaller than that of the core. This is true also in the present case (ref. Fig. 2). The

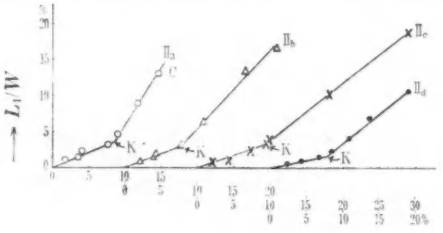

Fig. 2.

relation between the amount of this loss (L_1/W) and the acetic acid content (A) of the acetylated yarn is given by a broken line OKC. The amount of L_1/W corresponding to the inflection point $K-L_K/W$ in Table II—indicates the weight percentage of the outermost skin. These values and the thicknesses estimated from them are given in the second and third lines of the table.

TABLE II

Sample		IIa	IIb	IIc	IId
L_K/W, %		3.3	2.5	2.0	1.7
P_r % calculated from	Fig. 2	1.7	1.5	1.5	0.8
	Fig. 3	1.9	1.4	1.4	0.7

As the slopes of the lines OK and KC decrease in the order from IIa to IId, the rate of acetylation relative to the rate of dispersion of the acetylated portion increases with the growth of the stretching degree both in the skin and in the core. But the absolute rates do not necessarily change similarly.

In Figs. 3 and 4 rP_r and $r(P_r-P_s)$ are plotted against the acetylation time t, where r is the relative mean radius of each filament calculated from the denier, taking the denier of IIa as unity, so that the rate of the dispersion and the apparent rate of acetylation of IIa—IId can be compared directly, irrespective of the difference of their deniers.

As seen from Figs. 3–4, an inflection point appears on each curve, which tells that the

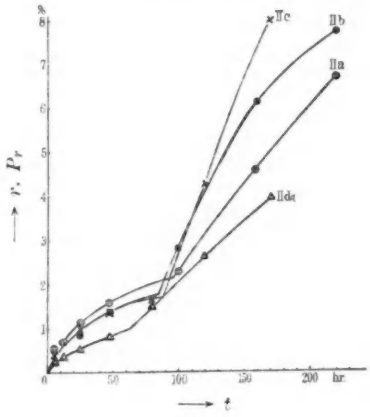

Fig. 3.

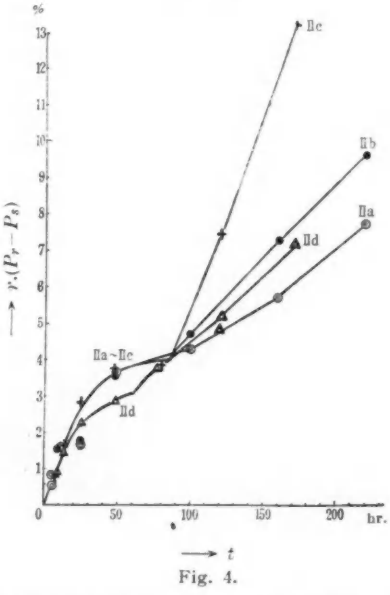

Fig. 4.

outermost skin exists and that the rates of the dispersion and the acetylation increase abruptly when the skin disappears from the filament. This is because the structure of the outermost skin is remarkably dense compared with that of the core or of the transition layer. Then the thickness of the skin layer is estimated also from the curve in Fig. 3 as shown in the fourth line of Table II. A good comformity between the corresponding values in the third and fourth lines

supports this view.

Among IIa—IId the outermost skin becomes thinner in the order from IIa to IId.

As to the effect of the stretching of a rayon fiber on its microstructure, the skin becomes slightly denser while the core becomes looser as the stretching increases, with an exception of IId, the structure of which is extraordinarily denser.

An electronmicrograph taken by Hermans[2] shows that a number of small pores exist within the outermost skin. These pores may be caused by the gasses evolved by the decomposition of viscose. Then we can suppose from the above two figures that the porosity within the outermost skin becomes the larger as the yarn is stretched the higher.

But this generalization can not be applied to the case of the yarn IId, the core of which is thought to have rather greater density and smaller porosity than that of IIb. To this point the authors shall return later.

(2) **Orientation Degrees of the Skin and of the Core.**—The relation between Γ and P_r is similar to these of the commercial viscose rayons already described in the second report. Three parts of the structure, i.e., the outermost skin, the transition layer and the core are clearly distinguished also here (rf. Fig. 5). The thickness of the outermost

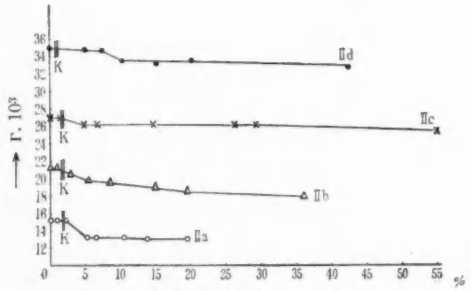

Fig. 5.

skin calculated from the inflection point (Figs. 2—3) coincides well with that found on the corresponding curve as indicated by K with an exception of IId, whose outermost skin is abnormally thick.

As to the orientation degree, both Γ of the skin and of the core grow almost linearly with the stretching degree or the difference between that of the skin and that of the core is kept nearly constant irrespective of the stretching (rf. Fig. 6). So if a fibre of nearly

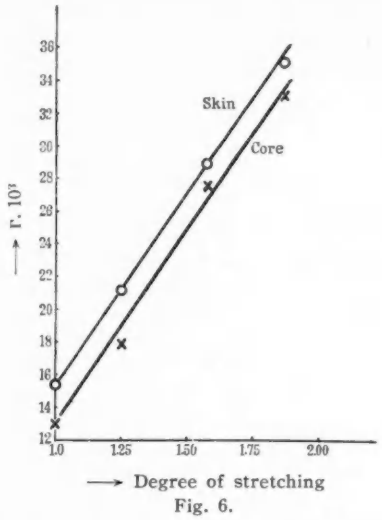

Fig. 6.

isotropic core is prepared by extructing a viscose slowly into a coagulating bath and not drafted[3] or stretched, its skin seems to be of low orientation. That it is truly the case is experimentaly proved. Then the orientation of xanthate molecules due to the high velocity gradient near the spinneret wall is considered to be feasible, if any, or the orientation seems not to be fixed in the hydrate cellulose fibre, even when the high orientation may occur in the viscose.

(3) **Abnormality of IId.**—As described above some properties of the filaments change systematically in the order from IIa to IId according to the degree of stretching, but IId often deviates from this order.

Many studies have been carried out on the mechanism of the viscose spinning process. They are however fragmentary and the results obtained are not yet conclusive. In order to explain the above results, attempt is made here to consider also this mechanism from author's view point. It is however partly a conjecture for which we hope future experiments will prove.

The first change of a viscose stream extruded from a spinneret orifice into the bath solution is the production of the Zn-xanthate layer on its surface and not the direct regeneration of the Na-xanthate. This layer is assumed to be hydrophobic compared with the ordinary Na-xanthate and cross-linked by Zn. Because of this the cellulose layer

2) P. H. Hermans, *Textile Research J.*, **20**, 105 (1950).

3) "Drafting" and "Stretching" are used as the same thing as "Verzug" and "Verstreckung" of Kauch and Harms; ct. Herbert Brandenberger; Melliand Textilber., **34**, 823 (1953).

regenerated from this Zn-xanthate has also a denser structure. This is the outermost skin considered in this study. It is well known that the addition of $ZnSO_4$ to the spinning bath retards the regeneration to follow. This is considered to be due to the stability of the Zn-xanthate, the retarded penetration of the sulfuric acid (inward) and the enhanced osmotic dehydration of viscose and xanthate (outward), because of the denser structures of the Zn-xanthate and of the hydrate cellulose layers derived from it.

The viscose stream is drafted by the first godet to attenuate the filament so that the orientation occurs during the osmotic dehydration. As the yarn IIa—IId are drafted equally and the stretching in the second bath is supposed to attenuate the cross section uniformly, the percentage occupied by the outermost skin of each filament must be equal to each other. But the observed thickness of the outermost skin of the yarn is thinner the higher it is stretched. This may be due to the slippage of the yarn on the first godet, the actual drafting not being kept constant as expected.

The drafting brings about the higher orientation of the outermost skin compared with that of the core, because the dehydration of the latter is not sufficiently high to be orientated effectively by this drafting.

Now in the second bath the yarn is stretched to various degrees and at the same time a sudden decomposition occurs because of the high temperature.

The orientation degrees of the outermost skin and of the core are raised further by this stretching and fixed as seen in Fig. 5.

The stretching also accelerates the dehydration of the core by the squeezing action, but at the same time the increase of the density of the outermost skin due to higher stretching retards the penetration of the liquids as shown in Fig. 7. As the result,

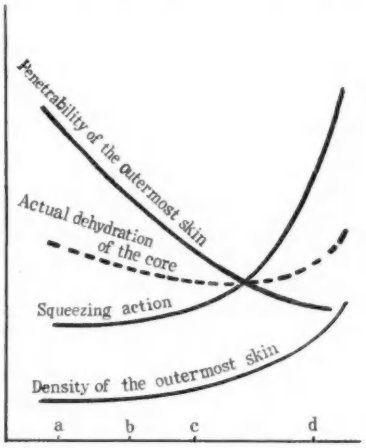

Fig. 7.

the actual dehydration goes through a minimum point with stretching.

Fig. 8.

(a) Dyed with Oxamine pure blue B

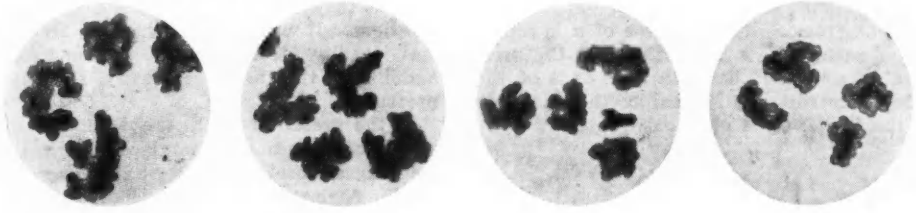

(b) Dyed with Oxamine blue 4R

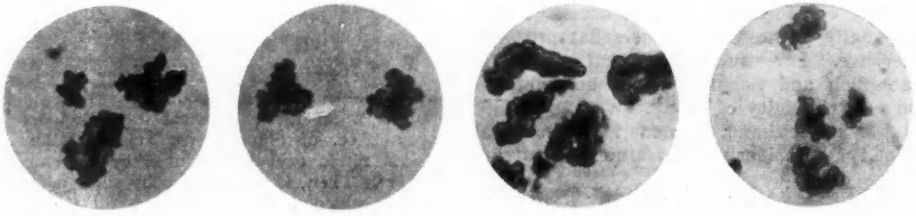

The sudden decomposition of viscose or xanthate evolves gasses and brings about a porous structure. But the more the viscose or xanthate core is dehydrated, the less is the destruction of the structure and the denser is it. So the outermost skin becomes denser in the order from IIa to IId, but the density of the core goes through a minimum (IIc).

In the case of IId the dehydration of the core proceeds and it approaches so near to the state of the outermost skin, that the orientation of that part is fixed effectively similarly to that of the outermost skin and the apparent outermost skin becomes extraordinarily thick. The origin of this outermost skin is thus dual and it can be distinguished only by the acetylation as shown in Fig. 5.

The relation between the outermost skin and the ordinary skin is as follows. The skin layer of an ordinary viscose filament has hitherto been recognized by metachromasis. The thickness of this skin seems to be larger than the authors' outermost skin. According to P.H. Hermans a number of tiny pores exist within an outermost layer (this seems to correspond to the authors' outermost skin), the pores being observed to grow larger toward the centre. Metachromasis is based on the distribution of the pore size so that the skin hitherto observed is thick and its thickness is dependent upon the state of the polydispersity of the dyes used.

Fig. 8 indicates the skins of IIa—IId dyed with Oxamine pure blue B and Oxamine blue 4R. These skins are thicker than our outermost skin and the latter dye seems to give a thicker skin than the former.

The cost of this research has been defrayed by the Grant in Aid for Fundamental Scientific Research from the Ministry of Education, to which the authors' thanks are due. The authors are also grateful to Mr. I. Okamura of the Teikoku Jinken Co. for his kind supply of the samples.

Faculty of Engineering, Tokyo Metropolitan University, Tokyo, and Faculty of Engineering, Yamagata University, Yonezawa

Structural Change in Some Solutions Having Structural Viscosity

By Masayuki NAKAGAKI and Shigeo SAKATA

(Received May 17, 1954)

The amount of liquid flowing out in unit time, Q, from a capillary tube of a in radius and l in length, is proportional to the pressure difference, P, between both ends of the tube. According to Poiseuille, the viscosity of the liquid, η_0, is obtained by:

$$\eta_0 = \alpha P/Q \tag{1}$$

where,

$$\alpha = \frac{\pi a^4}{8l} \tag{2}$$

For some colloidal solutions, however, the viscosity obtained from this equation shows abnormally large value for smaller pressure difference. For such abnormal viscosity, Freundlich and Schalek[1] gave an explanation of "elasticity of flow". Wo. Ostwald[2], on the other hand, named it "structural viscosity", considering that a net-work structure as in jellies has been formed in such solutions. It was assumed that the structure was readily destroyed by pressure, thus exhibiting the usual viscosity for higher pressure.

In the present report, the structural viscosity of vanadium pentoxide (V_2O_5) sol and mercury sulfosalicylate (Hg-SS) sol are measured. Then, the structural changes of these sols by shaking and by the irradiation of ultrasonic wave are observed under the electron microscope, and the structural viscosity is explained by it.

Experimental

V_2O_5 sol was prepared from ammonium vanadate by hydrolysis. 5 g. of ammonium vanadate was put in a mortar and smeared, adding drop by drop 25 cc. of dilute nitric acid (1 volume of d=1.4 nitric acid was diluted by 5 volume of water). Then, it was filtered by suction, washed with distilled water repeatedly, till the filtrate showed distinct red color. The precipitate on the

1) H. Freundlich and E. Schalek, *Z. physik. Chem.*, **108**, 153 (1924).
2) Wo. Ostwald, *Z. physik. Chem.*, **111**, 62 (1924).

filter paper was then put in 100 cc. of distilled water and stirred vigorously. The sol was aged about one month.

Hg-SS (mercury sulfosalicylate) was prepared by boiling 4 cc. of sulfosalicylic acid solution (containing 4 g. of solute) with 2 g. of yellow mercury oxide, stirring continuously. After the powders had been completely dissolved by the reaction, the solution was heated to dryness, and the powder obtained was ground. 0.3 g. of powder was dissolved in 200 cc. of water.

The structural viscosity was measured by Ostwald's overflow viscometer, shown in Fig. 1.

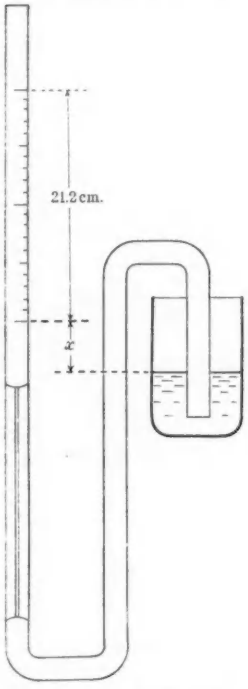

Fig. 1. Overflow viscometer.

A capillary tube of 21.2 cm. in length and 0.67 mm. in inner diameter was connected with a mess-pipette of 2 cc. in capacity. The grade of the pipette from 0.0 to 2.0 corresponded to the height of 21.2 cm. The height indicated by x in Fig. 1 was measured every time. It was usually 3.0—4.5 cm. The time, which 0.4 or 0.2 cc. of liquid required to flow down, was measured by stop watch, to calculate the mean amount of flow, Q. The pressure difference, P, was obtained from the mean difference of liquid levels.

The Electron microscope used was the Hitachi HU-4 type, operated under the direct enlargement of 10,000—5,000 ×. Plates were enlarged, 3—6 times, photographically. If necessary, a shadow was cast by Cr metal.

The ultrasonic apparatus was Shimazu P-200 type, used under the condition of 2 kV., 0.2 A. in input, and output current was also 0.2 A. The frequency was 610 kC.

Structural viscosity

Some of the results obtained for distilled water, V_2O_5 sol (about 0.6%), and Hg-SS sol (about 0.04%) are shown in Fig. 2. P/Q is proportional to the

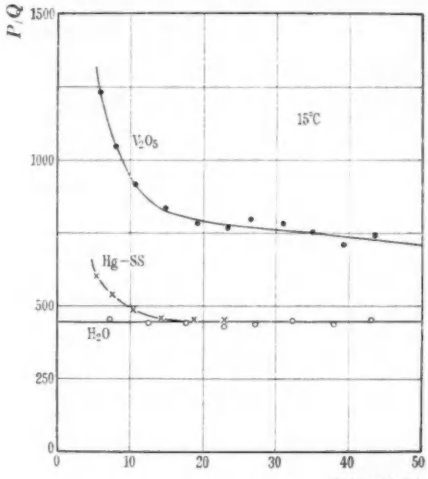

Fig. 2. P/Q-P relation at 15°C.

viscosity, as shown in Eq. (1). Curves for V_2O^9 and Hg-SS, therefore, show structural viscosity, as already known[1,2,3]. As for water, a typical Newtonian liquid, P/Q is constant regardless of pressure P. The mean value of $P/Q=446$ for water gives the α value, using the viscosity of water at 15°C[4], $\eta_0=11.45\times10^{-5}$ dyne. sec./cm.^{2}, $\alpha_{(obs)}=\eta_0/(P/Q)=2.57\times10^{-5}$ (dyne. cm./cmH$_2$O) (3) where cmH$_2$O means the pressure expressed by the height of the water column. On the other hand, using the size of capillary tube cited above,

$$\alpha_{(calc)}=\frac{\pi a^4}{8l}g=2.3\times10^{-5}\ \text{(dyne. cm./cmH}_2\text{O)} \quad (4)$$

where the constant of gravity, g, is used to recalculate the pressure to water pressure in cm. Values of Eq. 3 and 4 are in good agreement.

The ratio of P/Q for a specimen and for water is equal to the relative viscosity η/η_w. As shown in Fig. 3 and 5, the relative viscosity is linear to $1/Q$:

$$\eta/\eta_w=a+(b/Q) \quad (5)$$

at least in the measured range of pressure. This relation is explained as follows. In the pressure P applied to the liquid, P_0 is used to destroy the net-work structure, and the residue is effective to flow:

$$P_{eff}=P-P_0 \quad (6)$$

P_0 corresponds to the yield value. It is, then, assumed that the flow of broken net-work is Newtonian:

3) Wo. Ostwald and M. Mertens, *Kolloid-Beih.*, **23**, 242 (1927); S. Berkman and H. Zocher, *Kolloid-Z.*, **42** 322 (1927).
4) "International Critical Tables," Vol. 5 (1929), p. 10.

$$Q=\alpha P_{eff}/\eta_N, \tag{7}$$

η_N is the viscosity of this Newtonian flow. The apparent viscosity, η, is

$$\eta=\alpha P/Q=\eta_N+\alpha P_0/Q. \tag{8}$$

Then, the coefficients, a and b, in the empirical equation (5) are

$$\left.\begin{aligned} a&=\eta_N/\eta_w \\ b&=\alpha P_0/\eta_w=P_0/446. \end{aligned}\right\} \tag{9}$$

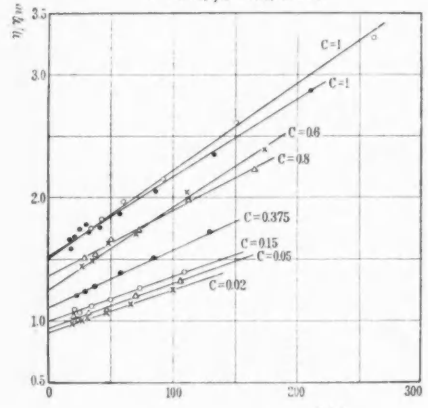

Fig. 3. $\eta/\eta_w-1/Q$ for V_2O_5 sol.

V_2O_5 sol of about 0.6% is diluted to various concentrations, left alone for 2 hrs., and the structural viscosity is measured. The results are shown in Fig. 3. The linear relation of Eq. (5) are verified. The concentration, C, is the relative one, assigning that of original solution (about 0.6%) as 1. Fig. 4 shows (η_N/η_w) and P_0 obtained from the data of Fig. 3, as a function of C. Fig. 4a shows that η_N/η_w increases linearly with the increase of C. Assuming the concentration of the original solution as 0.6%, and the density of V_2O_5 as 3.5[5], the relation.

$$\eta_N/\eta_w=0.91+128\phi \tag{10}$$

is obtained, where ϕ is the volume fraction of dispersed particles. The coefficient 128 is about 51 times larger than Einstein's 2.5. Comparing the fluctuation of plots in Fig. 4a and b, it is concluded that the yield value, P_0, sensitively depends on the structure, or the history of the specimen, while the Newtonian viscosity, or the viscosity after the structure has been broken, depends a little on its history.

As shown in Eq. (10), the relative viscosity becomes smaller than that of the solvent itself at smaller concentration. This is more clearly shown for Hg-SS in Fig. 5. This may be attributed to the slip of liquid on the surface of a capillary tube. The elasticity of flow will usually accompany the slip. Then, the amount of flow, Q, is assumed as the sum of the flow amount by Newtonian flow, Q_η, and the flow amount by slip, Q_s, on the surface of the tube (in this case, liquid is pushed out as a whole). Assuming that the slipping velocity at the tube surface, v_s, is

5) R. Abegg, "Handb anorg. Chem.," Vol. 3, p. 738 (1927).

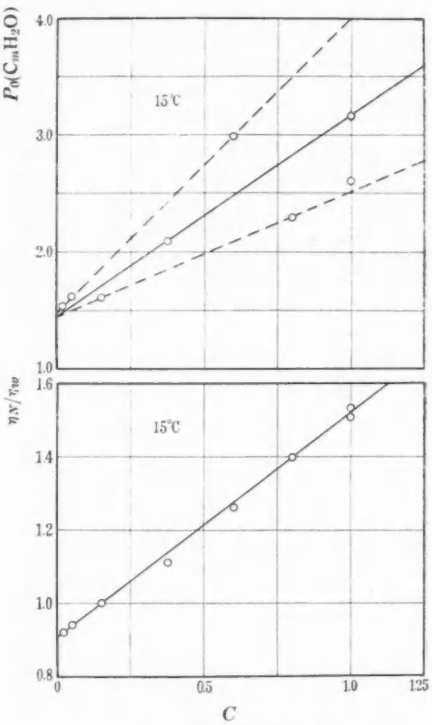

Fig. 4. η_N/η_w and P_0 for V_2O_5 sol.

proportional to the pressure P,

$$v_s=kP \tag{11}$$

Q_s becomes

$$Q_s=\pi a^2kP \tag{12}$$

On the other hand, Q_η is, using Eq. (6) and (7),

$$Q_\eta=\alpha(P-P_0^0)/\eta_N^0 \tag{13}$$

Then, the apparent viscosity η is obtained in the same form as Eq. (8)

$$\eta=\alpha P/Q=\eta_N+\alpha P_0/Q \tag{14}$$

But in this case, the apparent Newtonian viscosity η_N and the apparent yield value P_0 are related to their real values, η_N^0 and P_0^0, by the equation:

$$\left.\begin{aligned} P_0&=P_0^0/(1+\beta) \\ \eta_N&=\eta_N^0/(1+\beta) \\ \beta&=\pi a^2k\eta_N^0/\alpha \end{aligned}\right\} \tag{15}$$

Owing to this correction factor $(1+\beta)$, the apparent Newtonian viscosity η_N may become smaller than that of water. For example, at the infinite dilution of V_2O_5 sol,

$$\eta_N/\eta_w=\eta_N^0/\{\eta_w(1+\beta)\}=0.91 \tag{16}$$

is obtained from Eq. (10). Then, $\beta\simeq0.10$. If $P_0^0\ll P$ at infinite dilution,

$$Q_s/Q_\eta\simeq0.1. \tag{17}$$

For more concentrated sol, the slip may be more important by its greater elasticity, but no method to estimate it is found.

The effect of ultrasonic wave on the structural viscosity of Hg-SS is shown in Fig. 5. The time recorded in this Fig. show that elapsed after the

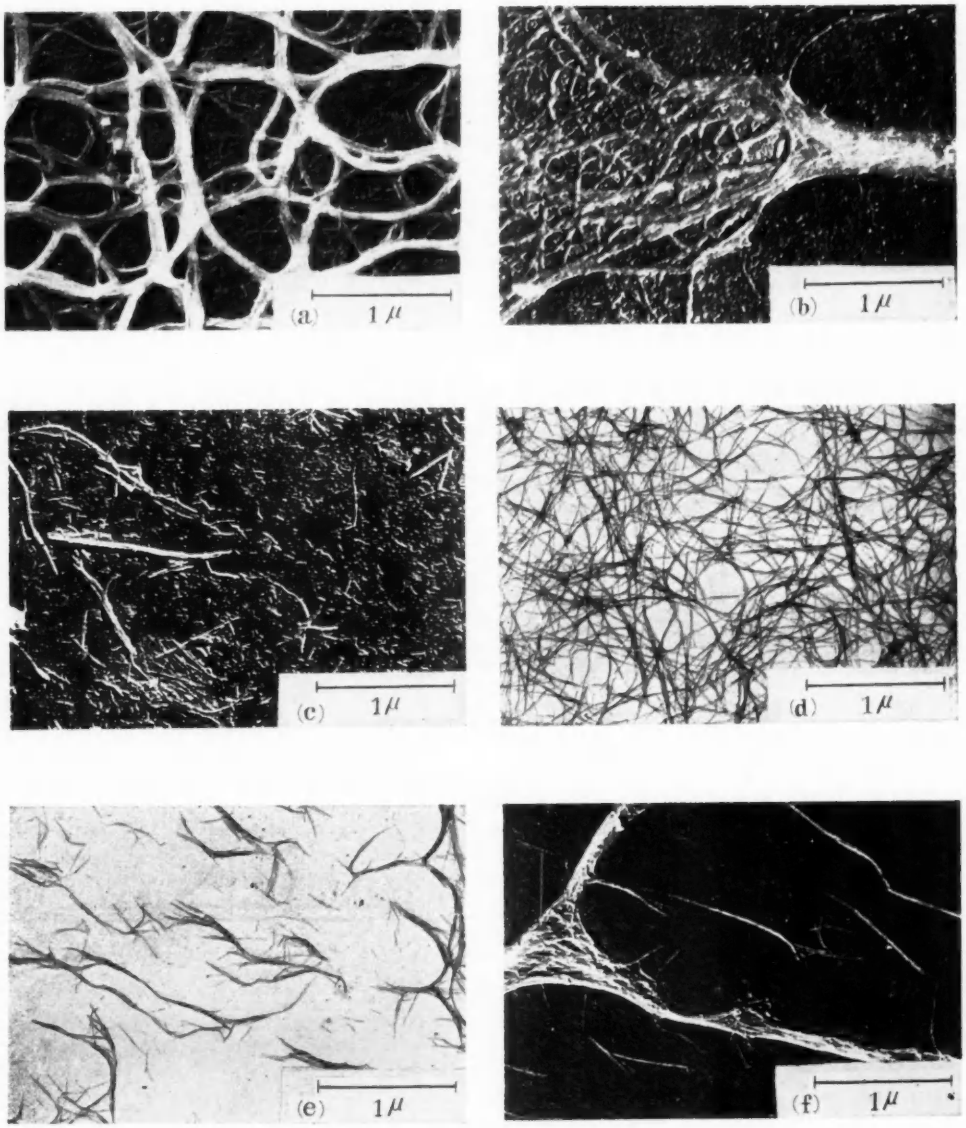

Fig. 6 Electron micrographs for Hg-SS:
(a) No treatment (b) Left alone for 3 min. after shaking
(c) Ultrasonic irradiation
and for V_2O_5:
(d) No treatment (e) Just after shaking (f) Just after shaking

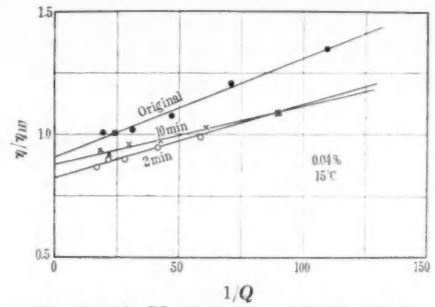

Fig. 5. Hg-SS after ultrasonic irradiation.

end of ultrasonic irradiation. It is shown that the Newtonian viscosity begins to recover after about 10 min., while the yield value does not recover yet. The net-work structure of Hg-SS seems to be destroyed by ultrasonic wave, but broken pieces soon join together to form fibers. Some time is spent, however, before these fibers form rigid knots to complete a net-work. This idea will be supported by electron micrographs shown later. The slip on the wall, however, is so great that a confident conclusion cannot be obtained.

Electron micrograph

Hg-SS has a typical net-work structure as shown in Fig. 6a. The net-work is built of yarns of about 0.1 μ in width, and the latter is a bundle of fibers of about 200 Å in its thickness. After shaking the solution in a test tube for 1 min., the net-work is destroyed and dispersed to single yarn or to single fiber, or on the other hand, they aggregate to a rope of 0.3–1 μ in thickness. Letting the solution stand for about 3 min., (Fig. 6b), the rope again disperses to reproduce a net-work. After 10 min., almost complete net-work structure has been reconstructed. By the irradiation of ultrasonic, (Fig. 6c), the net-work of Hg-SS is torn to pieces of 0.1–1 μ in length. When it is left alone for 3—10 min., broken pieces join together to form fibers, or further coagulaie to yarns and ropes. After 2.5 hrs. they reconstruct a complete net-work structure.

A similar change of structure is observed also for V_2O_5 sol. Original sol (Fig. 6d) has a net-work structure, constructed from fibers of about 100 Å in thickness. By vigorous shaking, the net-work is destroyed and torn to pieces as shown in Fig. 6e, or coagulates to thick ropes of ~0.1 μ

The structural changes observed above are favourable to explain their rheological behavior. Destruction of net-work structure may correspond to the lowering of viscosity under higher pressure. The recovery of the net-work structure may explain the recovery of its viscosity and elasticity of flow after keeping the sol standing, and the in thickness as shown in Fig. 6f. After being left alone for 2.5 hrs. or so, they recover a net-work structure again. The recovery of the net-work seems to take more time for V_2O_5 than for Hg-SS. Irradiation of ultrasonic brings nearly the same effects as that by shaking.
dependence of yield value on the history of teh specimen.

Summary

The structural viscosity of V_2O_5 sol is measured by Ostwald's overflow viscometer. A linear relation is found between the relative viscosity (η/η_w) and the reciprocal of flow amount ($1/Q$). Viscosity of Newtonian flow η_N and yield value P_0 are calculated from it. η_N and P_0 is nearly linearly varied with concentration. A decisive conclusion however, cannot be obtained owing to the slip of liquid on the capillary wall.

Hg-SS (Hg-sulfosalicylate) sol also showed a linear relation between η/η_w and $1/Q$. By the irradiation of ultrasonic wave, η_N and P_0 decreases. η_N again increases after about 10 min., but the recovery of P_0 took more time. A clear conclusion cannot be obtained due to the slip.

Electron micrographs showed that Hg-SS has a net-work structure, which is broken by shaking or by the irradiation of ultrasonic wave. When it is kept standing, the net-work is again constructed. V_2O_5 sol showed analogous structural changes.

Department of Chemistry, Faculty of Science, University of Tokyo, and Electron Microscope Laboratory, University of Tokyo

Heterogeneous Structure of Rayon. V. Effect of Stretching on the Heterogeneous Structure (2)

By Saburo OKAJIMA and Shigeru HAYAMA

(Received June 5, 1954)

In the preceding report the effect of the stretching of a rayon fiber in the second bath upon its heterogeneous structure was studied making use of a series of viscose rayons. Now the same experiment was repeated on another series of rayons which were spun by one-bath process but stretched to various degrees.

Experiment

(1) Sample of Rayons.—The spinning was also carried out in the laboratory of Teikoku Jinken Co. by one-bath process using an ordinary factory viscose. A constant volume of viscose was extruded through spinnerets of various orifice sizes and collected with an equal velocity so that the denier of the filament was kept constant. The peripheral velocity of the first godet was so controlled as to equalize it to the extrusion velocity of the viscose so that an equal drafting is given to every filaments. The details of the spinning condition and some of the properties of the yarns obtained are tabulated below.

TABLE I

No.	Diam of orifice, mm.	Stretch	Denier	Dry		Wet	
				Strength, g./den	Elong., %	Strength, g./den	Elong., %
IIIa	0.08	1.06	119.4	1.43	26.2	0.64	35.7
IIIb	0.085	1.20	120.3	1.69	20.5	0.74	29.9
IIIc	0.09	1.35	120.2	2.14	15.9	0.91	20.3
IIId	0.095	1.50	119.7	2.10	12.6	1.06	16.2

Collection velocity: 86.48 m./min.; Number of holes of a spinneret: 25; Bath composition: H_2SO_4 120 g./l, Zn 10 g./l besides Na_2SO_4, sp. gr. 1.25; Bath temperature: 50°C.

In this spinning the spinnerets with uniform holes were prepared with special precautions in order to keep the standard deviation of the denier as small as possible. And the actual standard deviations of the single filaments relative to the mean deniers were 5.8, 6.4, 7.3 and 7.6% in the order from IIIa to IIId.

The other operations were similar to those of the previous experiment, except that one bath-process was adopted in the present spinning.

The acetylation temperature was also controlled but it fluctuates so much that the discussion of the rate of acetylation is abandoned.

Experimental Results

(1) The Structure of the Skin and Core.—The relation between the loss during the acetylation (L_1/W) and the acetic acid content (A) is also similar to that of the previous report (Fig. 1). The weight percentages of the outermost skins IIIa—IIId are 4.6, 4.2, 4.2, and 4.4% respectively, or nearly constant irrespective of the stretching and the mean depth of the outermost skin is estimated to be 2.2% of the total radius. The slope of the line of the skin part, OK, is also nearly constant, but that of the inner structure decreases as the stretching increases. This means that the outermost skin is of nearly equal structure

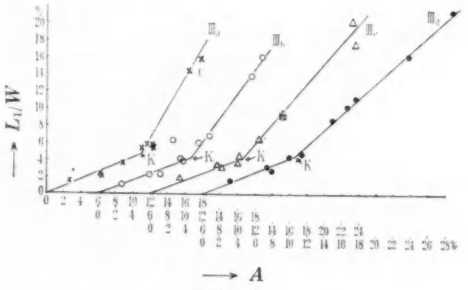

Fig. 1.

in each yarn but the structure within the skin becomes the more difficult to disperse as the filament is stretched the higher.

It is described in the previous paper that the origin of the outer most skin is related to the production of the Zn-xanthate. The constancy of this skin can be explained from this point of view as follows. If the diameter of an orifice is D, then the sectional area of each filament on the first godet will be k_1D^2. Of course the attenuation of a filament occurs due to some complex factors, such as drafting, gelling, dehydration, etc., and the cross section can not be circular. k_1 implies these complex changes of the sectional area and of the form but it is nearly constant and independent on the value of D in the range of the present spinning condition. Now the

thickness d of the Zn-xanthate layer formed is in proportion to the square root of the immersion time t, during which the yarn stays in the bath, so that d is given by

$$d=k_2t=k_3L^{1/2}D,$$

where L is the immersion length and k_2 and k_3 are numerical constants. Therefore d/D is independent on the orifice diameter D.

As the thickness of the outermost skin, which is derived from this Zn-xanthate layer is also proportional to d, and the further shrinkage of the cross section due to the regeneration, stretching and drying occurs uniformly the percentage of the outermost skin, P_r, must always be independent of D as shown above.

(2) Orientation.—The radial distribution of the intrinsic double refraction Γ is given in Fig. 2. The highly stretched filament has larger Γ.

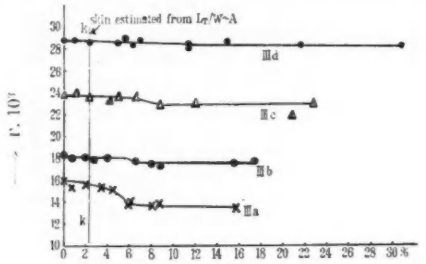

Fig. 2.

On the curves of Γ—P_r three parts of the structure are seen as already pointed out in the second paper of this study. The outermost skin indicated on these curves grows thicker in the order from IIIa to IIId and the last one appears to be of all skin types. But the skin which appears during the acetylation is a part of it as is indicated by a line k-k, in Fig. 2. So the outermost skin optically indicated as one layer is not simple but is composed of two layers. The inside layer may be caused as follows.

Because the viscose or xanthate close to the Zn-xanthate skin is dehydrated so much by osmotic diffusion and gelates, the flow property of that part is so similar to that of the Zn-xanthate layer, that the orientation of this layer is fixed during the stretching of the filament and the regeneration of cellulose as effectively as in the true outermost skin. The dehydration and syneresis of this layer is further enhanced by the stretching, so the apparent outermost skin thickens with the degree of stretching. For the same reason the destruction of the structure due to the gas evolution within the outermost skin is suppressed in the same order as actually observed in the acetylation.

The cost of this research has been defrayed by the Grant in Aid for Fundamental Scientific Research for the Ministry of Education, to which the authors' thanks are due. The authors are also grateful to Mr. I. Okamura of the Teikoku Jinken Co. for his kind supply of the samples.

Faculty of Engineering, Tokyo Metropolitan University, Tokyo, and Faculty of Engineering, Yamagata University, Yonezawa

Errors in Measuring the Wave-Height of Polarogram. I. Mathematical Discussion

By Yoshikazu YASUMORI

(Received June 16, 1954)

Introduction

In the polarographic quantitative analysis, we may know the amount of material by measuring the wave-height which is obtained after the graphical construction on a polarogram. Therefore it is one of the necessary conditions in the precise polarographic determination, that the polarogram is so taken that the errors of the graphical construction become the least possible.

According to Kolthoff and Lingane[1], any tendency of the limiting current to change with changing applied e.m.f. is greatly magnified by the magnification of a wave and so when the wave is not well-developed, mere magnification of a wave does not necessarily increase the accuracy with which it can be measured. This discussion may hold rather in precision than in accuracy where the so-called errors are related to reliability, precision and accuracy[2]. Therefore a degree of magnification of a wave should be selected in the precise polarographic analysis. In this paper this degree of magnification is discussed mathematically.

Mathematical Calculation of Errors

In order to measure the wave-height of the polarogram *ACB* (Fig. 1), we may use various methods of graphical construction. This discussion holds when the line intersection method[3] treats curves. That is, tangents ξ and η are drawn through the midpoints of straight parts or inflexion-points *A* and *B*, respectively, just before and just after the wave, and a third tangent is drawn through the inflexion-point C of wave. The vertical distance between the two intersection *X* and *Y* thus obtained corresponds to the wave-height *h*.

Now, when the voltage axis represents abscissa and the current axis ordinate, writing coordinates of A, B, C, *X* ane *Y*, as (a_1, b_1), (a_2, b_2), (a_3, b_3), $(x_1, y_1)$and (x_2, y_2), respectively and putting angles at which ξ, η, and ζ intersect the abscissa, φ, ψ and θ, respectively, we have

$$h=f\ (a_1,\ b_1,\ a_2,\ b_2,\ a_3,\ b_3,\ \theta,\ \varphi,\ \psi). \quad (1)$$

But three respective variables in bracket of (a_1, d_1, φ), (a_2, b_2, ψ) or (a_3, b_3, θ) are not independent of one another and the relations between these variables cannot be discussed generally.

On the other hand, the first procedure of construction is to determine (a_1, b_1) etc. and the next is to determine φ etc. And, for instance, on determining (a_1, b_1), b_1 will be

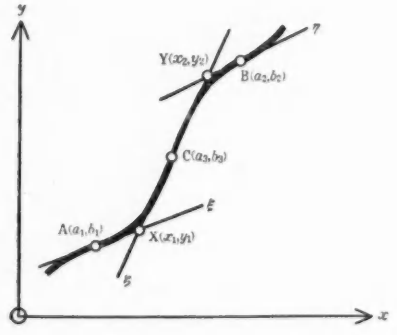

Fig. 1.

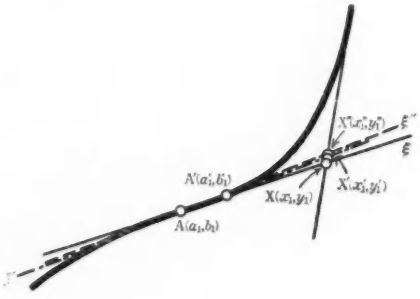

Fig. 2.

1) I. M. Kolthoff and J. J. Lingane, "Polarography," 2nd Ed. p. 328 (1952) Interscience Publishers, New York.

2) K. Ishikawa, *Kagaku-no-Ryoiki*, extra-ed. 10. ("Statistics for Chemists") p. 26 (1953).

3) D. F. Boltz, "Selected Topics in Modern Instrumental Analysis," p. 41 (1952) Prentice-Hall, Inc., New York.

determined after a_1 is fixed. Perhaps the error, which occurs in the determination of b_1, may be negligibly small, if a_1 is fixed. So assuming that b_1 responds strictly to a_1, we have

$$h=f\ (a_1,\ a_2,\ a_3,\ \theta,\ \varphi,\ \psi) \tag{2}$$

Nevertheless another assumption is needed, as two respective variables in a bracket of $(a_1,\ \varphi)$, $(a_2,\ \psi)$ or $(a_3,\ \theta)$ are not independent of each other.

That is, if a point $(a_1',\ b_1')$ is found instead of the actual point $(a_1,\ b_1)$ and a tangent ξ' is erected instead of the actual tangent ξ let us draw through the point $(a_1,\ b_1)$ a line ξ'' in parallel with ξ' (Fig. 2). The difference between the wave-height with ξ' and the one with ξ'' ($|y_1''-y_1'|$) shall be assumed as negligibly small in comparison with the difference between the wave-height with ξ and the one with ξ' ($|y_1'-y_1|$). And the corresponding assumptions of $(a_2,\ \psi)$ and $(a_3,\ \theta)$ shall be considered. With these assumptions the errors in determination of φ, ψ and θ contain those in determination of a_1, a_2 and a_3. Thus writing

$$h=f\ (\theta,\ \varphi,\ \psi) \tag{3}$$

we may calculate the amount of error of h.

Then, by transferring the origin to C in Fig. 1 and displacing the axes parallelly, the following equations can be obtained.

$$\left.\begin{aligned}\frac{b_1^0-y_1^0}{a_1^0-x_1^0}&=\tan\varphi=m\\ \frac{b_2^0-y_2^0}{a_2^0-x_2^0}&=\tan\psi=n\\ \frac{y_1^0}{x_1^0}=\frac{y_2^0}{x_2^0}&=\tan\theta=l\end{aligned}\right\} \tag{4}$$

Where $(a_1^0,\ b_1^0)$, $(a_2^0,\ b_2^0)$, $(0,\ 0)$, $(x_1^0,\ y_1^0)$ and $(x_2^0,\ y_2^0)$ are the coordinates of A, B, C, X and Y, respectively.

Hence we have

$$\left.\begin{aligned}y_1^0&=\frac{(b_1^0-a_1^0m)l}{l-m}\\ y_2^0&=\frac{(b_2^0-a_2^0n)l}{l-n}\end{aligned}\right\} \tag{5}$$

$$h=y_2^0-y_1^0=\frac{(b_2^0-a_2^0n)l}{l-n}-\frac{(b_1^0-a_1^0m)l}{l-m} \tag{6}$$

Now, assuming that the probability density functions of h, θ, φ and ψ are all symmetrical, we have from the familiar formula of error transmission[4]:

$$e_h^2=\left(\frac{\partial h}{\partial\theta}\right)^2e_\theta^2+\left(\frac{\partial h}{\partial\varphi}\right)^2e_\varphi^2+\left(\frac{\partial h}{\partial\psi}\right)^2e_\psi^2 \tag{7}$$

4) S. Miyamoto, "Theory and Calculation of Error," p. 81 (1951) Kosei-sha, Tokyo.

where e_h^2 etc. are the mean squares of errors of h etc., respectively. And from Eq. (6), it follows that

$$\left.\begin{aligned}\frac{\partial h}{\partial\varphi}&=\frac{(a_1^0l-b_1^0)l}{(l-m)^2}(1+m^2)\\ \frac{\partial h}{\partial\psi}&=\frac{-(a_2^0l-b_2^0)l}{(l-n)^2}(1+n^2)\\ \frac{\partial h}{\partial\theta}&=-\left\{\frac{(b_2^0-a_2^0n)n}{(l-n)^2}-\frac{(b_1^0-a_1^0m)m}{(l-m)^2}\right\}(1+l^2)\end{aligned}\right\} \tag{8}$$

Also the relative errors of h are more important than the absolute errors shown in Eq. (7), since the comparative method is usually used in the polarographic quantitative analysis. From Eq. (7) the relative errors are given by,

$$\left(\frac{e_h}{h}\right)^2=\frac{1}{h^2}\left(\frac{\partial h}{\partial\theta}\right)^2e_\theta^2+\frac{1}{h^2}\left(\frac{\partial h}{\partial\varphi}\right)^2e_\varphi^2+\frac{1}{h^2}\left(\frac{\partial h}{\partial\psi}\right)^2e_\psi^2 \tag{9}$$

The Variation of Magnitude of Error with Span Voltage and Sensitivity

When a polarogram is taken with span voltage p times as high and sensitivity q times as high as those with which the original polarogram in Fig. 1 is taken, the new polarogram will be transformed into one of dimensions one pth times in abscissa and q times in ordinate as great as the original. Let us compare the errors of construction on those polarograms as follows.

That is, if the transformation is performed without transferring the point C, the coordinates of A and B will be $(a_1^0/p,\ qb_1^0)$ and $(a_2^0/p,\ qb_2^0)$ respectively. Thus

$$\left.\begin{aligned}\tan\varphi_{pq}&=pqm\\ \tan\psi_{pq}&=pqn\\ \tan\theta_{pq}&=pql\end{aligned}\right\} \tag{10}$$

where φ_{pq}, ψ_{pq} and θ_{pq} are angles at which after the transformation tangents ξ, η and ζ intersect abscissa respectively.

Hence from Eq. (8) we have

$$\frac{\partial h_{pq}}{\partial\varphi_{pq}}=\frac{(a_1^0l-b_1^0)l}{(l-m)^2}\cdot\frac{1+p^2q^2m^2}{p}=\left(\frac{\partial h}{\partial\varphi}\right)\frac{1+p^2q^2m^2}{p(1+m^2)}$$

$$\frac{\partial h_{pq}}{\partial\psi_{pq}}=\frac{-(a_2^0l-b_2^0)l}{(l-n)^2}\cdot\frac{1+p^2q^2n^2}{p}=\left(\frac{\partial h}{\partial\psi}\right)\frac{1+p^2q^2n^2}{p(1+n^2)}$$

$$\frac{\partial h_{pq}}{\partial \theta_{pq}} = -\left\{\frac{(b_2^0 - a_2^0 n)n}{(l-n)^2} - \frac{(b_1^0 - a_1^0 m)m}{(l-m)^2}\right\} \frac{1+p^2q^2l^2}{p(1+l^2)} = \left(\frac{\partial h}{\partial \theta}\right)\frac{1+p^2q^2l^2}{p(1+l^2)} \tag{11}$$

And in such a transformation the wave-height varies also. writing the wave-height after the transformation as h_{pq}, it follows that

$$h_{pq} = qh \tag{12}$$

Furthermore, the magnitude of e_θ, e_φ and e_ψ may vary. Now we assume on these variations as follows.

(1) If the curvature on A, B or C of the polarogram in Fig. 1 are greater, or the curve near such a point is linear over a wider range, the amount of e_θ, e_φ or e_ψ will not vary with the transformation.

(2) If the curve near such a point is linear but the linear portion is shorter, the amount of e_θ, e_φ or e_ψ will be inversely proportional to the length of this linear portion.

With the assumption (1), for instance, it is seen that

$$\frac{1}{h_{pq}^2}\left(\frac{\partial h_{pq}}{\partial \theta_{pq}}\right)^2 e_{\theta pq}{}^2 = \frac{1}{h^2}\left(\frac{\partial h}{\partial \theta}\right)^2 e_\theta{}^2 \frac{(1+p^2q^2l^2)^2}{p^2q^2(1+l^2)^2} \tag{13}$$

And by partially differentiating Eq. (13) with respect to p or q, we have

$$\frac{\partial}{\partial p}\left\{\frac{1}{h_{pq}^2}\left(\frac{\partial h_{pq}}{\partial \theta_{pq}}\right)^2 e_{\theta pq}{}^2\right\} = \frac{1}{h^2}\left(\frac{\partial h}{\partial \theta}\right)^2 e_\theta{}^2 \frac{2(1+p^2q^2l^2)(p^2q^2l^2-1)}{p^3q^2(1+l^2)^2}$$

$$\frac{\partial}{\partial q}\left\{\frac{1}{h_{pq}^2}\left(\frac{\partial h_{pq}}{\partial \theta_{pq}}\right)^2 e_{\theta pq}{}^2\right\} = \frac{1}{h^2}\left(\frac{\partial h}{\partial \theta}\right)^2 e_\theta{}^2 \frac{2(1+p^2q^2l^2)(p^2q^2l^2-1)}{p^2q^3(1+l^2)^2}$$

Hence when $pql=1$ ($l \neq 0$), Eq. (13) takes the minimum value. As for

$$\frac{1}{h_{pq}^2}\left(\frac{\partial h_{pq}}{\partial \varphi_{pq}}\right)^2 e^2{}_{\varphi pq} \text{ or } \frac{1}{h_{pq}^2}\left(\frac{\partial h_{pq}}{\partial \psi_{pq}}\right)^2 e_{\psi pq}{}^2$$

it takes the minimum value also, when $pqm=1$ or $pqn=1$, respectively. But if $l=0$, $m=0$ or $n=0$, it takes the smaller value, with the increase of p and q.

Next, with the assumption (2), for instance, it is seen that

$$\frac{1}{h_{pq}^2}\left(\frac{\partial h_{pq}}{\partial \theta_{pq}}\right)^2 e_{\theta pq}{}^2 = \frac{1}{h^2}\left(\frac{\partial h}{\partial \theta}\right)^2 e_\theta{}^2 \frac{1+p^2q^2l^2}{q^2(1+l^2)} \tag{14}$$

where

$$e_{\theta pq}{}^2 = e_\theta{}^2 \frac{p^2(1+l^2)}{1+p^2q^2l^2} \tag{15}$$

and

$$\frac{\partial}{\partial p}\left\{\frac{1}{h_{pq}^2}\left(\frac{\partial h_{pq}}{\partial \theta_{pq}}\right)^2 e_{\theta pq}{}^2\right\} = \frac{1}{h^2}\left(\frac{\partial h}{\partial \theta}\right)^2 e_\theta{}^2 \frac{1+2pq^2m^2}{q^2(1+m^2)} > 0 \tag{16}$$

$$\frac{\partial}{\partial q}\left\{\frac{1}{h_{pq}^2}\left(\frac{\partial h_{pq}}{\partial \theta_{pq}}\right)^2 e_{\theta pq}{}^2\right\} = \frac{1}{h^2}\left(\frac{\partial h}{\partial \theta}\right)^2 e_\theta{}^2 \left\{\frac{-2}{q^3(1+m^2)^2}\right\} < 0 \tag{17}$$

Hence, Eq. (14) takes the greater value with increasing p and Eq. (14) takes the smaller value with increasing of q.

As for

$$\frac{1}{h_{pq}^2}\left(\frac{\partial h_{pq}}{\partial \varphi_{pq}}\right)^2 e^2{}_{\varphi pq} \text{ or } \frac{1}{h_{pq}^2}\left(\frac{\partial h_{pq}}{\partial \psi_{pq}}\right)^2 e^2{}_{\psi pq},$$

the same relationships hold.

Discussion

From the above mathematical calculation, the relative error of h should be minimum when $pql=1$ or $\theta_{pq}=45°$, if the error in construction of the tangent through C in Fig. 1 is more pronounced than other errors and its magnitude varies after the manner shown by the assumption (1). And if the errors in construction of the tangents through B and C are both pronounced and their magnitudes vary after the manner shown by the assumption (1), $1/m > pq > 1/l$, where $l > m$ or $\theta_{pq} > 45° > \varphi_{pq}$, is the necessary condition for the minimum value of the relative error of h.

On the other hand, when in all the errors the assumption (2) holds, the relative error of h becomes smaller, with decreasing p and increasing q.

But we must remember the fact that the manner of variation of error of σ_{pq} etc. can also change with the transformation of the curve.

Department of Agricultural Chemical
Faculty of Agriculture,
Kyoto University, Kyoto

Errors in Measuring the Wave-Height of Polarogram. II. Practical Errors of Graphical Construction

By Yoshikazu YASUMORI

(Received June 16, 1954)

Introduction

In the previous work[1] the errors in measuring the wave-height on a polarogram were mathematically discussed, and it was concluded that the relative errors in graphical construction on a polarogram might vary with the transformation of the polarogram by the changes of span voltage and sensitivity. In this paper the practical variations of errors are investigated for the sake of comparison with the mathematical conclusion.

Experimental

The intersections of tangents were constructed by ten polarographists on the polarograms printed photographically with a same printing ratio (0.45) from variously transformed original polarograms which were recorded of the same samples with various span voltages and sensitivities.

The original polarograms were recorded of the following three samples after oxygen removal with the initial voltage of −0.3V vs. Hg-pool; and the span voltage and sensitivity are shown in Table I.

Sample A: $1\times10^{-4}N$ $Pb(NO_3)_2+2\times10^{-2}N$ $CdCl_2$
Sample B: $1\times10^{-4}N$ $Pb(NO_3)_2+1\times10^{-2}N$ $CdCl_2$
Sample C: $4\times10^{-4}N$ $TlCl+8\times10^{-3}N$ $CdCl_2$
(Each sample contains $1\times10^{-1}N$ KCl as an indifferent salt)

TABLE I
NOTATIONS OF POLAROGRAMS TAKEN WITH VARIOUS SPAN VOLTAGES AND SENSITIVITIES

		Sensitivity microamp./mm.		
		High	Medium	Low
Polarogram	A	0.004	0.010	0.020
	B	0.006	0.015	0.030
	C	0.008	0.015	0.030
Span Voltage	3V	00	01	02
	1V	10	11	12
	0.5V	20	21	22

The polarograph used here was Sargent Model XXI Polarograph, on whose recorder-paper the 1 mm.-scales on current-axis are printed and so

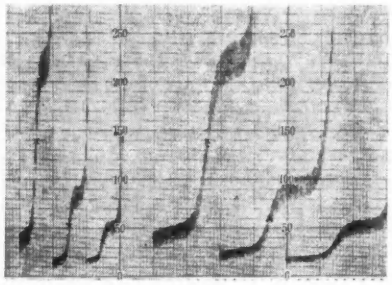

Fig. 3.

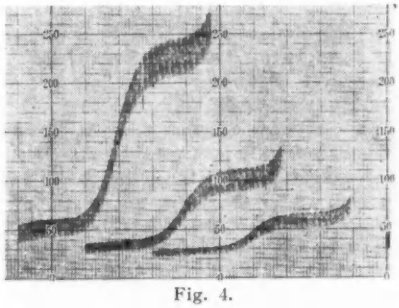

Fig. 4.

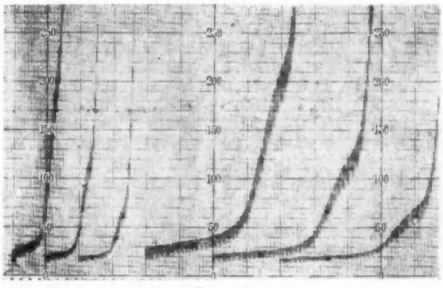

Fig. 5.

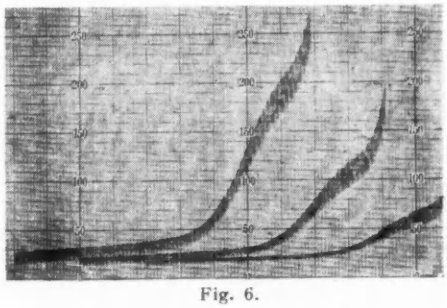

Fig. 6.

1) Y. Yasumori, This Bulletin, **27**, 554 (1954).

the positions of intersections of tangents could be read with these scales.

The tangents in polarogram A (Fig. 3 and 4) and B (Fig. 5 and 6) were drawn through the marked points corresponding to the inflexion-points. In Table II are shown the positions of intersections, in Table III the mean squares of relative deviations of positions of the points from their median to the respective wave-height and in Table 4 the mean squares of relative deviations of thh wave-heights from their median to the respective wave-height.

(The figures in Tables III & IV are values multiplied by 10^1 of the above mentioned.)

TABLE II

THE POSITIONS OF INTERSECTIONS

Sample	Point	Polaro-gram	Constructer A	B	C	D	E	F	G	H	I	J
A	Y	00	208.1	210.8	208.1	209.0	202.9	205.0	209.3	208.6	209.0	202.3
		01	77.7	79.3	80.0	83.1	79.8	80.3	79.8	81.0	81.1	80.6
		02	48.1	49.7	47.7	50.0	48.2	47.4	48.5	48.8	49.6	49.4
		10	215.0	216.4	214.4	219.8	214.2	210.9	215.0	216.8	215.2	212.5
		11	86.9	90.8	89.2	91.9	89.0	88.7	89.3	89.9	90.2	88.4
		12	48.2	48.7	49.4	50.3	50.3	49.2	48.3	49.8	49.3	49.2
		20	214.0	222.8	214.3	221.2	218.2	218.2	216.1	219.1	219.4	220.2
		21	98.3	97.7	97.1	100.9	100.0	98.3	97.3	98.9	98.5	97.5
		22	57.5	57.9	57.6	58.0	57.6	57.2	57.2	57.9	57.0	57.2
	X	00	44.4	49.9	47.8	46.0	46.3	47.7	47.7	45.7	45.7	49.0
		01	18.8	17.9	19.3	18.6	18.3	18.2	19.7	17.3	18.7	18.4
		02	18.0	19.1	18.5	18.4	18.7	18.5	18.1	17.3	18.0	17.2
		10	51.0	54.8	54.0	51.1	50.2	52.4	51.3	48.6	50.0	52.9
		11	26.8	27.4	27.0	25.7	26.7	26.9	26.2	25.9	26.1	21.8
		12	19.7	18.9	19.1	18.8	17.9	19.3	19.3	18.3	18.5	18.9
		20	55.2	57.2	58.3	53.9	53.4	56.3	56.0	54.2	55.3	55.6
		21	36.2	36.7	36.1	36.0	36.2	37.0	37.6	35.8	35.5	37.0
		22	28.9	28.3	28.3	28.3	28.1	28.4	28.3	28.0	29.9	28.3
B	Y	00	174.1	174.6	175.9	177.0	179.2	175.3	176.0	181.2	178.4	173.5
		01	74.3	74.8	74.0	76.9	75.9	73.8	76.4	77.6	77.7	73.7
		02	37.0	38.7	38.5	39.4	39.4	39.4	37.7	39.8	39.2	37.9
		10	191.2	195.3	192.2	198.8	191.0	191.3	194.1	194.6	194.8	189.3
		11	74.0	75.2	72.4	76.2	74.1	74.0	73.8	74.8	75.3	72.9
		12	35.8	35.9	36.1	37.0	35.1	36.9	35.9	36.8	37.0	35.9
		20	198.4	196.9	195.3	199.2	194.4	192.4	191.7	196.3	193.4	191.8
		21	75.1	76.8	75.7	77.9	76.3	78.3	77.2	78.7	76.8	75.8
		22	37.9	37.2	38.2	38.9	39.9	38.6	38.2	38.8	37.1	38.0
	X	00	46.9	49.2	51.1	47.5	46.6	49.2	50.1	44.3	49.9	50.1
		01	31.1	31.3	31.9	29.3	32.0	29.9	31.5	29.1	29.6	32.2
		02	17.2	18.9	18.7	15.8	15.8	15.9	17.6	15.1	16.2	17.1
		10	86.8	83.2	87.8	82.2	85.3	84.6	83.9	85.1	85.2	84.7
		11	30.1	30.1	31.8	28.3	31.8	30.6	31.0	29.0	30.5	31.0
		12	14.3	15.2	14.7	13.3	14.8	14.2	14.0	14.1	14.2	13.8
		20	85.0	80.1	86.4	82.8	84.8	84.2	83.4	78.3	83.0	88.4
		21	31.2	34.9	33.3	34.9	32.9	33.1	32.2	32.2	34.1	33.4
		22	14.5	17.0	16.0	15.3	15.7	16.0	16.5	15.9	16.0	16.0
C	Y	00	175.0	176.5	158.6	180.7	187.8	166.0	152.2	194.0	167.6	185.5
		01	104.2	99.9	87.2	97.1	99.7	87.0	96.8	100.1	90.0	95.9
		02	59.0	58.8	45.9	60.0	54.9	63.3	62.1	56.2	55.2	55.0
		10	173.8	174.8	155.1	180.9	164.0	166.2	169.5	179.0	184.1	153.4
		11	96.0	97.2	88.8	97.4	96.0	89.9	96.0	97.8	104.0	91.0
		12	55.8	55.8	51.5	55.1	54.0	53.9	53.0	54.5	58.9	56.0
		20	151.4	170.0	164.1	181.8	168.8	172.1	169.5	178.2	178.0	165.1
		21	88.8	100.9	98.6	101.9	94.4	103.0	94.1	96.9	99.8	92.2
		22	53.4	57.0	54.2	56.9	59.1	57.2	57.0	57.7	55.0	55.3
	X	00	33.7	32.5	34.3	31.8	32.4	32.4	33.0	32.4	31.4	32.3
		01	25.7	25.0	25.6	23.4	24.3	24.7	24.4	24.7	24.9	24.8
		02	21.4	20.7	21.9	20.8	20.9	20.7	20.7	21.7	21.1	21.3
		10	40.1	40.1	41.2	40.0	41.9	40.0	40.8	38.8	40.9	40.0
		11	25.2	25.9	26.6	26.3	26.2	26.8	26.4	25.2	26.3	26.4
		12	20.6	21.4	20.5	20.1	21.4	21.7	21.4	20.6	21.7	21.1
		20	36.0	36.4	37.7	34.7	34.5	35.3	39.1	35.1	34.4	35.6
		21	28.2	27.2	26.7	26.5	28.3	27.1	28.2	27.3	27.7	27.1
		22	22.4	21.0	21.9	21.6	20.7	21.0	21.9	21.3	22.1	20.6

TABLE III

THE MEAN SQUARES OF RELATIVE DEVIATIONS OF POSITIONS OF POINTS FROM TMEIR MEDIANS

Span Voltage	Sample	Sensitivity: High Y	High X	Medium Y	Medium X	Low Y	Low X	Sum Y	Sum X
3V	A	3.31	0.98	4.58	2.62	8.01	3.53	15.90	7.13
	B	3.50	2.76	11.56	5.95	24.80	30.47	39.86	39.18
	C	78.3	0.17	62.1	0.74	126.3	1.39	302.7	2.30
1V	A	1.96	1.28	4.41	0.83	5.29	2.69	11.66	4.80
	B	5.95	2.02	6.40	5.06	9.18	5.48	21.53	12.56
	C	54.9	0.40	38.2	0.61	32.1	3.10	125.2	4.11
0.5V	A	2.79	0.85	3.50	1.10	1.35	0.79	7.64	2.74
	B	5.29	6.15	6.60	6.71	12.67	8.29	24.56	21.15
	C	37.7	1.21	38.4	0.77	25.3	3.20	101.4	5.18
Sum	A	8.06	3.11	12.49	4.55	14.65	7.01	35.20	14.67
	B	14.74	10.93	24.56	17.72	46.65	44.24	85.95	72.89
	C	170.9	1.79	138.7	2.12	219.7	7.69	529.4	11.59

TABLE IV

THE MEAN SQUARES OF RELATIVE DEVIATIONS OF WAVE-HEIGHTS FROM THEIR MEDIANS

Span Voltage	Sample	Sensitivity: High	Medium	Low	Sum
3V	A	4.54	6.35	12.53	23.42
	C	82.8	67.1	191.0	340.9
1V	A	4.04	5.43	13.91	23.38
	C	61.9	35.2	29.9	127.0
0.5V	A	4.84	6.55	7.02	18.41
	C	44.9	46.4	36.2	127.5
Sum	A	13.42	18.33	33.46	65.21
	C	189.6	148.7	257.1	595.4

Discussion of the Results

(1) **Polarogram A.** — (*a*) *Intersection Y.* The values of respective sums in Table III become smaller with increasing sensitivity and decreasing span voltage. So this result is coincident with the mathematical result obtained with the assumption (2) in the previous paper. But in the high level of sensitivity and the low level of span voltage, this is not valid. In these levels the errors appear not to vary after such a manner that the assumption (2) alone holds.

(*b*) *Intersection X.* The values of the respective sum in Table III varies after the same manner as in (1, -a). But this is not valid in each level except the low level of sensitivity and the high level of span voltage. In this case, as each value is so small that the error in reading of the intersection may not be ignored, this result cannot be compared with the mathematical result.

(*c*) *Wave-height* (*h*). The values of respective sums in Table IV become smaller with increasing sensitivity, but they are not so affected by the change of span voltage. The cause for this seems to be, that the effect of error e_θ on construction of tangent through a inflexion-point of wave becomes more overwhelming with decreasing span voltage. For the errors of Y and X caused by e_θ are not independent of each other. If the errors of Y and X are independent of each other, the sum of these errors in a certain sensitivity and span voltage in Table III will be equal to the error of wave-height in the corresponding sensitivity and span voltage in Table IV[2], but if these errors are not independent of each other and further errors of Y and X are of the same sign, the sum of these errors will be smaller than the error of wave-height. It is obvious that the effect of error e_θ becomes more pronounced with decreasing span voltage, when the values in Tables III and IV are compared with each other on this standpoint.

(2) **Polarogram B.** — Polarogram B has almost the same wave-form as Polarogram A but its inflexion-points have not been marked on it previously.

(*a*) *Intersection Y.* The values of respective sums in Table III become smaller with increasing sensitivity, but they are not so much affected by the change of span voltage. And each value is greater than the corresponding value in Polarogram A. Perhaps the magnitude of error on construction of tangent may not vary after such a manner as discussed mathematically previously, where the point is not fixed, through which the tangent is to be drawn. The error of construction without the fixing of a point is greater than with the fixing of a point and this tendency becomes more effective when the span voltage and sensitivity are low.

(*b*) *Intersection X* The result is analogous to (2, -a).

(3) **Polarogram C.** — (*a*) *Intersection Y.* The values of respective sums in Table III

2) P. G. Hoel, "Introduction to Mathematical Statistics," (translated into Japanese by G. Taguchi) Kagaku-Shinko-Sha (Tokyo) (1950) p. 159.

become smaller with decreasing span voltage, but the effect of sensitivity is irregular. And the result in the medium level of span voltage is coincident with the mathematical result with the assumption (1), where the error in construction of a tangent along the curve just after the wave, is more remarkable. Nevertheless, the results in other levels of span voltage are inconsistent with the mathematical result with the assumption (1). In the high level of span voltage, the error in construction of a tangent through the inflexion-point of a wave may become more predominant with decreasing sensitivity.

(*b*) *Intersection X.* Each value in this case is so small that it may be nonsense to discuss this result with the above mathematical result.

(*c*) *Wave-Height h.* When the corresponding values in Table III and IV are compared with each other, it will be found that the error of wave-height is affected mainly by one of intersections (Y), but where the span voltage is low, by both intersections (Y and X), which are not independent of each other.

Summary

When the construction of tangent η on the curve just after the wave in a poralogram is more difficult, but the construction of other tangents are less difficult, it is concluded as follows.

In the case that the construction of η is a little more difficult, a polarogram with high sensitivity is desirable in order to minimize the relative error in measuring the wave-height. And here low span voltage is, to some extent, effective, but a polarogram too enlarged in abscissa is ill-conditioned. Next, in the case of the very difficult construction of η, the relative error of wave-height is minimum, when a polarogram is taken with lowered span voltage, in which the slope of a tangent is tan 45°. Here the error is not always minimum if the polarogram is recorded with lowered sensitivity.

The author wishes to express his hearty thanks to Prof. I. Tachi for his kind encouragement. The authors' thanks are also due to the members of the Polarographic Group in the Faculty of Agriculture, Kyoto University for their kind help in the construction.

Department of Agricultural Chemistry,
Faculty of Agriculture, Kyoto
University, Kyoto

Studies on Dimethylglyoximo-cobalt(III) Complexes. I. The Preparation and Some Properties of Tris-(dimethylglyoximo)-cobalt(III)

By Akitsugu NAKAHARA

(Received June 21, 1954)

Introduction

Since the work of Tschugaeff[1] a number of dimethylglyoximo-cobalt(III) complexes have been prepared, but the complex-compound having three ions* of dimethylglyoxime about a cobalt atom has never been described. Mann[2] has pointed out that chelating groups fall into two classes: (a) those that can fill all six co-ordination positions, e.g., ethylenediamine, oxalate radical etc.; (b) those which, while capable of filling four positions in the quadri-co-ordinate complex, cannot fill more than four-co-ordination positions when introduced into the sexa-co-ordinate complex. Dimethylglyoxime was cited by Mann as the typical example of the latter case. Thus it has been a definite opinion that the synthesis of tris-(dimethylglyoximo)-cobalt(III) cannot be reached or at least is very difficult[3]. This concept, however, has perfectly been overthrown since the present author has succeeded in preparing this pending compound by a quite simple method. The present paper deals with the method of preparation and properties of this new compound, with some discussions concerning the process of the complex formation.

1) L. Tschugaeff, *Z. anorg. Chem.*, **46**, 144 (1905); *Ber.*, **39**, 2692 (1906); **40**, 3498 (1907); **41**, 2226 (1908).

2) F. G. Mann, *J. Chem. Soc.*, **1933**, 412; H. J. Emeleus and J. S. Anderson, "Modern Aspects of Inorganic Chemistry," 2nd ed., George Routledge and Sons, Ltd. London, (1952), p. 125

3) L. Cambi and C. Coriselli, *Gazz. chim. ital.*, **66**, 91 (1936).

* The following symbols are used: the ion of dimethylglyoxime (DH^-), $CH_3C(NO)C(NOH)CH_3$; the undissociated molecule of dimethylglyoxime (DH_2), $CH_3C(NOH)C(NOH)CH_3$.

Experimental

The Preparation and Identification.—The preparation of tris-(dimethylglyoximo)-cobalt(III) was performed as follows: Six grams of dimethylglyoxime was completely dissolved in 60 ml. of hot water containing 6 g. of potassium hydroxide. After the solution was cooled to 40—50°C, 5 g. of crystalline cobaltous nitrate hexahydrate was added. The mixture was shaken vigorously and thoroughly, and to this 12 ml. of 50% acetic acid was poured. Then the air was bubbled vigorously through the reaction mixture for about three hours. Beautiful orange-yellow acicular crystals gradually were deposited. The mixture was allowed to stand for several hours, and then was filtered by suction. The crude substance was recrystallized from water containing a small amount of acetic acid. Four grams of pure substance was yielded.

In place of potassium hydroxide and cobaltous nitrate in the above described procedure, sodium hydroxide and cobaltous chloride, respectively, can also be used. Therefore, it will be concluded that the resulting products have nothing to do with K^+ and Na^+ or NO^-_3 and Cl^-. In fact, the products did not show any reaction characteristic of those ions. Nevertheless, if the product were not the uncharged complex molecule, the compound would necessarily have H^+ or OH^- as the external ion of the complex radical, and the aqueous solution of the compound would have to show, similarly to the case of $H_3O^+[Co(DH)_2(NO_2)_2]^-$ or $[Co(NH_3)_2(DH)_2]^+ OH^-$, considerably strongly acidic or basic property, respectively.[4] The present compound, however, was found to be neither acidic nor basic. In consequence, it was concluded that the product is an uncharged complex molecule. The results of analyses were as follows: Co, 12.90; C, 32.51; H, 5.98; N, 18.80; H_2O, 9.75 Calcd. for $[Co(DH)_3] \cdot 2.5\ H_2O$: Co, 13.12; C, 32.08; H, 5.83; N, 18.71; H_2O, 10.02%.

Furthermore, as far as the valency of cobalt is concerned, it is reasonably considered to be tervalent since the cobaltous salts in general are very easily oxidized in the presence of glyoximes to cobaltic complexes[5].

Thus it was finally decided that the present substance surely corresponds to the tris-(dimethylglyoximo)-cobalt(III) $[Co(DH)_3] \cdot 2.5\ H_2O$.

Measurements of the Absorption Spectra.—The absorption spectra of the complex and its ligand, dimethylglyoxime, were determined at room temperature with a Beckman Model DU quartz spectrophotometer. The results are shown in Fig. 1. The concentrations used were $1/10^3$—$1/10^5$ and $1/10^2$—$1/10^4$ mol./l., in (a) and (b), respectively. While the measurement of dimethylglyoxime was made in alcoholic solution, that of the complex was made in aqueous solution for the purpose of comparison with the data obtained in bis-(dimethylglyoximo)-derivatives. Molar extinction coefficients ε were calculated from the familiar equation $\varepsilon = \frac{1}{cd} \times \log_{10} (I_0/I)$, where c is the concentration of the compound in mol./l., and d the thickness of the layer in cm.

Description of the Properties.—The clear acicular crystals of tris-(dimethylglyoximo)-cobalt (III) obtained by successful recrystallization are orange-yellow or brownish-yellow. The bright-yellow coloured opaque fibroid crystals which we very often encounter are impure. The pure crystal is quite stable in the atmosphere, and hardly ever decomposes below 200°C. It is somewhat soft to the feel in comparison with ordinary inorganic complexes. This is probably attributable to the feeble intermolecular forces, which are possible in the spherical compound surrounded by many methyl-groups. It is soluble in water, alcohol, chloroform and dioxane, and insoluble in benzene and acetone. In concentrated acetic acid, it decomposes on dissolution.

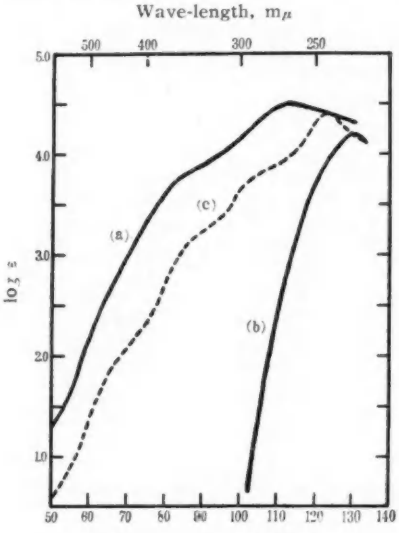

Fig. 1. Absorption spectra of: (a), tris-(dimethylglyoximo)-cobalt(III) in aqueous solution; (b), dimethylglyoxime in alcoholic solution, and (c), bis-(dimethylglyoximo)-diammine-cobaltic chloride in aqueous solution.

Discussion

The Absorption Spectra.—The absorption curve, (a), has only one maximum in the spectral region from 50 to 130×10^{13}/sec., and is quite monotonous. This will probably be due to the large and complicated specific absorption bands[6] of ligands, dimethyl-

4) L. Tschugaeff, *Ber.*, **41**, 2228 (1908); *J. Russ. Ges. chem.*, **41**, 1366 (1909); **41**, 218 (1909); *Z. anorg. Chem.*, **46**, 163 (1905); Gmelins Handbuch d. anorg. Chem., 8. Auflage, **58B**, 276, 324 (1930).

5) L. Cambi and C. Coriselli, *Gazz. chim. ital.*, **66**, 81 (1936); *Chem. Abstr.*, **30**, 8158 (1936).

6) R. Tsuchida, and M. Kobayashi, This Bulletin, **13**, 471 (1938); R. Tsuchida, ibid., **13**, 442 (1938); **13**, 388 (1938).

glyoxime. Although bis-(dimethylglyoximo)-cobalt(III) complexes[7,8] show similar absorption curves on the whole, they differ considerably from the present curve, (a). As is clear from Table I,[8] tris-(dimethylgyloximo)-cobalt(III) has the absorption maximum at 113×10^{13}/sec., while the maxima of bis-(dimethylglyoximo)-complexes are observed in the region from 121.5 to 123×10^{13}/sec. In other words, the former is bathochromic to the latter. Also with respect to the molar extinction coefficients the former is hyperchromic to the latter as shown in Table I.

TABLE I
ABSORPTION MAXIMA FOUND IN THE SHORTER WAVE-LENGTH

Complexes	absorption maxima	
	$\nu_{max.}$	log $\varepsilon_{max.}$
$[Co(NH_3)_2(DH)_2]Cl\cdot 5H_2O$	123.0	4.41
$[Co(NH_3)(DH)_2Cl]$	122.0	4.38
$[Co(DH)_2(NO_2)_2]NH_4\cdot H_2O$	122.0	4.44
$[Co(NH_3)(DH)_2(NO_2)]$	123.0	4.40
$[Co(H_2O)(DH)_2(NO_2)]$	121.5	4.41
$[Co(DH)_3]\cdot 2.5\ H_2O$	113.2	4.50
Dimethylglyoxime	130.4	4.20

It has long been known that the specific absorption bands are usually shifted bathochromically and hyperchromically with an increasing number of the concerned ligands.[6] If the present absorption band is assumed to be the specific absorption band of dimethylglyoxime, the relation between the absorption maximum of tris-(dimethylglyoximo)-complex and that of bis-(dimethylglyoximo)-derivative agrees with the above mentioned empirical rule. Moreover, judging from the curve in the longer wave-length, dimethylglyoxime seems probably to precede, at least, ethylenediamine in the spectrochemical series.[6] That is to say, dimethylglyoxime is a considerably hypsochromic ligand. The details concerning the absorption spectra of the dimethylglyoximo-cobalt(III) complexes will be reported later.[8]

Stabilities of Dimethylglyoximo-complexes.—According to Nakatsuka and Iinuma,[9] two ions of dimethylglyoxime in the bis-(dimethylglyoximo)-diamine-cobalt(III) complexes generally have a strong tendency to form the planar configuration. Certainly, this opinion is supported by many chemical evidences. For instance, it is necessary to assume such a strong tendency characteristic of dimethylglyoxime, in order to elucidate the reason why any pair of geometric isomers of those complexes has never been obtained, while it is capable of isolating *cis*- and trans-isomers for the bis-ethylenediamine- or bis-oxalato-complexes. The distinguished stability of planar co-ordinated bis-(dimethylglyoximo)-derivative can be recognized also in the fact that any type of complex radical other than the bis-(dimethylglyoximo)-derivative has never been prepared for the last five decades. Although no paper concerning the origin of this characteristic has ever been published, it may be considered that O—H—O hydrogen bonds in the planar configuration as shown in Fig. 2 are necessarily concerned

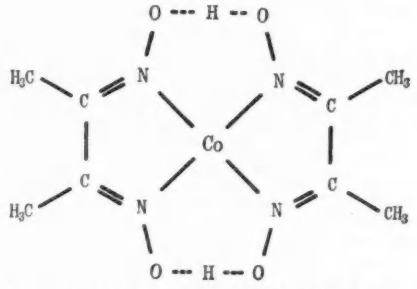

Fig. 2 Planar bis-(dimethylglyoximo)-cobalt(III)-complexes with O—H—O hydrogen bonds.

in the distinguished stability of those complexes.* This is probably because such a kind of hydrogen bond in bis-(dimethylglyoximo)-nickel(II) was demonstrated recently by Godycki and Rundle from the standpoint of X-ray analysis,[10] and directly by means of the measurement of infra-red absorption spectrum.[11] The existence of the above mentioned O—H—O hydrogen bonds in the cobalt(III) complexes will be expected reasonably from the evidence obtained in the nickel complex. If it proves to be the case, we can estimate this energy of hydrogen bond at several kilocalories per mol. from a large number of data.[12] Since there are two hydrogen bonds in one complex radical, the energy of at least 10—15 kilocalories will be expected per mol. On the other hand, so far as the ordinary cobalt(III) complexes are

7) H. Kuroya, *J. Inst. Polytech.*, Osaka City Univ., **1**, No. 2, Ser. C, 11 (1950),
8) To be published later.
9) Y. Nakatsuka and H. Iinuma, This Bulletin, **11**, 48 (1936).
10) L. E. Godycki, R. E. Rundle, R. C. Voter and C. V. Banks, *J. Chem. Phys.*, **19**, 1205 (1951); L. E. Godycki and R. E. Rundle, *Acta Cryst.*, **6**, 487 (1953).
11) R. E. Rundle and M. Parasol, *J. Chem. Phys.*, **20**, 1487 (1952).
12) See, for example, S. Seki, *Chem. and Chem. Ind.* (in Japanese), **6**, 2226—2227 (1953).
* On the contrary, the opinion that the origin of the tendency towards the planar configuration may be attributable to the π-electrons in the conjugated double bond system is out of the question, since tris-(dipyridyl)- or tris-(phenanthroline)-complexes generally are readily synthesized.

concerned, heats of formation are about 30—50 kcal/mol.[13] (Table II). Thus it may be supposed that the present O—H—O hydrogen bonds in the planar configuration contribute to a considerable degree towards the complex

TABLE II
HEAT OF FORMATION OF COBALT(III) COMPLEXES

Complex ions	Heat of formation kcal.
$[Co(NH_3)_5]^{3+}$	51.9
$[Co(NH_3)_5(NO_2)]^{2+}$	53.1
$[Co(NH_3)_5Cl]^{2+}$	41.7
$[Co(NH_3)_5(H_2O)]^{3+}$	45.0
$[Co(NH_3)_4(NO_2)_2^{(1)}_{(6)}]^{+}$	53.1
$[Co(NH_3)_4(NO_2)_2^{(1)}_{(2)}]^{+}$	53.9
$[Co(NH_3)_4Cl_2^{(1)}_{(6)}]^{+}$	32.0
$[Co(NH_3)_4Cl_2^{(1)}_{(2)}]^{+}$	30.2
$[Co(NH_3)_4(NO_2)Cl^{(1)}_{(6)}]^{+}$	49.3
$[Co(NH_3)_4(H_2O)(NO_2)^{(1)}_{(6)}]^{2+}$	45.6
$[Co(NH_3)_4(NO_2)_4]^{-}$	47.0
$[Co(NO_2)_3]^{3-}$	28.1

formation. The origin of the strong tendency towards the planar configuration characteristic of dimethylglyoxime will, therefore, be found in the above described O—H—O hydrogen bonds. It is then quite natural that the synthesis of tris-(dimethylglyoximo)-cobalt(III) should be very difficult in the ordinary conditions, since the planar bis-(dimethylglyoximo)-derivatives are exceedingly stable. The method of preparation of tris-(dimethylglyoximo)-cobalt (III) suggested by the present author, however, is compatible with the above conclusion. Namely, in this condition, the O—H—O hydrogen bonds are interrupted by potassium hydroxide in the process of the complex formation. In such a condition, three ions of dimethylglyoxime will be able to co-ordinate to a cobalt atom, quite similarly to the ethylenediamine or oxalate radical. And it may be supposed that the formation of the original form of the product already is finished before acetic acid is poured. This assumption is supported by the fact that the synthesis of tris-(dimethylglyoximo)-cobalt(III) is unsuccessful if acetic acid is poured on at the beginning. At any rate. the reactions adopted by many investigators differ in the starting form of dimethylglyoxime from the present method; i.e., in the former dimethylglyoxime exists as a molecule and in the latter as a bivalent anion.

13) K. B. Yatsimirski and L. L. Pankova, *J. Gen. Chem. U. S. S. R.*, **18**, 2051 (1948); **19**, 617, 623 (1949); *Chem. Abstr.*, **43**, 2855, 7805, 7806 (1949); **44**, 7701 (1950).

Summary

Tris-(dimethylglyoximo)-cobalt(III) was newly synthesized by making use of dipotassium dimethylglyoximate. The crystals are quite stable in the atmosphere similarly to other so-called luteo-complexes, and orange-yellow in color. It is soluble in organic solvents, e.g., chloroform, alcohol and dioxane, as well as in water, but insoluble in benzene and acetone.

The absorption spectrum of this compound in aqueous solution was measured, and it was concluded that dimethylglyoxime is a considerably hypsochromic ligand.

Some discussions concerning the stabilities of bis-(dimethylglyoximo)-cobalt(III) complexes were given and they reached the following conclusions: (1) the distinguished stability of bis-(dimethylglyoximo)-derivatives is probably due to the O—H—O hydrogen bonds which are expected for the planar configuration of two dimethylglyoximic ions, and (2) the synthesis of tris-(dimethylglyoximo)-cobalt(III) can be successfully achieved only by interrupting the formation of those hydrogen bonds in the course of co-ordination of the ligands.

The author wishes to express his sincere thanks to Prof. R. Tsuchida and Dr. S. Yamada for their guidance and encouragement throughout this work. This study was supported in part by a grant from the Ministry of Education.

Department of Chemistry, Faculty of Science, Osaka University, Nakanoshima, Osaka

LETTER

A New Type Mercury Electrode for Polarography

By Yuzo Yashiro

(Received May 28, 1954)

A new type mercury electrode has been designed for polarography. As shown in Figure 1, this electrode has a pin hole of which the diameter is so small that the mercury does not drop through the hole due to the large surface tension of mercury. The mercury is always kept on a suitable constant head level and poured at a slow steady speed. This electrode retains many of the

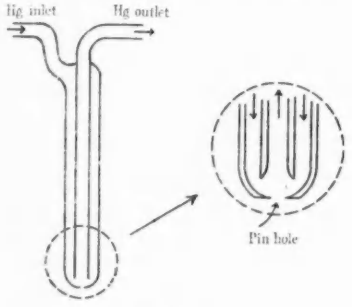

Fig. 1.

advantages of conventional procedures and has about the same sensitivity as compared with the dropping mecury electrode. The polarograms obtained by using this electrode are very smooth and the residual currents have noticeably less slope than those of Heyrovsky-Forejet's streaming mercury electrode.[1] For instance, the polarograms of air-free 0.1 N KCl solutions containing 5×10^{-4} M $CdCl_2$ and gelatin as a maximum suppressor give an experimental relation $h=45A+0.02$, where h is the wave-height(μA) and A is the sectional area(cm^2) of a pin hole of this type electrode. The residual currents, however, are always about 0.05 μA at -0.6 V in the above cases.

If a pair of this type electrode which has the same characteristics are used in a polarographic circuit, the residual currents may be almost completely eliminated. (The one electrode is immersed in the solution containing samples to be analysed and supporting electrolytes and the other electrode is immersed in the solution containing supporting electrolytes only.)

Thus, the electrode of this type will be well applied to the oscillographic polarography, the derivative and differential polarography, the potentiometric plot polarography, the amperometry and so on.

1) *Z. physik. Chem.*, **193**, 77 (1943).

Nagoya Institute of Technology, Nagoya

A Cytochrome and a Green Pigment of Sulfate-reducing Bacteria

By Makoto Ishimoto, Jiro Koyama and Yutaka Nagai

(Received July 31, 1954)

Some strains of sulfate-reducing bacteria, isolated from paddy fields, were found to contain a cytochrome-like red pigment and a green one in spite of their strictly anaerobic character. In cell suspension, the cytochrome was reduced by molecular hydrogen or by formate, which are the proper metabolites of the bacteria[1], and oxidized by sulfate, sulfite or thiosulfate. So they seem to behave as an intermediary carrier of hydrogen in sulfate reduction in a manner similar to usual cytochromes in aerobic organisms[2]. The presence of the cytochrome and the green pigment was reported recently by Postgate[3] in other strains of sulfate-reducing bacteria, but he did not notice the oxidation of the cytochrome by sulfate.

Both pigments could be easily extracted after being made soluble by grinding the cells of the sulfate-reducing bacteria with quartz sand or alumina. A preparation of the green pigment, almost free from the cytochrome, was obtained as precipitate from the saline extract, previously treated with 0.1 M manganese chloride, by addition of its half volume of acetone. The cytochrome, free from the green pigment, was extracted with M/15 disodium phosphate from the residue of the ground cells, which had been treated three times with saline. Their absorption spectra determined by Beckman spectrophotometer, Model DU, are indicated in Fig. 1 and 2.

The cytochrome has absorption maxima at 553 mμ, 524 mμ and 420 mμ in reduced form and at 528 mμ and 410 mμ in oxidized. The absorption bands did not change by the addition of cyanide or carbon monoxide. The

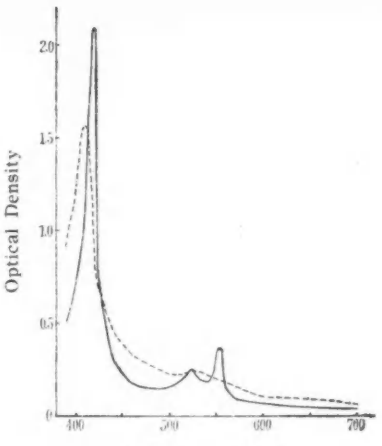

Fig. 1. Absorption spectra of the cytochrome of sulfate-reducing bacteria.
Continuous line: reduced form.
Broken line: oxidized form.

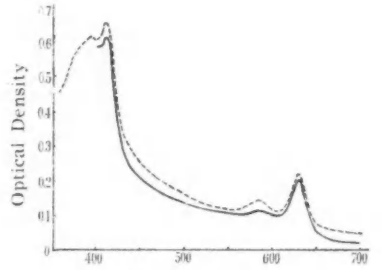

Fig. 2. Absorption spectra of the green pigment of sulfate-reducing bacteria.
Broken line: before reduction.
Continuous line: after reduction.

reduced form was autoxidizable. This cytochrome resembles fairly well cytochrome-b_1 in respect of the absorption spectra[4], but differs from it in autoxidizability and redox potential. rH_0 of the cytochrome of the sulfate-reducing bacteria falls in between 9.3 and 5.7, when measured by Ball's method[5].

The green pigment had absorption maxima at 630 mμ, 590 mμ and 410 mμ, which were not affected by reduction, but shifted by the addition of pyridine to 590 mμ and 555—545 mμ. This pigment seems to be also a hemoprotein.

1) M. Ishimoto, J. Koyama, T. Omura and Y. Nagai, *J. Biochem.* (Tokyo), **41**, 537 (1954).
2) M. Ishimoto, J. Koyama and Y. Nagai, *J. Japan Biochem. Soc.*, **26**, 304 (1954).
3) J. Postgate, *Biochem. J.*, **56**, xi (1954).
4) F. Egami, M. Itahashi, R. Sato and T. Mori, *J. Biochem.* (Tokyo), **40**, 527 (1953).
5) E. G. Ball, *Biochem. Z.*, **295**, 262 (1938).

Department of Chemistry Faculty of Science, Tokyo University

A Semi-empirical Approach to the Self-consistent Molecular Orbitals

By Hideo Kon

(Received August 12, 1954)

The semi-empirical ASMO method proposed recently by Pariser and Parr[1] presents a way to calculate the transition energy of a variety of π-electron systems without much labor in conformity with experimental results that is rarely to be found in this kind of calculations. One of the essential points of the method is to alter the values of Coulomb repulsion integrals over atomic orbitals by computing $(pp|pp)$ through the empirical ionization potential and electron affinity values of the atom p and by computing $(pp|qq)$ as the electrostatic interaction between the uniformly charged spheres.

It is of some interest to reflect this reasonable revision of integral values on the form of molecular orbitals. One way might be to resort to the iterative procedure of Roothaan[2], by incorporating Pariser and Parr's semi-empirical scheme into the former. In the present letter, the above mentioned idea is applied to the simple oxygen containing molecules (formaldehyde and glyoxal) as to which no account was given in Pariser and Parr's article.

The best set of coefficients (c_{tp}) in a molecular orbital (ϕ_t) expressed as a linear combination of atomic orbitals (χ_p),

$$\phi_t = \sum_p c_{tp}\chi_p,$$

is obtained by the iterative solution of a set of homogeneous equations derived by Roothaan, with the overlap integrals S_{pq} being replaced by δ_{pq},

$$\sum_q c_{tp}(L_{pq} - \delta_{pq}\epsilon_t) = 0,$$

δ_{pq} being Kronecker's delta. (As to the definitions of L_{pq} and ϵ_t, see ref. 2.) In computing the matrix elements L_{pq}, the simplifications by Pariser and Parr such as; 1) zero differential overlap, 2) neglect of non neighbor resonance integrals are taken in. In addition to this, following assumptions are made: 1) The Coulomb integral α_p can be approximated as the valence state ionization potential (W_{2p}) of the free atom, less the sum only of the Coulomb repulsion integrals $(pp|qq)$. This neglect of Coulomb penetration integrals is found to reduce the labor without having

a significant influence on the numerical results. 2) The resonance integral β_{pq} is proportional for a type of bond (C=C, C=N, or C=O, etc.) to the inverse sixth power of the bond length, the proportionality constants being selected so as to reproduce, as closely as possible, the observed N→V, transition of a particular molecule in the final result by the iterative process. In the case of formaldehyde, 2.95 ev is found suitable for β_{co} (1.20 Å), and the same value is used for predicting glyoxal N→V_1 transition. The geometricals and numberings for formaldehyde and glyoxal are shown in Fig. 1, together with the computed π-electron densities.

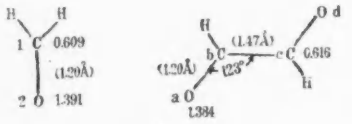

Fig. 1.

The calculated transition energies (E) and self-consistent molecular orbitals are given in the following, where V_1 and T_1 designate the lowest excited singlet and triplet state, respectively.

Formaldehyde,

$E(N\rightarrow V_1)$=8.09 ev, observed, 7.95 ev,[1]

$E(N\rightarrow T_1)$ 4.75 ev,

$\phi_1 = 0.5519\ \chi_1 - 0.8339\ \chi_2$,

$\phi_2 = 0.8339\ \chi_1 + 0.5519\ \chi_2$.

Glyoxal,

$E(N\rightarrow V_1)$ 7.47 ev, estimated, 7.51 ev*),

$E(N\rightarrow T_1)$=5.09 ev,

$\phi_1 = 0.5541\ (\chi_a + \chi_d) + 0.4393\ (\chi_b + \chi_c)$,

$\phi_2 = 0.6205\ (\chi_a - \chi_d) + 0.3390\ (\chi_b - \chi_c)$,

$\phi_3 = 0.4393\ (\chi_a + \chi_d) - 0.5541\ (\chi_b + \chi_c)$,

$\phi_4 = 0.3390\ (\chi_a - \chi_d) - 0.6205\ (\chi_b - \chi_c)$.

*) Estimated roughly from the 57,000 cm^{-1} band of diacetyl, assuming that the two $-CH_3$ groups cause the bathochromic shift of the same magnitude as the difference between the 60,600 cm^{-1} band of acetone and the corresponding band of formaldehyde.

Detailed discussion of these results will be published soon, with the result of calculations for several other molecules which are now in progress.

The author is grateful to Professor H. Tominaga for his kind guidance through the course of this calculation.

1) R. Pariser and R. G. Parr, *J. Chem. Phys.*, **21**, 466, 767 (1953).
2) C. C. J. Roothaan, *Rev. Mod. Phys.*, **23**, 69 (1951); R. G. Parr and R. S. Mulliken, *J. Chem. Phys.*, **18**, 1338 (1950).
3) A. D. Walsh, *Proc. Roy. Soc.* (London), **185A**, 176 (1946).

Department of Chemistry, Faculty of Science, Tôhoku University